POLITECNICO DI TORINO
Repository ISTITUZIONALE

ExtrusionBased Additive Manufacturing of Advanced Ceramics: Strengthening Mechanisms and Process Optimization Review

Original
ExtrusionBased Additive Manufacturing of Advanced Ceramics: Strengthening Mechanisms and Process Optimization Review / Bakhtiari, M., Sheikhansari, M.H., Borgaonkar, A., Dadkhah, M., Saboori, A.. - In: ADVANCED ENGINEERING MATERIALS. - ISSN 1527-2648. - 28:16(2026). [10.1002/adem.71088]

Availability:
This version is available at: 11583/3015988 since: 2026-09-27T10:57:58Z

Publisher:
John Wiley and Sons Inc

Published
DOI:10.1002/adem.71088

Terms of use:

This article is made available under terms and conditions as specified in the corresponding bibliographic description in the repository

Publisher copyright

(Article begins on next page)

31 October 2026

Check for updates

Advanced Engineering Materials

ADVANCED ENGINEERING MATERIALS
www.aem-journal.com

REVIEW OPEN ACCESS

Extrusion-Based Additive Manufacturing of Advanced Ceramics: Strengthening Mechanisms and Process Optimization Review

Meisam Bakhtiari[1] | Mohammad Hadi Sheikh-Ansari[1] | Avinash Borgaonkar[2,3] | Mehran Dadkhah[4] | Abdollah Saboori[2,3]

[1]Faculty of Materials Science and Engineering, K. N. Toosi University of Technology, Tehran, Iran | [2]Department of Management and Production Engineering, Politecnico di Torino, Torino, Italy | [3]Integrated Additive Manufacturing Center, Politecnico di Torino, Torino, Italy | [4]Department of Applied Science and Technology, Politecnico di Torino, Torino, Italy

Correspondence: Meisam Bakhtiari (m.bakhtiari@mail.kntu.ac.ir) | Abdollah Saboori (abdollah.saboori@polito.it)

Received: 10 December 2025 | **Revised:** 15 June 2026 | **Accepted:** 19 June 2026

Keywords: advanced ceramics | densification | extrusion-based additive manufacturing | process optimization | strengthening

ABSTRACT

Extrusion-based additive manufacturing (EAM) has become an increasingly important method for fabricating complex ceramic components due to its cost-effectiveness, design flexibility, and suitability for small-batch production. This review presents a comprehensive evaluation of EAM processes for advanced ceramics, including water-based and thermoplastic extrusion methods such as fused deposition modeling, extrusion free-form fabrication, thermoplastic 3D printing, and photoassisted extrusion techniques. This study critically examines how key process parameters, including extrusion pressure, velocity, nozzle diameter, and layer thickness, affect surface finish, dimensional accuracy, and defect formation. The occurrence of porosity and cracking in both single- and multistage processes highlights the necessity of advanced postprocessing techniques. Methods such as debinding, sintering, infiltration, and isostatic pressing are evaluated for their effectiveness in improving densification and microstructural integrity. Preprocessing routes including liquid silicon infiltration and spark plasma sintering are also explored. Additionally, the review addresses optimization strategies through toolpath planning, machine learning, and process simulation. Applications in biomedical scaffolds, aerospace components, and functional electronics are discussed to demonstrate the industrial potential of EAM. By synthesizing recent developments in materials, process control, and performance assessment, this work identifies major challenges and opportunities in ceramic additive manufacturing and offers guidance for future research and industrial applications.

1 | Introduction

Additive manufacturing (AM), known as three-dimensional (3D) printing, encompasses a variety of techniques for fabricating 3D objects through the incremental addition of material, typically in a layer-by-layer fashion, directly from digital 3D model information. With 3D printing technologies in manufacturing various industrial parts, extensive changes were made in the fabrication methods of parts. This includes ceramics and has enabled greater design freedom in component fabrication. It also eliminates the need for mold-making and the associated limitations. This approach enables the simultaneous and in situ fabrication of ceramic components, enhancing efficiency and design flexibility [1–5]. One of the primary benefits of AM for the ceramic industry is its capacity to facilitate the cost-effective production of prototypes, small-batch runs, and personalized components without relying on expensive specialized molding equipment. Because ceramic parts are often used in specialized or high-value applications, their required production volumes are typically much lower than those of metal or polymer parts. This renders AM

This is an open access article under the terms of the Creative Commons Attribution License, which permits use, distribution and reproduction in any medium, provided the original work is properly cited.

© 2026 The Author(s). *Advanced Engineering Materials* published by Wiley-VCH GmbH.

an especially appealing and cost-effective alternative to substitute injection molding for small-scale production quantities, mainly when components exhibit geometric intricacy.

AM methods for advanced ceramics can generally be classified into single- and multistep processes [6, 7]. In single-step AM methods, forming and sintering occur simultaneously, producing the final part directly. In multistep methods, a "green body" composed of ceramic powders, binders, and other additives is first fabricated using a 3D printer. This green body then undergoes heat treatment for debinding and sintering to achieve the final dense structure. The solid loading, the volume fraction of ceramic material within the green body, is a key factor influencing part quality; higher ceramic content tends to reduce distortion, shrinkage, and cracking during sintering [8, 9]. Despite notable progress, most AM techniques for ceramics are multistep processes, and none can yet produce fully defect-free parts. This shortcoming suggests that conventional heat treatment alone is insufficient to ensure structural integrity. Consequently, the fabrication of high-quality ceramic components remains a complex challenge. To address these limitations and optimize mechanical and microstructural properties, postprocessing treatments are often required after AM fabrication. Such treatments aim to increase density, improve surface finish, and enhance the microstructure of the printed ceramic parts. At this stage, efforts should focus on enhancing density, surface quality, and the microstructural properties of the ceramic parts [10–12].

Densification of the manufactured parts is one of the most important criteria for increasing the quality of products [8]. In general, single- or multistage AM methods, each for some reason, can create cavity defects such as porosity and cracking. For instance, in single-stage methods, especially in manufacturing ceramic parts using the direct selective laser sintering (D-SLS) method, some challenges lead to defects in parts, among which the inherent properties of ceramics, such as low thermal ductility and high melting point, can be mentioned [13, 14]. This is due to the high speed and very low duration of laser radiation in the process, the possibility of poor curing of ceramics, and low density with high thermal stress created in the parts [15]. Also, multistage methods based on slurry are inherently porous due to the sintering and release of binders and solutions [16].

The postprocessing methods of extrusion-based additive manufacturing (EAM) of advanced ceramic materials involve several key techniques to enhance the quality and functionality of the final products. These methods include debinding, where the binder material is removed from the printed part through thermal or chemical processes. Sintering is another crucial step involving heating the part to high temperatures to fuse ceramic particles for increased strength and density. Additionally, surface finishing techniques like polishing and coating are employed to improve aesthetics and functionality. At the same time, machining processes such as milling or grinding may be used for precise dimensions and surface characteristics. These postprocessing steps are essential in ensuring the production of high-quality ceramic components through EAM processes.

This study presents a compilation of reviews concerning the AM of ceramics spanning the last two decades. However, these reviews have concentrated on specific ceramics-related AM processes, neglecting recent advancements. Over the past few years, significant developments and technological innovations have emerged, some of which have not been addressed in prior reviews. This article offers a comprehensive overview of the present advanced ceramic materials in AM. It systematically evaluates the capabilities of each AM technology, delving into an in-depth analysis of its advantages, limitations, opportunities, and associated challenges in processing advanced ceramics. Additionally, it sheds light on the industrial and commercial market landscape for ceramic AM.

2 | EAM Methods

When an extrusion nozzle is used during ceramic AM, the process is referred to as an extrusion-based EAM technique. AM methods for advanced ceramics can be broadly classified into three categories: powder-based, bulk solid-based, and slurry-based manufacturing methods. In slurry-based EAM, a suspension composed of ceramic particles, polymers, aqueous or nonaqueous solvents, and other additives is used. The viscosity of this suspension plays a critical role in selecting the appropriate manufacturing method, which can be divided into two approaches [10]. First, ink refers to a low-viscosity suspension (∼mPa·s) in which the ceramic loading is limited, typically not exceeding 30 volume percent. This form is primarily used in techniques such as inkjet printing. Second, paste refers to a high-viscosity suspension (∼Pa·s), containing a higher concentration of ceramic particles, which gives it a paste-like consistency. Paste is mainly applied in extrusion-based methods.

Parts manufactured using slurry-based AM methods must first undergo heat treatment for debinding, during which organic materials and polymers in the structure are removed as completely as possible. Following this, the ceramic body is sintered by gradually increasing the temperature and holding it for a sufficient time to densify the material and reduce porosity. The ceramic content in the structure plays a critical role in part quality: higher ceramic loading helps minimize shape distortion, shrinkage, and the likelihood of cracks in the final component [8, 17, 18]. A key challenge in slurry-based methods is achieving a uniform distribution of ceramic particles within the suspension. Proper particle dispersion prevents agglomeration during manufacturing and ensures consistent properties in the printed part. Consequently, debinding and sintering processes must be carefully controlled to preserve the part's integrity and optimize its microstructure [19–22].

Furthermore, the average particle size and particle size distribution are critical parameters that influence not only the viscosity of the slurry but also the behavior of the suspension during printing. For example, smaller particle sizes can decrease the reactivity of the suspension, affecting its flow and consolidation during fabrication [23]. This study provides an overview of various EAM techniques for ceramic materials and discusses the different EAM methods and related research conducted in this field. The types of AM methods used for fabricating advanced ceramics are summarized in Table 1. The primary focus of the present review is on multistep extrusion-based AM technologies for ceramic materials. Since 2009, AM technologies have been

15272648, 2026, 16, Downloaded from https://advanced.onlinelibrary.wiley.com/doi/10.1002/adem.71089 by Abdollah Saboori - Politecnico Di Torino Sist. Bibl Del Polit Di Torino , Wiley Online Library on [27/09/2026]. See the Terms and Conditions (https://onlinelibrary.wiley.com/terms-and-conditions) on Wiley Online Library for rules of use; OA articles are governed by the applicable Creative Commons License

TABLE 1 | Type of various AM methods used in the manufacture of advanced ceramics.

AM process	Single step				Direct selective laser sintering (D-SLS) Selective laser melting (SLM) Direct energy deposition (DED)
	Multi step	Slurry based	Photo polymerization-based technology		Two-photon polymerization (2PP) Digital light processing (DLP) Stereolithography (SL) Vat photopolymerization (VPP)
			Slurry jetting		Direct inkjet printing (DIP) Wax-direct inkjet printing (W-DIP)
			Extrusion-based technology	Water based	Direct ink writing (DIW) Robocasting (RC) Freeze-form extrusion fabrication (FEF) 3D gel printing (3DGP) Ceramic on-demand extrusion (CODE)
				Wax based	Fused deposition modeling of ceramics (FDM/FDC) Extrusion free-form fabrication (EFF) Thermoplastic 3D printing (T3DP) Photopolymerization-assisted syringe-based extrusion (PHASE)
		Powder based			Three-dimensional printing (3DP) Direct energy deposition (DED) Selective laser melting (SLM) Selective laser sintering (SLS)
			Binder jetting		Powder binder jetting (P-BJ) Slurry binder jetting (S-BJ)
		Bulk solid based	Sheet lamination manufacturing		Laminated object manufacturing (LOM) Computer-aided manufacturing (CAM)
			Extrusion-based technology		Fused deposition modeling (FDM)

intensively developed and applied across a wide range of applications. Figure 1 illustrates the timeline of AM evolution from 2009 to 2025.

In Figure 2, various types of nozzles used in extrusion-based 3D printers are illustrated. In pneumatic extrusion, continuous air pressure is applied to the paste inside the extrusion chamber, causing a steady flow of material onto the build platform. In piston-driven extrusion, a piston applies uniform mechanical pressure to the paste inside the nozzle to control its flow [24]. In torsional (or screw-assisted) extrusion, the paste enters the nozzle and encounters spiral impellers, which generate a torsional flow that directs the material toward the nozzle outlet. This mechanism not only facilitates the deposition of the paste onto the platform but also overcomes material selection limitations and enables the homogeneous mixing of multiple components within the paste [25].

Prepared raw materials must be carefully formulated to achieve desirable properties, such as minimal shrinkage and the reduction or elimination of porosity and cracks during manufacturing, particularly during heat treatment and sintering. To this end, the solid content in the slurry should be high, and the solid particles must be uniformly distributed within the slurry matrix. Additionally, the slurry viscosity must be optimized, ensuring smooth extrusion through the nozzle and consistent part formation during printing [26]. Slurries with a paste-like consistency generally exhibit viscoelastic behavior. These viscoelastic materials require appropriate tensile strength in addition to exhibiting the rheological characteristics of yield-pseudoplastic fluids [24]. For EAM, the most suitable tensile strength is typically in the range of 100–1000 Pa [27–30]. For this purpose, pastes can be formulated with high concentrations of both ceramic particles and binders, such as methylcellulose [31], polyvinylpyrrolidone (PVP) [32], and polyethyleneimine (PEI) [33]. A schematic of the extrusion process of a ceramic part is demonstrated in Figure 3. There are two main types of ceramic material extrusion (MEX) processes: (i) wax-based extrusion processes and (ii) water-based extrusion processes, which are discussed in the following sections.

2.1 | Water-Based Ceramic EAM

The water-based ceramic EAM (WBCEAM) method allows for the layer-by-layer building of components using three-dimensional model data, distinct from traditional subtractive or formative manufacturing methods. The advantage of the WBCEAM method over other slurry techniques is the higher ceramic material loading in the suspension. In addition to forming an aqueous solution, this leads to reduced use of organic materials and polymers and a more straightforward debinding process. This results in a decrease in

15272648, 2026, 16, Downloaded from https://advanced.onlinelibrary.wiley.com/doi/10.1002/adem.71089 by Abdullah Saboori - Politecnico Di Torino Sist. Bibl Del Polit Di Torino , Wiley Online Library on [27/09/2026]. See the Terms and Conditions (https://onlinelibrary.wiley.com/terms-and-conditions) on Wiley Online Library for rules of use; OA articles are governed by the applicable Creative Commons License

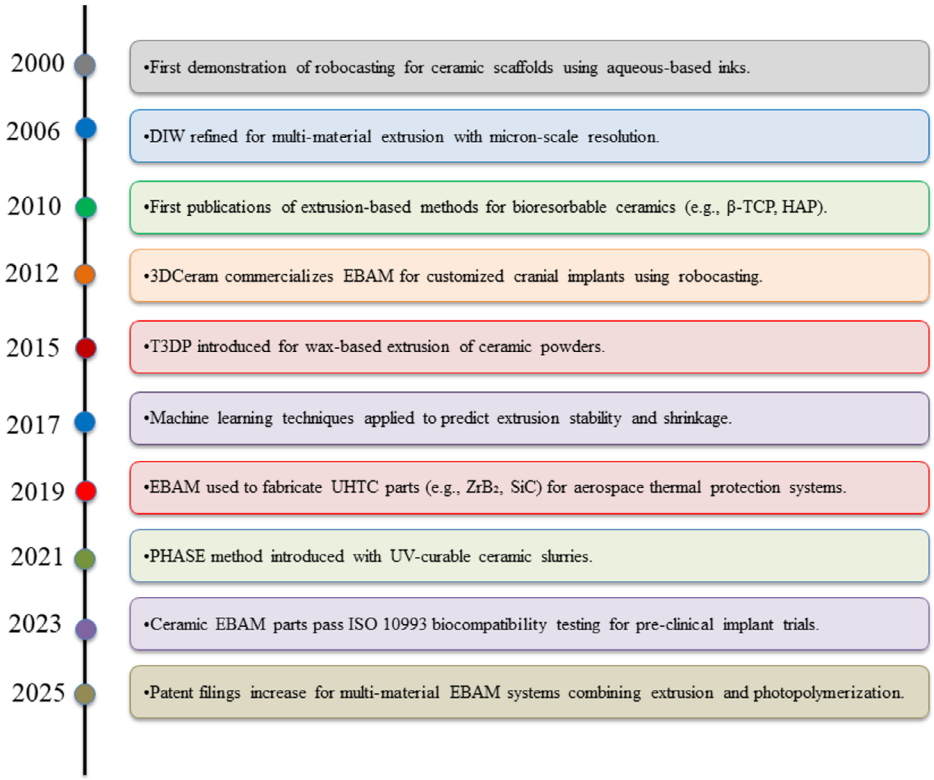


FIGURE 1 | Timeline of the development of additive manufacturing technologies for advanced ceramics from 2009 to 2025.

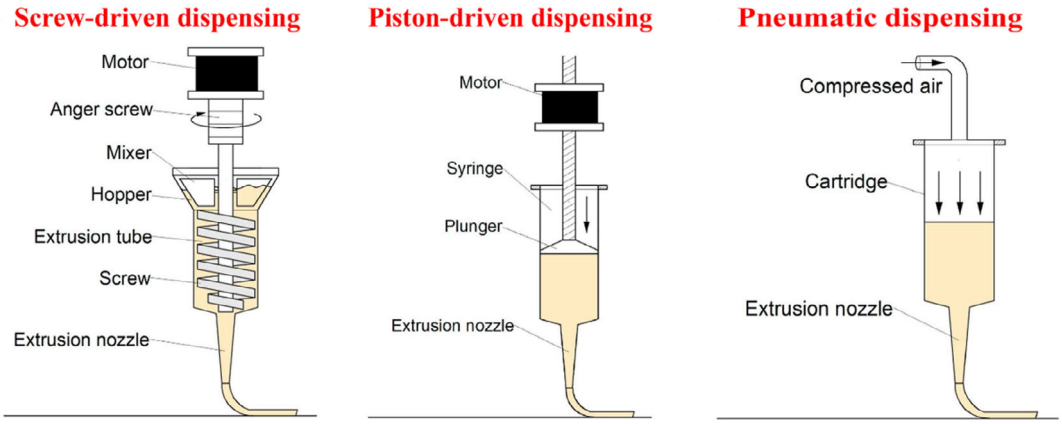


FIGURE 2 | Schematic illustration of the main nozzle configurations used in slurry-based extrusion 3D printing.

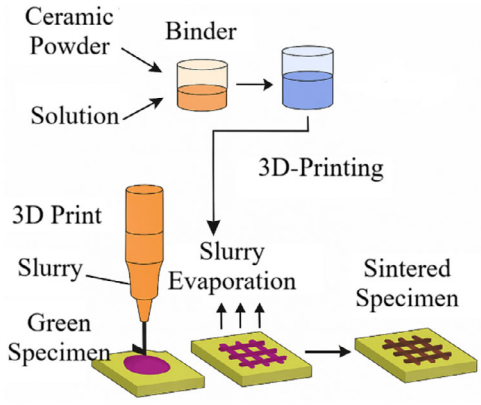


FIGURE 3 | Schematic of making a manufactured part using the extrusion method.

many issues related to the manufacture of parts, which is why most ceramic extrusion methods are based on aqueous-based pastes. Various ceramics such as zircon, alumina, bioglass, and zirconia can be used as feedstock materials in this process. The use of these materials enables the fabrication of ceramic components with tailored properties suitable for aerospace, automotive, biomedical, and energy applications. The following section discusses the techniques classified under this category.

2.1.1 | *Robocasting*

Robocasting (RC) is an EAM process that uses highly concentrated powder suspensions or inks to create intricate ceramic structures. RC is based on the extrusion of pastes with high solid material volume, which leads to an independent structure after heat treatment, debinding, and sintering [34–36]. A schematic of

15272648, 2026, 16, Downloaded from https://advanced.onlinelibrary.wiley.com/doi/10.1002/adem.71088 by Abdollah Saboori - Politecnico Di Torino Sist. Bibl Del Polit Di Torino , Wiley Online Library on [27/09/2026]. See the Terms and Conditions (https://onlinelibrary.wiley.com/terms-and-conditions) on Wiley Online Library for rules of use; OA articles are governed by the applicable Creative Commons License

the RC-AM process is shown in Figure 4. The filament diameter of the materials used in this process depends on the nozzle diameter (typically in the range of 200–800 μm). Another critical factor is the deposition behavior of the extruded filament onto the build platform. To ensure the fabrication of integrated and dimensionally stable samples, the spacing between adjacent filaments within each layer is set to zero, thereby preventing sample distortion [37]. However, the distance between the deposited filaments on the platform is a positive factor in manufacturing porous ceramics. In these types of ceramics, the pore size varies from 50 μm to 2 mm. Management of the deposits allows controlling pore geometry and size by altering and rotating the movement pattern of the nozzle between layers. This method allows for the precise layer-by-layer deposition of materials to build complex ceramic components with tailored properties. While RC-AM is not inherently water-based, it is a versatile technique that can be adapted to work with various suspensions or inks, including water-based ceramic pastes. By adjusting the composition of the ink used in RC-AM, it is possible to create ceramic structures with specific characteristics suitable for different applications in aerospace and automotive industries.

Cai et al. [38] used RC-AM to manufacture complex silicon carbide (SiC) samples, and after sintering using spark plasma sintering (SPS), a part with 97% density was produced. Feildern et al. [39] investigated the fabrication of ultra-high-temperature ceramics (UHTCs) made of HfB_2 using RC-AM, in which they were able to obtain a part with a complex shape and 94%–97% density with the bending strength of 196 ± 5 MPa at 1950 °C, where pressure less sintering was used to densify it. Wahl et al. [40] prepared a suspension containing SiC particles and carbon and then manufactured a SiC/C raw body using RC-AM. Subsequently, they used reaction sintering (RS) and liquid silicon infiltrate (LSI) to manufacture the final part. The density and bending strength (four-point) of this produced part were measured about 98% and 224 MPa, respectively.

2.1.2 | *Direct Ink Writing*

Direct ink writing (DIW) is a ceramic suspension technique applied by a nozzle onto a platform at room temperature. It directly dries and solidifies, and this drying is caused by the solvent escaping the printed paste-like structure [26]. However, despite the differences this technique has from RC-AM, some researchers consider them the same, and of course, their differences will be discussed in the following section. While RC-AM and DIW are often used interchangeably to describe similar AM processes involving ceramic materials, RC-AM emphasizes its origins and application within the ceramic AM domain. At the same time, DIW highlights the broader versatility of the technique across various material types and applications. DIW stands out from RC-AM due to its room temperature deposition. It also offers versatility in material selection, ability to produce multimaterial prints. Additionally, it provides control over architecture and composition during AM [26]. Figure 5 shows a schematic of the DIW process.

Additionally, to increase the stability of the suspension and provide rheological properties, small amounts of other additives such as viscosifier plasticizer thickener could be applied in the range of 0–5 wt% [41, 42]. However, some problems are observed during the manufacture of parts, among which residual porosities, strength data sparsity, and eventually unreliability of the manufactured parts and interfilament delamination could be mentioned [43]. For example, Xia et al. [44] utilized DIW to fabricate a part made of SiC and carbon short fibers (Csf). The final manufactured part demonstrated 30.9%–34.8% porosity, and ultimate strength was measured in the 84–123 MPa range.

Costakis et al. [30] fabricated an aqueous suspension containing ceramic boron carbide (B_4C) particles and PEI and 2.7 vol% tungsten carbide (WC) shown a tensile strength of 43 Pa. They showed that the probability of cracking increased with increasing solid particles. Kemp et al. [45] fabricated a ceramic composite part derived from polysilazane reinforced with hBN using DIW. The bending strength of the obtained parts was approximately 56.4 MPa, with microhardness of 111.4 HV indicative of lower porosity and more uniform pore distribution. In another investigation, Rueschboff et al. [30] prepared an aqueous suspension containing alumina particles using DIW. In this suspension, 5 v/v% PVP and 1-ethyl-2pyrrolidinone homopolymer were used as binder and strengthener of the raw part. In part containing 55 v/v% alumina, the final sintered part had a density of 98.2% and the bending strength was calculated in the range of 134–157 MPa. Miranda et al. [46] used the DIW technique to fabricate 3D scaffolds where β-triphosphate calcium (β-TCP)

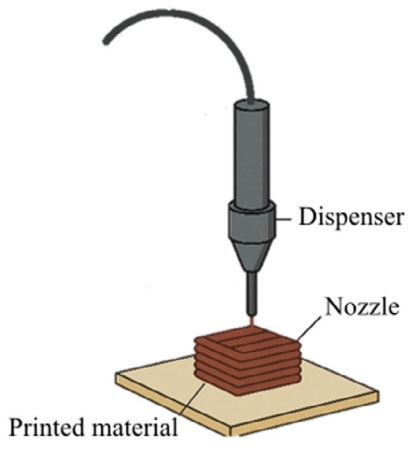


FIGURE 4 | Schematic of the RC-AM.

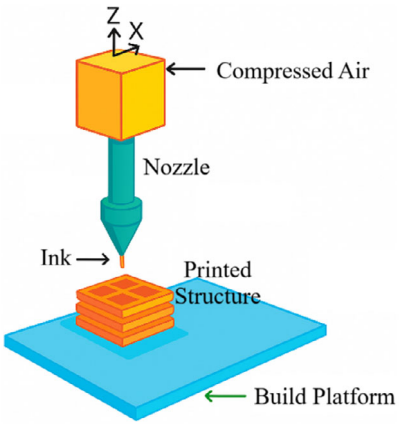


FIGURE 5 | Schematic diagram of DIW used for manufacturing ceramic parts.

15272648, 2026, 16, Downloaded from https://advanced.onlinelibrary.wiley.com/doi/10.1002/adem.71089 by Abdollah Saboori - Politecnico Di Torino Sist. Bibl Del Polit Di Torino , Wiley Online Library on [27/09/2026]. See the Terms and Conditions (https://onlinelibrary.wiley.com/terms-and-conditions) on Wiley Online Library for rules of use; OA articles are governed by the applicable Creative Commons License

samples were made, which eventually achieved a density of 92% after drying and sintering. Elsayed et al. [47] fabricated calcite-based composite scaffolds in which the silicon polymer paste was mixed with calcite ($CaCO_3$) powder, and they manufactured the intended samples using DIW. Then they were exposed to 600 °C for ceramication, and resulted part exhibited 56% porosity. Shao et al. [48] fabricated glass-based scaffolds in which a paste based on calcium silicate ($CaSiO_3$ containing 4.5 g ceramic powder with 4.0 g polyvinyl alcohol (PVA)) was formed and was applied on a platform using DIW and sintered. The characterization results show a part possessing 60% porosity with a compressive strength between 48 and 88 MPa. Franchin et al. [49] prepared a SiC ceramic suspension containing 30% chopped carbon fibers and then manufactured the parts using DIW. They finally observed that chopped carbon fibers decreased cracks inside the part.

2.1.3 | Freeze-Form Extrusion Fabrication

In the freeze-form extrusion fabrication (FEF) process, a water-based suspension containing ceramic particles or colloidal gel is extruded through a nozzle and subsequently frozen onto the substrate after deposition [50]. One of the main issues associated with parts fabricated using this technique is poor dimensional accuracy, which often results in noticeable surface bumps [27]. In general, ceramic materials, processed through FEF, DIW, or RC methods, are considered the most important approaches among aqueous-based extrusion techniques. The key aspect of these processes is controlling the viscosity of the extruded slurry. This control directly affects the rheological properties of the paste or slurry, which, in turn, determine the characteristics of the final product [51]. Compared with the DIW and RC methods, FEF stands out for its environmentally friendly nature, high solid-loading capability for diverse material production, and advanced control features. However, it faces several challenges, including complex binder removal procedures, demanding postprocessing requirements, material transition difficulties, and potential warping or cracking during part fabrication.

2.1.4 | 3D Gel Printing

3D gel printing (3DGP) is used to manufacture raw parts pertinent to the gelation process of 2-hydroxyethyl methacrylate (HEMA) [52]. This method is considered one of the newest methods of EAM, and not much information is available from active researchers in this field yet. This technique enables the fabrication of complex ceramic structures with high precision and customization, making it valuable for various biomedical and aerospace applications. 3DGP presents several advantages over traditional methods such as FEF, DIW, and RC. One of its primary advantages lies in its ability to fabricate intricate ceramic structures with high precision and complexity. This is made possible by the gel-like consistency of the material, which allows for intricate geometries and fine details. Additionally, 3DGP printing offers better control over material deposition, resulting in improved surface finish and dimensional accuracy. However, it also possess some limitations. One major drawback is the relatively slower printing speed compared to other methods due to the viscous nature of the gel materials. Moreover, postprocessing steps such as curing or sintering may be more complex and time-consuming, impacting the overall production time. Furthermore, the availability of suitable ceramic gel materials may be limited, restricting the range of applications for which 3DGP is feasible. In contrast, FEF, DIW, and RC methods often offer faster printing speeds and a wider selection of printable materials. Still, FEF, DIW, and RC methods may struggle with achieving the same level of intricacy and precision as 3DGP.

2.1.5 | Ceramic On-Demand Extrusion

The ceramic on-demand extrusion (CODE) method possesses a key advantage that enables the alteration of material composition within a single layer or between interlayers. It also allows the fabrication of parts with densities exceeding 98%. In this method, a suspension containing more than 50% ceramic particles is deposited layer by layer onto a substrate at room temperature, followed by infrared heating to partially dry each layer after deposition [53]. Subsequent layers are then deposited, and by controlling the moisture gradient around the part, cracking can be prevented. Through careful regulation of heat and moisture, the parts are gradually dried and sintered [54–56].

In the extrusion process, materials can be extruded continuously, cooled by gelation or UV curing after being applied drop by drop onto the substrate, or self-solidified under rheological influences [41]. Yield–pseudoplastic rheology provides the ink with structural integrity up to its yield stress, followed by shear-thinning behavior [57, 58]. This behavior is critical for the ink, as it must be capable of flowing through the nozzle under high shear conditions while maintaining its shape once deposited on the substrate. McMillen et al. [59] utilized the CODE method to fabricate UHTCs from ZrB_2, achieving a density of 99%. A PVA binder, along with various nitride and carbide additives, was used in the process. As a pioneering approach, this technique shows strong potential for manufacturing components with complex geometries.

2.2 | Wax or Thermoplastic-Based Extrusion Process

Wax-based methods often excel in achieving high-resolution prints, enabling the fabrication of intricate ceramic structures with fine details. They are typically cost-effective due to the affordability of wax materials. However, these methods may suffer from lower mechanical strength and limited temperature resistance compared to water-based counterparts. Conversely, water-based processes offer environmental friendliness and biocompatibility, making them suitable for specific biomedical applications [60–62]. While they may exhibit higher strength and durability in printed objects, they often face challenges in achieving high-resolution prints and typically require drying or curing processes postprinting. Ultimately, the choice between wax- and water-based extrusion-based ceramic AM (EAM) depends on specific requirements such as resolution, material properties, and intended applications, highlighting the importance of evaluating these factors when selecting the most appropriate fabrication method [63, 64]. In both approaches, the prepared paste, ceramic slurry, or filament is loaded into a container that replaces the nozzle assembly of the 3D printer. The material is then extruded through the nozzle and deposited layer by layer onto the build platform, forming a three-dimensional structure [65, 66].

15272648, 2026, 16, Downloaded from https://advanced.onlinelibrary.wiley.com/doi/10.1002/adem.71088 by Abdollah Saboori - Politecnico Di Torino Sist. Bibl Del Polit Di Torino , Wiley Online Library on [27/09/2026]. See the Terms and Conditions (https://onlinelibrary.wiley.com/terms-and-conditions) on Wiley Online Library for rules of use; OA articles are governed by the applicable Creative Commons License

2.2.1 | *Fused Deposition Modeling of Ceramics*

After printing, the green parts undergo a thermal debinding process in a furnace to remove the polymeric binder, followed by sintering to densify the ceramic structure. The filament typically consists of an elastomer-based polymer (as a tackifier), a plasticizer, and wax to reduce viscosity, ensuring adequate strength, elasticity, plasticity, and flexibility during extrusion. To date, numerous oxide and nonoxide ceramics have been successfully fabricated using this method. Table 2 lists common additives used in ceramic-loaded filaments for the fused deposition modeling of ceramics (FDM/FDC) process along with their respective characteristics [66]. The FDM process, often referred to as FDC (fused deposition of ceramics) when applied to ceramic-based filaments [67, 68] is a technique derived from fused filament fabrication (FFF) [69–72]. In this method, a filament comprising a high ceramic particle loading dispersed in a thermoplastic polymer binder system typically containing materials such as wax is extruded. The mixture is processed using conventional FDM printers through hot-melt extrusion, where the filament is fed into the nozzle by rotating pinch rollers. The filament softens and melts under the applied heat and is subsequently deposited layer by layer onto the build platform [73, 74]. This process is considered analogous to injection molding due to its reliance on thermoplastic binder systems. Compared with other AM technologies, FDM/FDC is cost-effective, utilizes relatively simple and inexpensive equipment, and relies on widely available raw materials [60]. After printing, the green parts undergo a thermal debinding process in a furnace to remove the polymeric binder, followed by sintering to densify the ceramic structure. The filament typically consists of an elastomer-based polymer (as a tackifier), a plasticizer, and wax to reduce viscosity, ensuring adequate strength, elasticity, plasticity, and flexibility during extrusion.

To date, numerous oxide and nonoxide ceramics have been successfully fabricated using this method. Table 2 lists common additives used in ceramic-loaded filaments for the FDM/FDC process along with their respective characteristics [68].

Limitations of this method include its mechanical and rheological properties of the filaments, which may be unsuitable for manufacturing various parts [75]. Therefore, proper evaluation and determination of rheological parameters are essential to ensure suitable flow and stable extrusion of the melted filament through the nozzle [76]. For example, insufficient filament hardness may result in filament breakage during feeding, preventing continuous flow and disrupting the manufacturing process [77, 78]. One effective solution for fabricating dense parts via FDM is the use of screw-based extrusion systems. This approach enables better control over the printing process, enhances the reliability of ceramic feedstocks, and provides improved management of filament rheology. However, since each ceramic-loaded filament exhibits distinct rheological characteristics, the screw design must be adapted accordingly for each formulation. Another challenge in this technique is the elimination of the stepping effect on printed surfaces. To address this issue, some studies have implemented gear- or piston-driven mechanisms to improve layer uniformity and facilitate the fabrication of precision components [79].

Scheithauer et al. [80] successfully fabricated dense alumina ceramics with a relative density of 99% using a screw-extrusion-based system. In another study, Lyer et al. [81] investigated the fabrication of dense Si_3N_4 components using the FDM technique. The filaments used contained 55 vol% silicon nitride with a grain size of approximately 0.5 μm, achieving bending strengths of approximately 908 MPa in the X–Y direction and 888 MPa in the Z direction. Additional extrusion-based approaches that utilize thermoplastic polymers or wax binders include the extrusion freeform fabrication (EFF) method [63, 64] and the multiphase jet solidification (MJS) process [65], both of which share similar manufacturing principles. In these methods, a multiphase feedstock comprising ceramic powders dispersed within a polymer-based binder system is extruded as a paste through a nozzle onto the build platform [82–84]. These techniques are capable of fabricating parts from a wide range of ceramic materials. For optimal process performance, the suspension used in these systems should exhibit a viscosity in the range of 10–200 poise, the binder melting point should be approximately 200 °C, and the ceramic solid loading should be relatively high, typically around 60 vol% [84].

2.2.2 | *EFF*

In EFF method, the raw materials are first dispersed in a solvent at high solid loading to form a ceramic paste with high volume fraction. The paste is then extruded through a nozzle using mechanical force, typically driven by oxygen or air pressure, to build the three-dimensional green part layer by layer. After printing, the fabricated part undergoes debinding and sintering. The main difference between RC and EFF is that, in RC, an aqueous-based paste is used, and unlike in FDC, partial melting of the polymer does not occur [85]. Therefore, EFF can be considered a specialized form of RC, involving the deposition and cooling of a colloidal gel containing thermoplastic materials onto the substrate [46].

Several studies have demonstrated the potential of extrusion-based methods for ceramic fabrication. For instance, Gomez et al. [86] fabricated silicon carbide part using EFF 3D printing, and after SPS sintering, the final parts exhibited 65%–85% porosity. Zhang et al. [87] produced SiC-based composites reinforced with carbon black and chopped carbon fibers achieving a three-point bending strength of approximately 300 MPa. McClain et al. [88] prepared a suspension using ceramic precursors with 45 wt% chopped carbon fibers and 10 wt% carbon black; after EFF printing and pyrolysis, they obtained the final ceramic structure. Huang et al. [89] fabricated alumina components that achieved

TABLE 2 | Characteristic parameters of various binder.

Binder constituents	Characteristics
Base polymer	The backbone of the filament provides strength
Elastomer	Providing elasticity and flexibility
Plasticizer	Providing plasticity to filament for spooling
Tackifier	Enable tackiness and provide flexibility
Wax	Reduces viscosity

15272648, 2026, 16, Downloaded from https://advanced.onlinelibrary.wiley.com/doi/10.1002/adem.71088 by Abdollah Saboori - Politecnico Di Torino Sist. Bibl Del Polit Di Torino , Wiley Online Library on [27/09/2026]. See the Terms and Conditions (https://onlinelibrary.wiley.com/terms-and-conditions) on Wiley Online Library for rules of use; OA articles are governed by the applicable Creative Commons License

a final density of 98% after sintering, with strengths ranging from 50 to 327 MPa. In summary, although different EAM methods share certain similarities, they also exhibit notable distinctions. One key difference lies in the viscosity of the suspensions used: EFF and RC typically utilize high-viscosity, paste-like feedstocks, whereas DIW employs lower-viscosity, ink-like suspensions [90].

2.2.3 | *Thermoplastic 3D Printing*

Thermoplastic 3D printing (T3DP) was developed by Scheithauer et al. by combining principles from RC and FDM methods, enabling the fabrication of various metallic and ceramic composites [80]. In this method, ceramic powders are dispersed in a paraffin-based thermoplastic polymer and and subsequently milled at approximately 100 °C. The resulting feedstock is then supplied to a heated extrusion system compatible with 3D printing. This technique also supports the production of metallic components and offers flexibility by accommodating both continuous and droplet-based deposition strategies for part fabrication [91].

2.2.4 | *Photopolymerization-Assisted Syringe-Based Extrusion*

The photopolymerization-assisted syringe-based extrusion (PHASE) process was developed by Faes et al. [92] at KU Leuven, Belgium, which involved the combination of ceramic extrusion and photopolymerization to integrate the distinct benefits of each technology. The formulation consisted of a UV-curable ZrO_2 suspension containing 30 vol% 3Y-TZP powder dispersed within a commercial photopolymeric resin. This mixture was successfully extruded using a 3D printer equipped with a syringe. During printing, the as-deposited layers underwent only partial polymerization due to insufficient UV irradiance, which led to deformation of the lower layers. Consequently, an additional thermal curing step was required to achieve complete polymerization. The sintered samples exhibited a density of 92%. However, the relatively low solids loading (30 vol%) resulted in extensive shrinkage during firing, causing significant cracking. Although the extrusion-based techniques discussed above share the common characteristic of depositing material through a nozzle, their operating principles differ significantly in terms of feedstock state, extrusion mechanism, shape-retention strategy, and postdeposition solidification route. These differences are important because methods that appear similar, such as RC and DIW, or FDM/FDC and T3DP, often require substantially different feedstock formulations, rheological properties, thermal histories, and postprocessing procedures. To highlight these distinctions and facilitate a direct comparison of the major ceramic EAM techniques, Table 3 summarizes their feedstock types, deposition principles, solidification mechanisms, related processes, distinguishing features, and key limitations. As shown in Table 3, RC and DIW are closely related extrusion-based methods; however, RC typically employs higher viscosity ceramic pastes with greater solid loading, whereas DIW offers broader material flexibility through ink- or paste-based formulations deposited at room temperature. FEF and CODE incorporate additional shape-retention mechanisms through freezing and infrared-assisted drying, respectively. In contrast, FDM/FDC, EFF, and T3DP are characterized by the use of thermoplastic- or wax-based feedstocks. PHASE differs further from conventional extrusion techniques by integrating syringe-based extrusion with photopolymerization-assisted solidification. Consequently, selecting an appropriate EAM method should depend not only on the target ceramic material but also on the required feedstock form, solidification mechanism, printing resolution, dimensional stability, and postprocessing requirements.

2.3 | Evaluation of Performance and Properties AM Techniques

As various EAMs are reviewed, different properties of ceramic parts using different extrusion 3D printing methods are listed in Table 4.

The key EAM methods for ceramics have been explored, covering both traditional and emerging approaches including water-based pastes, thermoplastic filaments, and hybrid techniques. Each method has its own set of strengths and limitations, whether related to feedstock type, part density, mechanical properties, or process complexity. Table 5 provides a clear comparison of these methods. By presenting their trade-offs and performance characteristics side by side, Table 5 helps readers to better understand the relative advantages of each technique. This comparison can assist researchers and engineers in making informed decisions when improving or applying these methods in practical applications.

To complement the qualitative comparison of ceramic EAM methods, a quantitative performance benchmark is necessary because the suitability of each technology strongly depends on measurable outcomes such as final density, residual porosity, mechanical strength, shrinkage, and postprocessing requirements. Table 6 compares representative EAM technologies in terms of ceramic system, relative density, porosity, flexural strength, and selected process conditions. These quantitative indicators provide a practical basis for evaluating the applicability of each method to oxide ceramics, nonoxide ceramics, bioceramics, and UHTCs. Beyond the comparison among individual EAM methods, it is also important to position extrusion-based technologies relative to other ceramic AM routes. Table 7 compares EAM with vat photopolymerization-based methods, selective laser sintering, binder jetting, and laminated object manufacturing in terms of working principle, typical density range, surface quality, geometrical complexity, build speed, material versatility, equipment cost, advantages, and limitations. This comparison clarifies the technical advantages and practical boundaries of EAM within the broader field of ceramic AM. The comparison in Table 7 shows that EAM is particularly advantageous for processing highly loaded ceramic pastes, thermoplastic feedstocks, multimaterial systems, porous scaffolds, and large or customized components at relatively low equipment cost. Compared with SLA/DLP, EAM offers broader feedstock flexibility and easier processing of high-solid-loading suspensions, although it usually provides lower surface quality and dimensional resolution. Compared with binder jetting and SLS, EAM avoids several powder-bed-related limitations and enables continuous filament or paste deposition, but it remains sensitive to nozzle clogging, filament deformation, interlayer delamination, and anisotropic shrinkage. Therefore, EAM is most suitable for low-cost, material-flexible, and structurally complex ceramic components, whereas SLA/DLP remains more appropriate for high-resolution parts and binder jetting is more favorable for rapid production of large powder-based components.

15272648, 2026, 16, Downloaded from https://advanced.onlinelibrary.wiley.com/doi/10.1002/adem.71088 by Abdollah Saboori - Politecnico Di Torino Sist. Bibl Del Polit Di Torino , Wiley Online Library on [27/09/2026]. See the Terms and Conditions (https://onlinelibrary.wiley.com/terms-and-conditions) on Wiley Online Library for rules of use; OA articles are governed by the applicable Creative Commons License

TABLE 3 | Comparative analysis of working principles and distinguishing characteristics of ceramic EAM methods.

Method	Feedstock type	Deposition principle	Solidification mechanism	Similar methods	Main distinction	Main limitation	Ref.
RC	High-viscosity aqueous paste	Pneumatic/piston extrusion of concentrated ceramic suspension	Solvent evaporation and subsequent sintering	DIW	Higher solid loading (40–55 vol%) and larger nozzle diameter	Limited resolution; drying-induced cracking	[35]
DIW	Low-to-medium viscosity ink/paste	Room-temperature extrusion with shear-thinning flow	Solvent evaporation and drying	RC	Lower viscosity inks and greater material versatility	Interfilament delamination; shrinkage	[49]
FEF	Water-based slurry/paste	Extrusion onto cooled substrate	Immediate freezing after deposition	RC, DIW	Freeze-assisted shape retention	Poor dimensional accuracy; surface roughness	[50]
3DGP	Gel-forming ceramic suspension	Extrusion combined with gelation	Gelation of HEMA-based system	DIW	High precision and complex geometry capability	Slow printing speed; limited material systems	[52]
CODE	High-solid aqueous paste	Layer-by-layer extrusion with interlayer drying	Infrared-assisted partial drying	RC, DIW	Moisture-gradient control and composition variation	Process complexity; sensitive drying control	[55, 59]
FDM/FDC	Ceramic-loaded thermoplastic filament	Hot-melt filament extrusion	Thermal solidification after deposition	T3DP	Uses solid filament feedstock similar to FFF	Filament brittleness; staircase effect	[68, 69]
EFF	Thermoplastic ceramic paste	Extrusion of paste using pneumatic/piston force	Cooling and partial polymer solidification	RC, FDM	Combines paste extrusion with thermoplastic binders	Rheology-sensitive processing	[65, 66]
T3DP	Paraffin-based thermoplastic paste	Heated extrusion or droplet deposition	Thermal cooling/solidification	FDM/FDC, EFF	Supports multimaterial ceramic/metal fabrication	High equipment complexity and cost	[80, 91]
PHASE	UV-curable ceramic slurry	Extrusion with simultaneous UV curing	In situ photopolymerization	DIW, T3DP	Hybrid extrusion-photopolymerization approach	Low solid loading and large shrinkage	[92]

15272648, 2026, 16, Downloaded from https://advanced.onlinelibrary.wiley.com/doi/10.1002/adem.71088 by Abdollah Saboori - Politecnico Di Torino Sist. Bibl Del Polit Di Torino , Wiley Online Library on [27/09/2026]. See the Terms and Conditions (https://onlinelibrary.wiley.com/terms-and-conditions) on Wiley Online Library for rules of use; OA articles are governed by the applicable Creative Commons License

TABLE 4 | Different properties of ceramic parts using different extrusion 3D printing methods.

Category	Method	Resolution	Size of parts made	Geometrical complexity	Surface roughness	Cost	Suitability grade	State of suspension	Ref.
Water-based EBCAM	RC	High	Large	Medium	Medium	Low	High	Paste	[38, 40]
	DIW	High	Large	Medium	Medium	Low	High	Ink	[44–46]
	FDM	Moderate	Small	Medium	Medium	Medium	Very High	Filament	[68, 80]
	FEF	Moderate	Large	Medium	Medium	Low	High	Paste	[50, 51]
	3DGP	High	Large	Medium	Medium	Low	Medium	Ink	[52]
	CODE	High	Large	High	Medium	Medium	Medium	Paste	[54–58, 93]
Wax-based EBCAM	FDC	Medium	Large	Medium	Low	Low	High	Filament	[80, 81]
	EFF	High	Large	High	Low	Low	High	Filament	[85–88]
	T3DP	Moderate	Large	High	Medium	Low	Medium	Paste	[80, 91]
	PHASE	Moderate	Small	High	Medium	Medium	Medium	Paste	[92]

TABLE 5 | Comparative performance of EAM techniques for advanced ceramics.

Method	Feedstock type	Reported density, %	Porosity, %	Resolution	Complexity of shapes	Key strengths	Key weaknesses
RC	Paste (high-viscosity aqueous)	94%–98%	~2%–6%	High	Moderate	High strength, low porosity, good for dense parts	Requires postprocessing, brittle green bodies
DIW	Ink/Paste (room-temp)	84%–98%	5%–35%	High	Medium	Versatile materials, low temp, fine control	High porosity, delamination, drying shrinkage
FDM	Thermoplastic Filament	~99% (HIP)	<1% (w/ HIP)	Moderate	Moderate	Low-cost, scalable, high strength	Requires debinding/ sintering, brittle filament
FEF	Paste (freeze-on-substrate)	Not specified	High	Moderate	Low–moderate	Eco-friendly, good solids loading	Poor dimensional accuracy, hard to control shrinkage
3DGP	Gel (HEMA-based)	Up to ~90%	Moderate	High	High	Precise features, biomedical potential	Slow printing, limited materials available
CODE	Paste (IR drying, >50% solid)	Up to 99%	<2%	High	High	High density, controlled drying	Moisture control critical, still maturing
EFF	Paste (thermoplastic)	85%–98%	Moderate	Moderate	High	Good for complex parts	Less standardized, viscosity-sensitive
T3DP	Wax/paraffin + powder	90%–99%	1%–10%	High	Medium	Fine resolution, comaterial printing	Expensive equipment, limited commercial use
HASE	UV-curable slurry	~92%	Significant shrinkage	High	High	Combines photopolymerization + extrusion	Low solids loading, shrinkage cracking

3 | Feedstock Development

Research on suitable feedstocks for EAM of ceramics remains both vital and dynamic. To improve the quality, reliability, and geometric complexity of fabricated ceramic components, efforts in this field mostly aim at optimizing material properties and processing parameters. The precise formulation of feedstocks is fundamental to this goal, as it directly influences critical factors

15272648, 2026, 16, Downloaded from https://advanced.onlinelibrary.wiley.com/doi/10.1002/adem.71089 by Abdollah Saboori - Politecnico Di Torino Sist. Bibl Del Polit Di Torino , Wiley Online Library on [27/09/2026]. See the Terms and Conditions (https://onlinelibrary.wiley.com/terms-and-conditions) on Wiley Online Library for rules of use; OA articles are governed by the applicable Creative Commons License

TABLE 6 | Core quantitative performance comparison of ceramic EAM technologies.

EAM method	Ceramic system	Density, %	Porosity, %	Flexural strength, MPa	Representative optimal process conditions	Ref.
RC	SiC (nonoxide)	94–98	2–3	224 (four-point)	Nozzle diameter: 200–800 μm; SPS postprocessing	[38, 40]
RC	HfB_2 (UHTC)	94–97	3–6	196 ± 5	Pressureless sintering at 1950 °C	[39]
DIW	Al_2O_3 (oxide)	98.2	1.8	134–157	55 vol% solid loading; PVP binder	[28]
DIW	β-TCP (bioceramic)	92	8	N/R	Drying and sintering of β-TCP scaffold	[46]
DIW	Csf/SiC composite	65–69	31–35	84–123	SiC with carbon short fibers; DIW followed by postprocessing	[44]
FDM/FDC	Al_2O_3 (oxide)	99	<1	N/R	Screw-extrusion system; 55 vol% solid loading	[80]
FDM/FDC	Si_3N_4 (nonoxide)	~99	<1	908 (X–Y)/888 (Z)	55 vol% solid loading; 0.5 μm grain size	[81]
CODE	ZrB_2 (UHTC)	99	<2	N/R	>50 vol% solid loading; PVA binder	[59]
FEF	Al_2O_3 (oxide)	98	2	50–327	Aqueous-based freeze-form extrusion fabrication followed by sintering	[89]
EFF	SiC (nonoxide)	15–35	65–85	N/R	Filament/paste-printed SiC architecture with limited densification	[86]
PHASE	ZrO_2 (oxide)	92	8	N/R	30 vol% solid loading; UV-curable suspension	[92]

Note: N/R indicates that the value was not reported in the cited source.

such as flow behavior during extrusion, shape retention after deposition, and the sinterability of the printed parts. Researchers have explored a variety of feedstock systems, including liquid-based, solid powder-based, and thermoplastic formulations, each offering unique advantages and presenting specific processing challenges. These feedstocks will be discussed in detail in the following sections, along with their material characteristics, processing behavior, and suitability for different EAM applications [94].

3.1 | Type of Feedstock

3.1.1 | *Liquid Feedstocks*

For EAM, liquid feedstocks including sol–gel solutions and preceramic polymers offer several benefits, most importantly lower viscosity and reduced risk of clogging during extrusion. Despite these advantages, their use is sometimes constrained by challenges including instability and drying-induced defects in printed structures. Nevertheless, liquid systems have proven particularly useful in processes like vat photopolymerization, where their natural transparency and resistance to sedimentation are significant advantages. Highlighting the unique properties of preceramic polymers and other liquid-based feedstocks in addressing issues such as high-temperature sintering and the inherent brittleness of ceramics, Travitzky et al. [95] provided a comprehensive review of the potential of various AM techniques, including stereolithography, inkjet printing, and RC, based on these principles. Building on this work, Schwentenwein and Homa [96] introduced the lithography-based ceramic manufacturing (LCM) technique, which successfully produced complex alumina components with densities exceeding 99.3% of the theoretical value. This study demonstrated the feasibility of photosensitive slurry-based systems for manufacturing high-performance ceramic parts with complex geometries.

Mühler et al. [97] investigated the layer-wise slurry deposition (LSD) technique, highlighting its ability to achieve better microstructural uniformity and higher green body packing densities compared to conventional powder-based methods. More recently, Wang et al. [102] introduced a stereolithographic approach for processing preceramic polymers based on thiol-ene click chemistry. This method enabled the fabrication of high-density, fracture-free ceramic components and allowed exact control over shrinkage behavior. In this context, Franchin et al. [103] demonstrated that particle-based systems are particularly well suited for high-resolution techniques such as two-photon polymerization (TPP) and digital light processing (DLP), as they significantly mitigate viscosity issues and sedimentation commonly encountered in these methods. Furthermore, the use of blends such as photocurable polymers combined with preceramic resins provides design flexibility and decouples ceramic yield from printability. By controlling filler particle size in combination with DIW, the authors successfully produced components with engineered macro- and microporosity, improving surface area and permeability for applications including catalysis and filtration. For example, SiOC scaffolds fabricated via DIW exhibited compressive strengths of up to 130 MPa and porosities exceeding 50%, matching or even surpassing those of conventional ceramic foams. Figure 6 illustrates the morphological characteristics of these scaffolds.

3.1.2 | *Solid Powder Feedstocks*

EAM using solid powder feedstocks mixed with binders is considered more cost-effective and design-flexible compared to

15272648, 2026, 16, Downloaded from https://advanced.onlinelibrary.wiley.com/doi/10.1002/adem.71088 by Abdollah Saboori - Politecnico Di Torino Sist. Bibl Del Polit Di Torino , Wiley Online Library on [27/09/2026]. See the Terms and Conditions (https://onlinelibrary.wiley.com/terms-and-conditions) on Wiley Online Library for rules of use; OA articles are governed by the applicable Creative Commons License

TABLE 7 | Comparison of EAM with other ceramic additive manufacturing technologies.

Technology	Working principle	Typical density, %	Surface quality	Geometrical complexity	Build speed	Material versatility	Equipment cost	Main advantages	Main limitations	Ref.
EAM	Extrusion-based deposition	85–99	Medium–high	Medium–high	Slow–medium	High	Low–Medium	Low cost; wide material compatibility; scalable feedstocks	Nozzle clogging; support requirement; anisotropic shrinkage	[7, 10, 94]
SLA/DLP	Photopolymerization of ceramic slurry	95–99	Very high	Very high	Medium	Medium	Medium–High	High resolution; smooth surface finish; excellent dimensional accuracy	Requires photosensitive resin; high shrinkage during debinding	[95–97]
SLS	Laser sintering of ceramic powder	70–90	Low–medium	High	Medium	High	High	Support-free fabrication; complex geometries	Residual porosity; thermal cracking; expensive equipment	[10–13, 98]
Binder Jetting	Selective binder deposition onto powder bed	60–85	Low	High	Fast	High	Medium	High productivity; suitable for large parts	Low green strength; infiltration and postprocessing required	[99, 100]
LOM	Layered sheet lamination	85–95	Medium	Low	Slow	Limited	Low	Simple process; low equipment cost	Limited geometric complexity; high material waste	[95, 101]

15272648, 2026, 16, Downloaded from https://advanced.onlinelibrary.wiley.com/doi/10.1002/adem.71088 by Abdollah Saboori - Politecnico Di Torino Sist. Bibl Del Polit Di Torino , Wiley Online Library on [27/09/2026]. See the Terms and Conditions (https://onlinelibrary.wiley.com/terms-and-conditions) on Wiley Online Library for rules of use; OA articles are governed by the applicable Creative Commons License

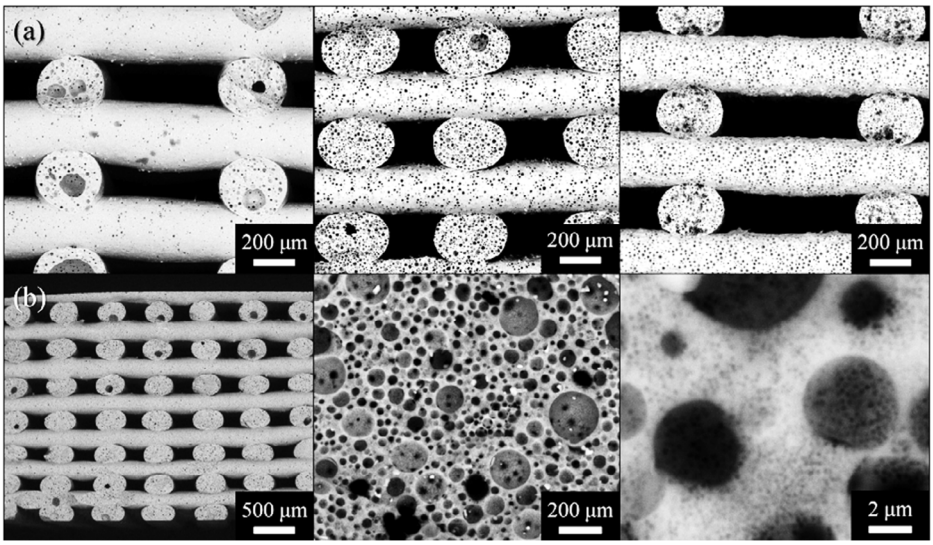


FIGURE 6 | SEM images of: (a) SiOC pyrolyzed porous scaffolds printed via DIW, derived from the removal of varying amounts of PMMA particles (50, 60, and 80 vol%); and (b) a SiOC scaffold exhibiting a hierarchical pore structure, obtained by combining PMMA particles of different nominal sizes (25 and 0.46 µm). Reproduced with permission [103]. Copyright 2022, Elsevier.

high-energy beam techniques. Although historically less common, this technique is gaining increasing prominence in the literature due to its ability to produce complex-shaped ceramic components. In this context, Rane et al. [104] demonstrated that higher solid loading increases feedstock viscosity, which enhances dimensional stability, particularly in vertical extrusion where gravity affects filament elongation. Under these circumstances, the feedstock shows pronounced shear-thinning (pseudoplastic) behavior, which is perfect for extrusion since viscosity decreases with increasing shear rate. Scanning electron microscopy (SEM) imaging data confirmed that feedstocks with higher powder content show more homogeneous particle dispersion and smoother surfaces morphology as represented in Figure 7.

The extensive body of previous research provides a solid foundation for the investigation of AM techniques and powder–binder extrusion. German and Bose [105] established a basic understanding of powder injection molding (PIM), outlining the key stages of feedstock preparation, injection, debinding, and sintering, thereby creating a processing framework that was later adapted for extrusion-based technologies. Trunec [106] examined the shape and dimensional stability of ceramic tubes under various thermoplastic extrusion conditions, revealing critical correlations between material flow behavior and final part geometry. Similarly, Grida and Evans [83] developed extrusion free-forming of ceramics using fine nozzles, addressing challenges related to flow stability, nozzle-induced deformation, and die swell phenomena.

Highlighting the influence of process parameters in metal powder extrusion for rapid prototyping, Bin Li et al. [107] identified key factors affecting layer deposition and dimensional accuracy. Through a theoretical analysis of extrusion instabilities, especially die swell in viscoelastic materials, Pettas et al. [108] provided insightful analysis of the processes generating dimensional variations in extruded filaments. Ren et al. [109] proposed process control strategies for extrusion-based metal AM, including real-time compensation techniques to mitigate flow inconsistencies, while Rane and Date [110] investigated the rheology of MIM feedstocks, demonstrating how variations in powder loading and binder composition affect flow behavior and stability. By conducting a

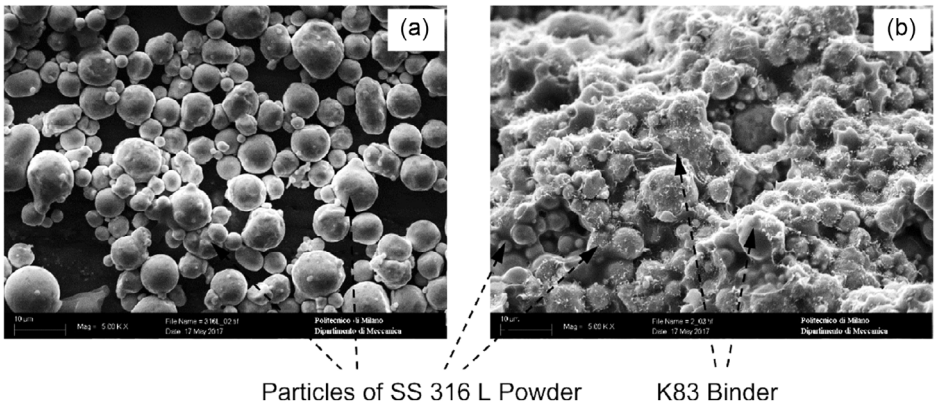


FIGURE 7 | SEM images of (a) SS316L powder and (b) the fractured surface of a feedstock pellet with a solid loading of SS316L powder. Reproduced with permission [104]. Copyright 2019, Elsevier.

15272648, 2026, 16, Downloaded from https://advanced.onlinelibrary.wiley.com/doi/10.1002/adem.71088 by Abdollah Saboori - Politecnico Di Torino Sist. Bibl Del Polit Di Torino , Wiley Online Library on [27/09/2026]. See the Terms and Conditions (https://onlinelibrary.wiley.com/terms-and-conditions) on Wiley Online Library for rules of use; OA articles are governed by the applicable Creative Commons License

comprehensive rheological analysis of SS316L–TiC feedstocks, Khakbiz et al. [111] further confirmed the significance of non-Newtonian, pseudoplastic behavior in predicting extrusion performance in powder-binder systems. Collectively, these studies form the theoretical and technical underpinning for contemporary research in EAM of metal and ceramic feedstocks.

3.1.3 | *Filament-Based Techniques*

With research efforts mostly focused on developing fully dense ceramic components through optimal material-binder systems, filament-based extrusion techniques have seen significant advancements in recent years. The intentional design of filaments, combined with continuous improvements in processing technologies, has greatly enhanced the performance and structural integrity of the final products [94]. Recent developments in MEX for ceramics have greatly strengthened the feasibility of producing reliable, mechanically robust components with complex geometries. Nötzel et al. [112] made a notable contribution by establishing a process chain similar to ceramic injection molding, using PEG/PVB-based binder systems. Their method resulted in sintered alumina parts achieving densities close to 98% of their theoretical maximum. In parallel, Orlovská et al. [113, 114] investigated the influence of critical printing parameters particularly layer height on the mechanical performance and microstructure of printed parts. Their findings demonstrated that reducing layer thickness enhanced flexural strength while decreasing the frequency of internal defects.

Gorjan et al. [115] developed a rheological model that clarified the effects of stearic acid (SA) saturation on the printability and flow characteristics of EVA-based filaments, thereby advancing feedstock formulation. These findings significantly contributed to optimizing binder content and improving processing behavior. Through thermogravimetric analysis, fourier transform infrared spectroscopy, and SEM analyses, Truxová et al. [116] further refined debinding and sintering techniques, ultimately achieving near full-density parts with densities reaching up to 99.5%. Despite these advancements, issues such as brittleness and shrinkage control remained unresolved. In pursuit of more environmentally friendly processing routes, Smirnov et al. [117] developed a solvent-free approach using polylactic acid (PLA) composites, identifying a workable formulation at 50 vol% alumina. Although promising, this method still faced challenges related to viscosity control and print quality. Emphasizing the importance of dimensional accuracy and thermal cycle optimization to minimize shrinkage-induced defects, Tosto et al. [118] evaluated a tool-free MEX strategy for small-scale production in application oriented contexts. Similarly, Hadian et al. [119] proposed fundamental geometric constraints for features such as overhangs, arches, and thin-walled structures, along with preliminary design guidelines for ceramic MEX, highlighting significant anisotropic shrinkage, particularly along the build direction. Collectively, these studies provide a comprehensive and evolving framework for the development of ceramic MEX technologies. While they address the persistent challenges associated with fabricating dense, high-performance ceramics via AM, they also underscore opportunities to enhance feedstock formulations, optimize process parameters, and incorporate more effective postprocessing strategies.

3.1.4 | *Thermoplastic Feedstocks*

Thermoplastic feedstocks have attracted significant attention in ceramic AM, particularly in processes such as FFF and T3DP, due to their ability to produce high-precision, complex ceramic geometries. While FFF is valued for its cost-effectiveness and accessibility, it is limited by relatively lower resolution and surface quality. In contrast, T3DP offers superior dimensional accuracy and surface finish, making it suitable for applications requiring fine detail and enhanced visual appeal [120]. Nötzel et al. [121] made significant contributions by adapting FFF methods for ceramic processing, thereby advancing thermoplastic-based ceramic AM. Their efforts concentrated on developing feedstocks composed of paraffin wax, low-density polyethylene, and SA, effectively addressing challenges associated with high ceramic loading and defect formation during the debinding stage. In particular, their study emphasized the similarities between feedstock formulation, rheology, and postprocessing considerations. Building on this, Scheithauer et al. [80] developed and refined T3DP, a substitute AM technique capable of achieving improved surface quality and higher precision. Wax-based suspensions enabled consistent deposition of high-solid-content ceramic slurries, allowing the fabrication of intricate, multimaterial structures. Their work also demonstrated the feasibility of co-processing ceramics with metals, thereby expanding the functional range of ceramic AM.

Further advancing the field, Cano et al. [122] concentrated on optimizing highly filled thermoplastic polymer formulations for ceramic FFF. Their studies provided critical guidance for adjusting binder systems to maximize filament mechanical integrity, improve flow behavior during extrusion, and increase the final part density all essential for consistently producing high-quality ceramic prints. A notable contribution was also made by Weingarten et al. [123], who investigated the aesthetic and functional potential of ceramic AM. They successfully fabricated black and white zirconia components for jewelry applications using T3DP, demonstrating the process's capability for fine spatial resolution and controlled color differentiation. Their work also offered valuable insights into the rheological requirements of multimaterial, droplet-based AM systems, advancing understanding of feedstock behavior in such processes.

3.2 | Feedstock Material Composition and Types

Depending on the extrusion system employed, the main forms of feedstocks are filament-based, pellet/granule-based, and, less commonly, paste or slurry-based. Additionally, strategies to improve processability and part properties have included the use of hollow filaments and bimodal or trimodal powder distributions. Table 8 summarizes various feedstocks utilized in EAM, along with their compositions and key processing characteristics. While pellet-based feedstocks offer greater compositional flexibility and can achieve higher solid loadings [124], filament-based systems are widely adopted because they are compatible with standard 3D printers.

3.3 | Ceramic Powder Properties and Optimization

The ceramic component of feedstocks—most commonly alumina, zirconia, silicon nitride, or boron carbide—is selected based on

15272648, 2026, 16, Downloaded from https://advanced.onlinelibrary.wiley.com/doi/10.1002/adem.71089 by Abdollah Saboori - Politecnico Di Torino Sist. Bibl Del Polit Di Torino , Wiley Online Library on [27/09/2026]. See the Terms and Conditions (https://onlinelibrary.wiley.com/terms-and-conditions) on Wiley Online Library for rules of use; OA articles are governed by the applicable Creative Commons License

TABLE 8 | Feedstock type, composition, and processing characteristics in EAM.

Feedstock type	Ceramic loading, vol%	Binder system components	Extrusion method(s)	Representative materials	Ref.
Filament-based	50–60 (up to 82)	Thermoplastics, backbone binders, waxes	FFF, FDC	Alumina, zirconia, Si_3N_4	[80, 113–115, 122]
Pellet/Granule-based	≥60	Thermoplastics, wax, surfactants	FFD, screw/plunger-based	Alumina, Ti6Al4V, composite blends	[124]
Paste/Slurry-based	∼60	Polymeric or aqueous, plasticizers	Specialty/plunger-based	Clay-based, alumina, composites	[34–38]

mechanical strength, thermal stability, and application-specific requirements. Researchers have employed multimodal, typically trimodal, particle size distributions to optimize the proportions of nano-, submicron-, and micron-sized powders, thereby achieving high packing density and uniform sintering. Spherical morphologies reduce internal porosity after sintering and improve powder flow and compounding. For specialized applications, the typical particle sizes of high-quality feedstocks range from several microns down to the nanoscale [124, 125].

3.4 | Binder Systems and Additives

Binder systems are carefully engineered mixtures of polymers and additives designed to control flow behavior, ensure printability, and enable effective debinding, making them essential in ceramic feedstock formulation. They typically consist of three main components, each serving a distinct function within the AM process [126–131]:

- The primary binder controls the cohesiveness and processability of the feedstock. Common low-molecular-weight thermoplastics used in this role include polyolefins, polyethylene glycol (PEG), low- or high-density polyethylene (LDPE/HDPE), and polyoxymethylene (POM) due to their favorable melting behavior and ease of removal during the initial debinding stages.
- After early binder removal, backbone binders provide strength to the green body. Common options include higher molecular weight thermoplastics such as polyvinyl butyral (PVB) or certain polyolefins.
- Surfactants (e.g., SA), dispersants, and plasticizers (e.g., waxes, dibutyl phthalate) reduce melt viscosity and promote homogeneity in the feedstock.

The surface area of the ceramic powder, its chemical reactivity, the desired viscosity, and intended debinding technique all influence the specific composition and ratios of binder components. For example, SA has been shown to significantly reduce melt viscosity while enhancing particle dispersion, thereby improving both process stability and the quality of the final part.

The selection of an appropriate ceramic feedstock for EAM depends not only on the ceramic material itself but also on the compatibility among powder chemistry, feedstock form, binder composition, rheological behavior, and the selected extrusion process. Oxide ceramics, such as Al_2O_3 and ZrO_2, are generally compatible with both aqueous and thermoplastic binder systems owing to their relatively stable surface chemistry and well-established sintering behavior. In contrast, nonoxide ceramics, including SiC, Si_3N_4, and B_4C, require more carefully engineered binder formulations and postprocessing strategies because of their high sintering temperatures, susceptibility to oxidation, and limited self-diffusion. Bioceramics, such as hydroxyapatite (HA), β-tricalcium phosphate (β-TCP), and bioglass, are commonly processed using water-based or hydrogel-assisted systems to maintain biocompatibility and facilitate the development of controlled porous structures. Table 9 summarizes the compatibility of representative ceramic systems with different feedstock forms, binder formulations, suitable EAM technologies, and their associated processing challenges. The material–binder–process relationships presented in Table 9 demonstrate that feedstock design must be tailored to both the ceramic composition and the requirements of the extrusion mechanism. Filament-based processes are primarily compatible with thermoplastic feedstocks employed in FDM/FDC, whereas paste- and slurry-based formulations are more suitable for RC, DIW, CODE, and gel-assisted extrusion techniques. For oxide ceramics, achieving high densification is generally more straightforward through conventional sintering or hot isostatic pressing (HIP). In contrast, nonoxide ceramics and UHTCs often require advanced densification techniques, such as SPS, liquid silicon infiltration (LSI), polymer infiltration and pyrolysis (PIP), chemical vapor infiltration (CVI), or RS, to overcome limited sinterability and residual porosity. In biomedical ceramic systems, binder selection must additionally account for biocompatibility, pore architecture stability, and controlled degradation behavior. Consequently, water-based and hydrogel-assisted formulations are often preferred over highly organic thermoplastic systems for such applications.

3.5 | Mechanical and Rheological Needs

- Feedstocks used in successful extrusion-based AM of ceramics must demonstrate well-balanced mechanical and rheological properties. Several key rheological characteristics are essential for successful processing.
- Shear-thinning behavior, in which viscosity decreases with increasing shear rate, is critical for enabling smooth and continuous flow through the print nozzle while maintaining sufficient viscosity at rest to support deposited layers.
- The presence of a yield point indicating the transition from elastic to viscous flow is important to prevent

15272648, 2026, 16, Downloaded from https://advanced.onlinelibrary.wiley.com/doi/10.1002/adem.71089 by Abdollah Saboori - Politecnico Di Torino Sist. Bibl Del Polit Di Torino , Wiley Online Library on [27/09/2026]. See the Terms and Conditions (https://onlinelibrary.wiley.com/terms-and-conditions) on Wiley Online Library for rules of use; OA articles are governed by the applicable Creative Commons License

TABLE 9 | Compatibility comparison among ceramic systems, feedstock forms, binder systems, and suitable EAM technologies.

Ceramic system	Typical feedstock form	Representative binder system	Suitable EAM technologies	Key processing characteristics	Main challenges	Ref.
Al_2O_3 (Alumina)	Paste, slurry, filament	PVA, PVP, PEG/PVB, LDPE/HDPE + wax	RC, DIW, FDM/FDC, EFF	High solid loading achievable; excellent sinterability; high dimensional stability	Shrinkage during debinding and sintering, filament brittleness, and dimensional distortion	[30, 80, 89, 112–114]
ZrO_2 (Zirconia)	Slurry, paste, UV-curable suspension, thermoplastic feedstock	Photocurable resin, PVA, PEG, paraffin wax	DIW, CODE, PHASE, T3DP	High density (>98%) and fine surface finish possible	High shrinkage sensitivity; crack formation during debinding	[80, 92, 106, 121]
SiC (Silicon carbide)	Paste, slurry, thermoplastic feedstock	Carbon precursor + polymer binder, PVB, paraffin wax	RC, DIW, EFF, FDM/FDC	Excellent thermal resistance; suitable for high-temperature and structural applications; compatible with infiltration-based postprocessing	Difficult densification; residual porosity; oxidation sensitivity; need for advanced postprocessing	[38, 40, 44, 86–88, 124, 125]
Si_3N_4 (Silicon nitride)	Filament, thermoplastic paste	Wax/polyolefin systems, PEG/PVB	FDM/FDC, T3DP	High flexural strength achievable after sintering	Complex debinding; warpage; anisotropic shrinkage; feedstock brittleness	[81]
B_4C (Boron carbide)	Paste/slurry	PEI, PVA, thermoplastic binders	DIW, RC	Lightweight and high hardness; suitable for armor applications	Crack formation at high solid loading and difficult sintering	[30]
HfB_2/ZrB_2 (UHTCs)	High-solid paste	PVA + carbide/nitride additives	RC, CODE	High-temperature resistance (>3000 °C); excellent thermal stability	Poor oxidation resistance; difficult densification	[39, 59]
Hydroxyapatite (HA)	Slurry, paste	PVA, alginate, gelatin-based systems	DIW, RC, 3DGP	Excellent biocompatibility and porous scaffold fabrication	Low mechanical strength; pore collapse during sintering	[34–36]
β-TCP	Paste/slurry	PVA, hydrogel systems	DIW, RC	Controlled bioresorbability; suitable for bone scaffolds	Fragility after sintering; limited load-bearing capability	[46]
Bioglass	Ink/slurry	Hydrogel binders, PVA	DIW, 3DGP	Good bioactivity and controlled porosity	Crystallization and cracking during heat treatment	[48]

15272648, 2026, 16, Downloaded from https://advanced.onlinelibrary.wiley.com/doi/10.1002/adem.71088 by Abdollah Saboori - Politecnico Di Torino Sist. Bibl Del Polit Di Torino , Wiley Online Library on [27/09/2026]. See the Terms and Conditions (https://onlinelibrary.wiley.com/terms-and-conditions) on Wiley Online Library for rules of use; OA articles are governed by the applicable Creative Commons License

deformation, collapse, or distortion of newly deposited layers under their own weight or during subsequent material deposition.

- Low viscosity at elevated temperatures facilitates continuous extrusion of filaments or pellets while minimizing the risk of excessive pressure buildup within the nozzle.

From a mechanical perspective, the binder system must provide printed components with sufficient green strength to allow safe handling and postprocessing. At the same time, adequate flexibility is required to prevent brittle fracture during the early stages of layer deposition or filament feeding. EAM has greatly benefited from recent studies that have enhanced the understanding and control of thixotropic and viscoelastic behaviors in ceramic feedstocks. These advances have enabled the fabrication of highly intricate geometries that were previously unattainable using conventional ceramic forming techniques.

One major improvement lies in the development of customized binder systems designed to optimize the thixotropic and viscoelastic properties of ceramic pastes. These systems typically consist of primary binders, backbone components, and additives that work together to achieve the desired rheological performance. During debinding, the primary binder is usually removed first, while the backbone component remains intact to maintain the structural integrity of the printed part [94, 132, 133].

3.6 | Problems and Restraints in Feedstock Development

- Although EAM of ceramics has made great progress, processing ceramic-rich, polymer-bound feedstocks [124, 134, 135] still presents several ongoing difficulties. If these problems go unaddressed, the manufacture of ceramic components may suffer as well as final properties.
- While high ceramic loadings are desired for reducing shrinkage and obtaining high-density sintered parts, they inevitably lead to increased brittleness in filaments and pellets. During extrusion, handling, feeding, and processing this brittleness can lead to cracking and breakage.
- Rheological control: Crucially, binder component and surfactant ratios must be balanced appropriately. Inappropriate formulations can cause phase separation, too high viscosity, or poor stick-slip behavior where intermittent material flow disturbs printing consistency and quality.
- Often, poorly controlled rheological properties or variations in feedstock lead to flaws during printing. Common problems include under- or over-extrusion, weak interlayer bonding, surface warping, and dimensional errors, all these can result into poor structural integrity and aesthetic quality of the printed parts.
- Eliminating organic binders is a delicate operation; incomplete or uneven debinding can cause internal voids and flaws. Moreover, too low densification or too great shrinkage during sintering can reduce dimensional accuracy, compromise mechanical performance, and create residual stresses.
- Environmental and financial issues arise from the use of hazardous catalytic debinding agents and environmentally damaging binders, affecting workplace safety and sustainability. These techniques can also raise running expenses and restrict the scalability of ceramic AM technologies for more general industrial acceptance.

Advancement in the field of ceramic AM still depends on addressing these challenges with better process control, optimized feedstock formulations, and the development of greener, more reasonably priced substitutes.

3.6.1 | Strategies to Improve Feedstock Flexibility and Lower Brittleness

Overcoming the natural brittleness of highly loaded ceramic feedstocks, especially filament-based ones, is one of the main difficulties in EAM of ceramics. While achieving dense sintered parts with minimum shrinkage depends on high ceramic solid loadings, these tend to make feedstocks brittle and prone to cracking during handling, filament extrusion, and printing. Several approaches have been developed aiming at both the feedstock composition and processing techniques to solve these problems [136, 137].

3.6.1.1 | Ratio Optimizing Binder Composition. Carefully tailoring the polymeric binder system to improve flexibility while maintaining high solid loading is an effective approach to mitigating the brittleness of ceramic-rich feedstocks. A commonly used strategy involves combining LDPE and HDPE with waxes to fine-tune both mechanical properties and melt rheology. Research has shown that increasing the proportion of HDPE improves the green strength and dimensional stability of printed parts, while the presence of LDPE and waxes helps retain sufficient flexibility in filament or pellet form to reduce brittleness during handling and extrusion.

Furthermore, plasticizers and surfactants such as SA are useful in reducing melt viscosity and improving powder dispersion. These modifications enhance feedstock flow, flexibility, and overall printability. However, the concentration of SA requires careful optimization. While moderate amounts improve rheological behavior and filament printability, excessively high levels can compromise the mechanical integrity of the green body by promoting the formation of overly rigid polymer networks within the binder matrix. Therefore, achieving a reliable balance of surfactants and plasticizers is essential for producing dependable, defect-free ceramic components via EAM [94].

3.6.1.2 | Particle Size Distribution and Powder Morphology. Specifically, trimodal blends combining nano-, submicron-, and micron-sized ceramic powders through multimodal particle size distributions improve packing density and reduce the volume fraction of binder required. By enhancing particle–particle and particle-binder interactions, these optimized powder blends help decrease brittleness and improve feedstock flow properties, thereby minimizing internal stresses likely to induce cracking. By encouraging simpler flow and homogeneous dispersion in the binder matrix, Additionally, spherical powder particles facilitate easier flow and more homogeneous dispersion within the binder matrix, reducing stress concentration points that could lead to filament or pellet fracture [125], thus enhancing feedstock flexibility.

15272648, 2026, 16, Downloaded from https://advanced.onlinelibrary.wiley.com/doi/10.1002/adem.71088 by Abdollah Saboori - Politecnico Di Torino Sist. Bibl Del Polit Di Torino , Wiley Online Library on [27/09/2026]. See the Terms and Conditions (https://onlinelibrary.wiley.com/terms-and-conditions) on Wiley Online Library for rules of use; OA articles are governed by the applicable Creative Commons License

3.6.1.3 | *Compounding and Processing Guidelines.* The mechanical behavior and feedstock homogeneity are strongly influenced by careful control of the compounding process including temperature and mixer-kneader settings. Lower compounding temperatures help to preserve surfactant integrity, maintaining their beneficial effects on flow and flexibility. Ensuring uniform particle wetting and distribution minimizes phase separation-induced defects and brittleness caused by agglomerates. Achieving high solid loading for densification while retaining sufficient polymer content for flexibility often requires a careful balance during feedstock preparation. For example, reducing solid loading slightly, from 55 to 50 vol% in alumina feedstocks, can significantly improve filament ductility and extrudability, illustrating the delicate trade-off between mechanical properties and printability [121].

3.6.1.4 | *Process Parameter Optimization and Print Strategy.* Brittleness is also influenced by the selection of printing parameters including extrusion temperature, nozzle diameter, and cooling rate. Precise control of cooling, along with higher nozzle temperatures, helps reduce internal stresses in extruded filaments or deposited layers, minimizing the risk of delamination or cracking. The use of external cooling fans to rapidly solidify printed layers further preserves structural stability, indirectly mitigating brittleness. Additionally, minimizing internal defects in brittle feedstocks and optimizing build orientation can reduce print failures caused by brittle filament behavior; consequently, adjustments to layer height and infill patterns can significantly influence the mechanical performance of printed parts [94].

3.7 | Future Directions and Trends

Looking ahead, both industrial and academic research are increasingly focused on addressing the remaining challenges of EAM along several key directions [138–141]. One major priority is increasing the solid loading of feedstocks which improves densification and reduces sintering shrinkage while still maintaining essential properties such as mechanical flexibility and printability. Achieving and maintaining this delicate balance remains a significant challenge in the field.

Simultaneously, there is growing interest in environmentally sustainable binder systems. Water-soluble or bio-derived polymers are being actively developed as safer, more eco-friendly alternatives to conventional, often hazardous or nonbiodegradable binders [142]. These innovations not only reduce the environmental impact of ceramic AM processes but also simplify debinding techniques. Another important area of research is the enhancement of rheological control. By employing advanced material characterization methods and molecular-level binder design, feedstock flow behavior can be optimized, enabling consistent extrusion across a wide range of geometries, feature sizes, and build scales.

Furthermore, the development of feedstocks capable of producing functionally graded and multimaterial structures presents new opportunities for high-performance, application-specific ceramic components. This includes the fabrication of composite systems, multiphase ceramics, and structures with customized spatial property distributions. In postprocessing technologies, major advancements are also underway. Rapid and effective debonding and sintering techniques, such as microwave sintering, ultra-high-speed (UHS) sintering, and HIP, are expected to improve both productivity and final part quality, so accelerating the larger acceptance of ceramic AM in industrial environments [143, 144].

Despite extensive research into paste formulation for EAM, several critical questions remain unanswered. For example, which binder systems can simultaneously provide excellent printability and clean thermal decomposition during debinding without causing cracks or defects? Additionally, how can the surface chemistry and particle morphology of ceramic powders be engineered to ensure uniform dispersion and minimal agglomeration in high-solid-loading pastes? Another unresolved challenge concerns the rheological thresholds that define printable behavior: is it possible to establish generalized printability criteria applicable across various extrusion platforms and materials?

4 | Process Parameters and Print Quality

Various process parameters in EAM significantly influence the mechanical qualities and print quality of the final ceramic parts. Achieving high-quality prints with the desired mechanical performance requires a thorough understanding of these parameters and their optimization. Highlighting that imbalances can lead to defects such as delamination and shape distortion, Travitzky et al. [145] provided a foundational framework emphasizing the critical role of paste formulation and extrusion parameters in achieving defect-free printing. Building on this foundation, Zocca et al. [95] investigated major EAM methods and demonstrated that controlling sintering shrinkage and guaranteeing dimensional accuracy depend on achieving high green body density and uniform filament deposition.

Chen et al. [10] conducted systematic parametric studies to investigate the relationship between process parameters and print quality. They found that, although associated with reduced build speed, lower layer heights and moderate extrusion rates produced parts with better surface finish and dimensional accuracy. Recognizing the need for effective decision-making tools, Peng et al. [146] developed a process map linking extrusion rate, layer thickness, and print speed to key quality criteria including print integrity and surface morphology. The integration of process monitoring systems has further advanced quality assurance in ceramic AM. Li et al. [147] developed a real-time, in situ image analysis method capable of detecting layer misalignment, pore development, and filament deformation during printing, thereby enabling early defect detection and instantaneous process intervention. In this work, the directed energy deposition (DED) process is monitored in situ using the coherent gradient sensing (CGS) technique. This approach, which is crucial for enhancing manufacturing quality, addresses the challenge of achieving high resolution and capturing the step-wise evolution of full-field deformation during the monitoring process. Figure 8 presents a schematic illustration of this customized tool. In parallel, Wang et al. [148] emphasized the critical role of ceramic paste rheology in extrusion dynamics. They noted that paste viscosity and yield stress directly influence extrusion continuity, filament stability, and defect occurrence. Collectively, these efforts have

15272648, 2026, 16, Downloaded from https://advanced.onlinelibrary.wiley.com/doi/10.1002/adem.71088 by Abdollah Saboori - Politecnico Di Torino Sist. Bibl Del Polit Di Torino , Wiley Online Library on [27/09/2026]. See the Terms and Conditions (https://onlinelibrary.wiley.com/terms-and-conditions) on Wiley Online Library for rules of use; OA articles are governed by the applicable Creative Commons License

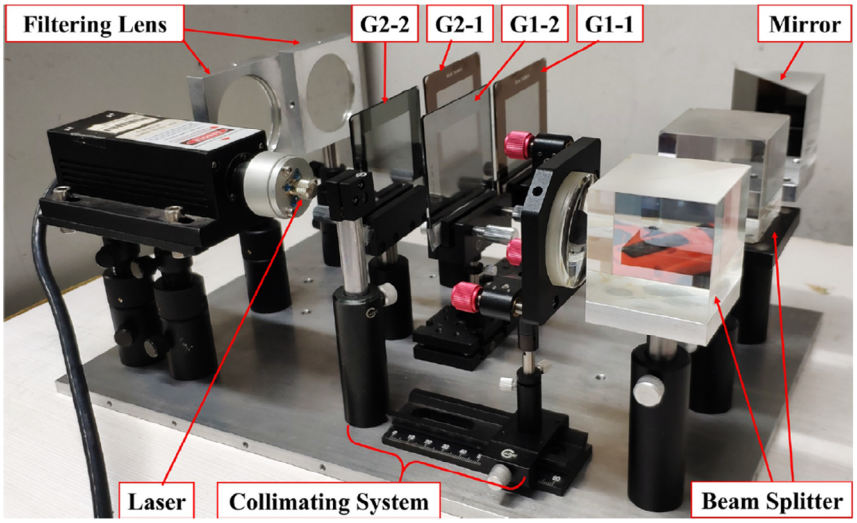


FIGURE 8 | Schematic representation of the customized coherent gradient sensing (CGS) system used for in situ process monitoring. Reproduced with permission [147]. Copyright 2020, Elsevier.

greatly advanced knowledge of the interactions among process parameters to affect print quality in EAM.

4.1 | Key Process Parameters in EAM

The quality and performance of ceramic parts produced by EAM are governed by a combination of process parameters, paste properties, and nozzle design. These factors collectively control dimensional accuracy, mechanical performance, surface quality, and defect formation. Each of these elements interacts closely to influence dimensional accuracy, mechanical properties, surface finish, and defect formation in printed components. This section provides a systematic review and clarification of the key parameters affecting EAM.

4.1.1 | Extrusion Pressure

In EAM technologies, extrusion pressure plays a critical role in regulating material flow, densification, and interparticle bonding. It directly influences mechanical qualities, packing density, and defect formation in both green and sintered parts. Experimental studies on alumina ceramics have identified an optimal extrusion pressure range of 2.2–2.5 bar, which enhances densification, compressive strength, and microhardness while minimizing shrinkage-induced deformation. Deviations from this range can lead to suboptimal outcomes: low pressures often result in insufficient compaction, whereas high pressures may cause filament distortion and cracking. Therefore, achieving reliable, high-quality printing requires maintaining extrusion pressure within a carefully controlled window, calibrated according to the paste rheology and nozzle geometry [149].

4.1.2 | Extrusion Velocity

Build speed and the material deposition rate are governed by extrusion velocity. Although its impact on mechanical characteristics including hardness and flexural strength seems limited within some ranges, it greatly influences process stability and print consistency. For example, studies using alumina and zirconia pastes showed that changing the extrusion velocity between 7.5 and 17.5 mm/s did not significantly change mechanical strength but rather affected layer uniformity and dimensional accuracy. Filament discontinuity, irregular layer deposition, and surface flaws can result from imbalances between extrusion speed, pressure, and paste rheology. Thus, extrusion velocity has to be maximized in combination with other factors to get defect-free prints and effective manufacturing rates [150, 151].

4.1.3 | Part Orientation

The mechanical performance of a printed component is strongly influenced by its orientation with respect to the build platform. Vertically printed components often exhibit higher hardness due to favorable alignment of interlayer bonding whereas horizontally oriented parts generally demonstrate increased flexural strength, attributed to continuous, uninterrupted filament paths along the load-bearing direction. Therefore, part orientation should be carefully selected depending on the application to balance compressive strength, tensile strength, and wear resistance. Comparing samples printed in XY (flat) and ZX (vertical) orientations, Mohd Aidil Nashruffi et al. [152] reported that YZ (on-edge)-oriented samples exhibited superior tensile strength (15.45 MPa) and impact toughness (1.55 J/cm^2), a result of improved stress distribution and interlayer bonding due to filament paths aligning more favorably with the loading direction. In contrast, Eryıldız [153] observed a 36% decrease in tensile strength for upright orientations in FDM 3D-printed PLA parts, indicating that horizontally printed specimens can achieve higher tensile strength. This reduction is attributed to layers being oriented perpendicular to the loading direction, which weakens interlayer adhesion. In a recent study, Bakhtiari et al. [5, 154] have demonstrated that raster angle variation from 0° to 90° in FDM-printed PLA caused reductions of 38%, 18%, and 41% in tensile strength, impact resistance, and bending strength, respectively, highlighting the pronounced effect of filament alignment on load-bearing capacity.

4.1.4 | Layer Thickness and Print Speed

The surface quality, dimensional accuracy, and interlayer adhesion of printed ceramics depend on closely related parameters,

15272648, 2026, 16, Downloaded from https://advanced.onlinelibrary.wiley.com/doi/10.1002/adem.71088 by Abdollah Saboori - Politecnico Di Torino Sist. Bibl Del Polit Di Torino , Wiley Online Library on [27/09/2026]. See the Terms and Conditions (https://onlinelibrary.wiley.com/terms-and-conditions) on Wiley Online Library for rules of use; OA articles are governed by the applicable Creative Commons License

namely, layer thickness and print speed. Lower layer thickness generally results in finer surface finishes and better feature resolution, but it also increases the build time. Print speed must be carefully coordinated with the extrusion rate to maintain filament continuity and prevent under- or over-deposition, which can lead to weak interlayer bonding and contour distortions. Achieving precise geometries, lower surface roughness, and improved mechanical integrity requires carefully balancing these parameters [155].

4.1.5 | *Nozzle Diameter and Overlap Rate*

The width of the extruded filament is directly determined by the nozzle diameter, which also influences the achievable resolution and build rate. Smaller nozzles provide better resolution and finer feature detailing, though they increase shear stress on the paste and clogging risk. Conversely, larger nozzles allow faster builds but may compromise surface smoothness and resolution. Ensuring appropriate bonding between filaments depends equally on the overlap rate, which is the distance between consecutive deposition lines relative to the nozzle diameter. While either insufficient or too much overlap can produce weak interfaces or surface irregularities, appropriate overlap reduces voids, so improving mechanical strength and surface integrity [156–158].

4.1.6 | *Paste Properties*

The printability and final quality of AM-produced parts are primarily determined by the rheological properties of ceramic pastes, including viscosity, yield stress, solids loading, and binder content. Appropriate flow behavior ensures consistent extrusion, smooth filament deposition, and dependability of shape retention during layer stacking. While overly low-viscosity formulations risk nozzle clogging and discontinuities, pastes with high viscosity and yield stress prevent sagging and filament collapse. Different extrusion techniques, such as freeze-form extrusion and RC, require specific paste characteristics to maintain green body stability. Advances in UV-curable or chemically gelable pastes further enhance immediate postdeposition shape retention, enabling complex geometries with improved surface finish and dimensional accuracy. Defect control depends critically on the interaction between paste rheology and process parameters, including extrusion pressure and print speed. For example, mismatches between extrusion speed and curing behavior can lead to morphological irregularities, porosity, or microcracking [139, 159], while extrusion pressure must be tuned to the flow's characteristics to ensure consistent filament formation.

4.1.7 | *Adjustments in Real-Time Parameters*

Real-time control and adjustment of process parameters during EAM of ceramics can significantly enhance the mechanical characteristics and overall print quality of ceramic parts. Dynamic tuning of parameters such as extrusion pressure, print speed, and extrusion velocity enables adaptation to material behavior and environmental variations as the fabrication advances. Unlike static settings, this approach reduces defects and increases consistency. Extrusion pressure is one important parameter for real-time adjustment; it needs to be closely regulated and matched to the rheological characteristics of the ceramic paste or slurry to guarantee consistent material flow and best densification. Studies on alumina ceramics indicate that extrusion pressures in the range of 2.2–2.5 bar achieve superior densification, compressive strength, and microhardness while minimizing shrinkage and defects. Maintaining pressure within this optimal range during printing helps prevent issues such as porosity or microcracking caused by uneven flow rates or pressure fluctuations. Real-time monitoring and feedback control systems can dynamically adjust pressure to compensate for changes in paste viscosity or nozzle resistance [160]. Print speed must also be synchronized with the extrusion rate to maintain filament shape and interlayer bonding. Ensuring consistent material deposition and bonding quality through coordinated extrusion speed and print head motion reduces defects such as small cracks, voids, and irregular geometries. Filament thinning or breakage results from a print speed higher than an extrusion rate; under speed causes over-extrusion and surface flaws. Adaptive control systems that adjust print speed in response to flow conditions help preserve dimensional accuracy and surface quality throughout the build process [161, 162]. Table 10 gives a general summary of the main EAM process parameters.

4.2 | Control of Print Quality by Process Parameters

Many interdependent elements define the print quality of components made by EAM. These cover surface finish, dimensional accuracy, mechanical integrity, and the frequency of process-generated flaws. Consistent, high-quality ceramic parts require careful optimization and control of process parameters. The effects of key process parameters on various quality characteristics are systematically reviewed in this section.

4.2.1 | *Surface Quality*

The practical and aesthetic performance of ceramic components majorly depends on the surface finish. Changing extrusion parameters such as air pressure, print speed, extruder height, and layer thickness has been shown in many studies to greatly increase surface smoothness and lower surface porosity. For porcelain AM processes, experimental feasibility maps indicate that optimal combinations of air pressure and extruder height result in uniform filament deposition and minimal surface irregularities. While excessively low speeds increase the risk of surface bulging and roughness, higher print speeds when properly balanced with appropriate extrusion pressure help achieve smoother surfaces by preventing over-deposition and filament sagging. Therefore, attaining ideal surface quality requires precise calibration of multiple extrusion parameters [163]. In practice, a widely used schematic diagram shows the link between extrusion parameters, particularly, air pressure, print speed, extruder height, and layer thickness, and the resultant surface finish of ceramic components [164]. A representative diagram of this type is shown in Figure 9, summarizing the relationships between key extrusion parameters and surface finish in porcelain AM processes.

- The *y*-axis shows resulting surface roughness or smoothness, while the *x*-axis typically shows variations in air pressure or extrusion pressure.
- Experimental feasibility maps distinguish regions prone to surface defects, such as bulging or roughness caused by

15272648, 2026, 16, Downloaded from https://advanced.onlinelibrary.wiley.com/doi/10.1002/adem.71088 by Abdollah Saboori - Politecnico Di Torino Sist. Bibl Del Polit Di Torino , Wiley Online Library on [27/09/2026]. See the Terms and Conditions (https://onlinelibrary.wiley.com/terms-and-conditions) on Wiley Online Library for rules of use; OA articles are governed by the applicable Creative Commons License

TABLE 10 | List of the main EAM process parameters.

Parameter	Type of visual	Key visual elements	Outcome or insight
Extrusion pressure	Cross-sectional schematic	Pressure zones, flow streamlines	Links pressure to compaction/defect formation
Extrusion velocity	Flowchart, parameter plot	Velocity-deposition coupling, surface result zones	Highlights need for speed-rheology synchronization
Part orientation	Schematic with a bar chart	Orientation diagrams, mechanical property bars	Visualizes anisotropy in mechanical response
Layer thickness/ speed	Ishikawa diagram, line plot	Cause–effect paths, surface profile panels	Quantifies trade-offs among precision, build time
Nozzle and overlap	Cross-sectional/top-view	Filament placement, overlap quantification	Demonstrates effect on voids and resolution
Paste properties	Rheology/triangular map	Shear curve, triaxial map, green body images	Defines printability domain with composition
Real-time adjustments	Closed-loop flowchart	Sensor-controller loop, "before/after" print images	Shows reduction in defects, enhanced consistency

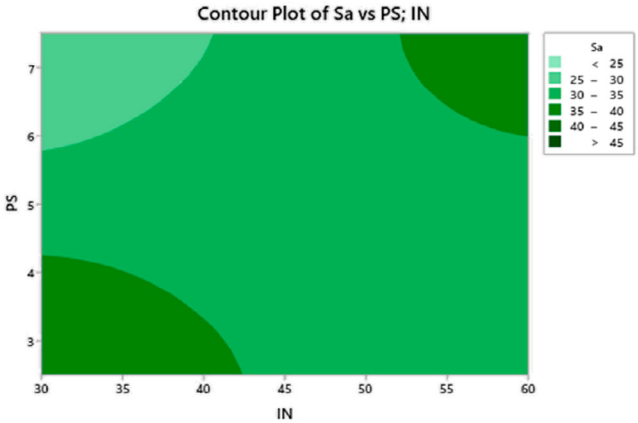


FIGURE 9 | Mean arithmetical roughness S_a (μm) as a function of infill and printing speed plotted conturally. Reproduced with permission [164]. Copyright 2020, MDPI.

inadequate parameter selection, from areas where uniform filament deposition is achieved, indicating optimal surface quality.

- Additional graphs illustrate surface roughness (R_a, in micrometers) as a function of print speed and layer thickness, highlighting that lower layer thickness combined with properly balanced print speed generally minimize surface roughness.
- Additional graphs illustrate surface roughness (R_a, in micrometers) as a function of print speed and layer thickness, highlighting that lower layer thickness combined with properly balanced print speed generally minimizes surface roughness.

4.2.2 | *Dimensional Accuracy*

A crucial performance indicator especially for applications needing exact fit and tolerances is dimensional accuracy. Print speed, extrusion pressure, and layer thickness, among other factors, directly influence the geometric integrity of printed goods. Recent developments have used genetic algorithms and machine learning models as well as optimization techniques to forecast and raise dimensional accuracy in ceramic AM. Using these data-driven techniques, ideal parameter combinations are found, so attaining dimensional deviations as low as 0.05 mm in intricate ceramic sculptures. Dimension consistency and process repeatability can be greatly improved by combining controlled parameter tuning and feedback systems, so lowering the postprocessing needs [165, 166]. Flow charts created for process control in EAM clearly show how closely controlled parameter tuning [167] determines dimensional accuracy outcomes. Usually, these flow charts show:

- Process inputs such as extrusion pressure, print speed, layer thickness, and nozzle height feed into a system block that simulates filament deposition and part fabrication.
- Measurement and feedback loops detect dimensional errors in the printed part, triggering either automatic or algorithmic adjustments to the process parameters.
- Machine-learning-based optimization modules iteratively refine parameter settings to achieve dimensional deviations as low as 0.05 mm.

A representative flowchart of this process is shown in Figure 10.

4.2.3 | *Mechanical Properties*

Typically assessed in terms of compressive strength, flexural strength, and microhardness, the mechanical integrity of extrusion-printed ceramic parts is closely linked to process parameters that influence material densification and interlayer bonding. Among these, extrusion pressure is particularly critical, as it governs packing density and interparticle cohesion. High-performance ceramic parts require a careful balance: sufficient extrusion pressure for appropriate green body strength and minimizing pressure-induced deformation or shrinkage during sintering. Strong interlayer adhesion is further achieved by appropriate synchronizing extrusion pressure, print speed, and paste rheology, thereby enhancing the overall mechanical robustness of the printed structure [168].

15272648, 2026, 16, Downloaded from https://advanced.onlinelibrary.wiley.com/doi/10.1002/adem.71089 by Abdollah Saboori - Politecnico Di Torino Sist. Bibl Del Polit Di Torino , Wiley Online Library on [27/09/2026]. See the Terms and Conditions (https://onlinelibrary.wiley.com/terms-and-conditions) on Wiley Online Library for rules of use; OA articles are governed by the applicable Creative Commons License

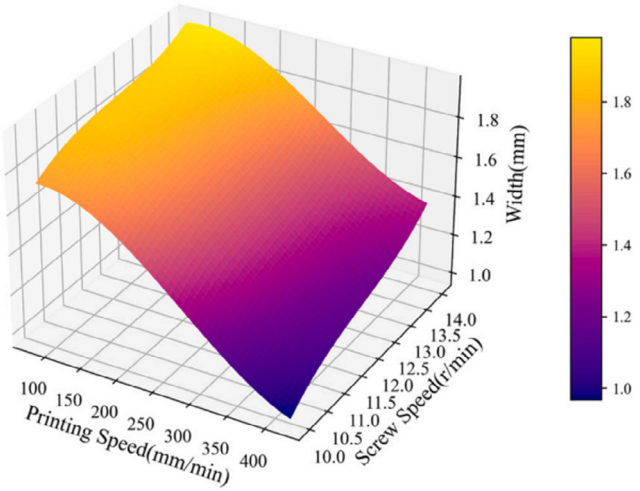


FIGURE 10 | Response surface showing the influence of print speed and screw rotation speed on deposition line width. Reproduced with permission [164]. Copyright 2020, MDPI.

4.2.4 | *Defects and Process Challenges*

Defect formation remains a major challenge in EAM, with common issues including microcracks, porosity, voids, filament discontinuities, and irregular morphologies [169]. These defects often arise from suboptimal parameter settings, such as mismatched print and extrusion speeds, excessive or insufficient extrusion pressure, or inappropriate nozzle geometries. For instance, high print speeds without a corresponding increase in extrusion rate can cause under-extrusion and filament gaps, while low extrusion pressure may result in poor interlayer bonding and increased porosity. Recent research has focused on establishing quantitative relationships between process parameters and defect occurrence, enabling predictive defect mitigation. Such data-driven process control frameworks are critical for preventing quality issues and enhancing overall process reliability [170].

4.3 | Optimization Techniques in EAM

4.3.1 | *Process Parameter Optimization*

A key approach to optimizing EAM involves the careful adjustment of process parameters such as extrusion temperature, print speed, layer thickness, and infill density. Statistical methods including Taguchi designs, Box–Behnken designs, and full-factorial experiments are commonly employed to systematically investigate parameter interactions and identify settings that produce parts with desired characteristics. These methodologies enable exploration of the parameter space to balance mechanical integrity, surface quality, and process efficiency, thereby reducing defects and material waste. Machine learning and heuristic optimization complement these classical approaches by analyzing multidimensional datasets and predicting optimal parameter configurations in real time [171–174]. Table 11 presents visual tools alongside their respective focus areas for enhancing print quality in ceramic extrusion-based EAM.

4.3.2 | *Build Orientation and Adaptive Slicing*

Geometric accuracy, surface finish, and mechanical anisotropy of a part are much influenced by its building orientation. Recent developments have brought multiobjective optimization, where adaptive slicing strategies coupled with build orientation decisions minimize geometric errors and simultaneous printing time. These models often co-optimize objectives using weighted sum techniques and iterative improvements, so enhancing dimensional integrity without too much resource use [165].

4.3.3 | *Toolpath Planning and Nozzle Design Optimization*

Surface roughness, void creation, and build rate are strongly influenced by the path followed by the printhead (or toolpath). Adaptive toolpath algorithms, which can dynamically adjust to part geometries, enable strategies such as zigzag, raster, and non-retraction patterns to be tested for their effects on accuracy and speed [175]. In addition, optimization of nozzle geometry, using both global and local shape optimization techniques, has demonstrated significant improvements, including enhanced flow control, temperature uniformity, and compatibility with different material types. These advancements contribute to improved mechanical performance, reduced surface defects, and stronger interlayer bonding [176, 177].

4.3.4 | *Support Structure and Material Waste Minimization*

Although support structures increase material usage and post-processing effort, they are sometimes essential for fabricating overhangs and intricate geometries in EAM. Knowledge-driven

TABLE 11 | Visual tools with respective focus areas for print quality.

Figure/diagram type	Key process parameters visualized	Print quality attribute highlighted
Experimental feasibility map	Air pressure, extruder height, print speed	Surface quality
Cause-and-effect (Ishikawa) diagram	Extrusion pressure, print speed, nozzle design	Defect formation
Response surface plot	Extrusion pressure, print speed, paste rheology	Mechanical properties (strength, etc.)
Process parameter–performance flowchart	Pressure, speed, layer thickness, nozzle height	Dimensional accuracy
Optimization workflow flowchart	Temperature, speed, layer thickness, density	Global optimization (all traits)

15272648, 2026, 16, Downloaded from https://advanced.onlinelibrary.wiley.com/doi/10.1002/adem.71088 by Abdollah Saboori - Politecnico Di Torino Sist. Bibl Del Polit Di Torino , Wiley Online Library on [27/09/2026]. See the Terms and Conditions (https://onlinelibrary.wiley.com/terms-and-conditions) on Wiley Online Library for rules of use; OA articles are governed by the applicable Creative Commons License

algorithms and topology optimization techniques have been developed to minimize the volume and complexity of supports required while maintaining process stability. Innovative process planning not only reduces material waste but also improves surface finish in regions that would otherwise be obstructed by supports [178, 179].

4.3.5 | *AI-Assisted Process Optimization, In Situ Monitoring, and Process Simulation*

Integration of machine learning frameworks and surrogate models for accelerated, adaptive decision-making represents a major trend in EAM optimization. Machine learning-enabled systems enhance part quality and reproducibility by dynamically tuning process parameters during printing, predicting faults, and detecting process inconsistencies [180]. Surrogate-based multifidelity modeling provides a computationally efficient approach to exploring complex parameter spaces by balancing predictive accuracy with simulation cost [181, 182].

Artificial intelligence (AI)-assisted optimization and data-driven modeling are emerging as powerful tools for enhancing the reliability, repeatability, and scalability of EAM. Their importance is particularly evident in ceramic EAM, where print quality depends on complex interactions among feedstock formulation, rheological properties, extrusion pressure, nozzle geometry, printing speed, layer thickness, drying behavior, debinding, and sintering. Traditional trial-and-error approaches are often labor-intensive and highly material-specific, whereas machine learning and surrogate modeling techniques can identify relationships between processing variables and final part quality using experimental, simulation-generated, or hybrid datasets [167, 174].

One of the most promising applications of AI in ceramic EAM is the prediction and optimization of feedstock printability. The performance of ceramic pastes, inks, and thermoplastic feedstocks is governed by factors such as solid loading, particle-size distribution, powder morphology, binder composition, dispersant concentration, viscosity, yield stress, and shear-thinning characteristics. Together, these parameters influence extrusion stability, shape retention, interlayer bonding, and susceptibility to defects such as nozzle clogging and filament collapse. Data-driven approaches can therefore accelerate the screening of ceramic–binder formulations and identify processing windows that ensure stable extrusion, adequate green strength, minimal defect formation, and controlled shrinkage during postprocessing. Such methods are particularly valuable for high-solid-loading ceramic filaments and highly filled suspensions, where increased ceramic content improves densification but may simultaneously reduce flexibility and compromise extrusion stability [94, 115].

AI-based parameter optimization can further support the selection of extrusion pressure, printing speed, layer height, nozzle diameter, extrusion temperature, infill strategy, and build orientation. These variables directly influence filament continuity, dimensional accuracy, surface quality, porosity, and anisotropic shrinkage. Machine learning-assisted quality optimization has already been demonstrated for ceramic extrusion printing, highlighting the potential of data-driven approaches to improve deposition consistency and geometric fidelity [167, 170]. Likewise, surrogate-based and multifidelity optimization frameworks provide efficient means of exploring large parameter spaces while substantially reducing experimental effort and computational cost [181, 182].

In situ monitoring represents another important pathway toward robust ceramic EAM. Defects such as nozzle clogging, filament discontinuity, over- or under-extrusion, layer misalignment, pore formation, surface irregularities, and crack initiation may arise from rheological fluctuations, pressure instability, nonuniform drying, or environmental disturbances. Monitoring systems incorporating machine vision, thermal imaging, extrusion-force sensing, pressure feedback, and acoustic emission analysis can be integrated with AI algorithms to identify abnormal deposition behavior in real time. Studies on quality recognition in MEX processes and investigations of porosity evolution and geometrical accuracy in ceramic EAM demonstrate that real-time process data can facilitate early defect detection and mitigation [183]. When coupled with adaptive control systems, these monitoring approaches enable dynamic adjustment of extrusion pressure, printing speed, and material flow rate, thereby improving process stability and repeatability [161].

Process simulation complements AI-driven optimization by providing mechanistic insight into material flow, filament formation, deformation, and postprocessing behavior. Numerical models can predict nozzle flow characteristics, pressure drop, shear-rate distribution, die swelling, filament spreading, and layer deformation after deposition. For ceramic feedstocks exhibiting viscoelastic or yield-stress behavior, rheology-informed simulations are particularly valuable for evaluating shape retention, sagging, and interlayer fusion. Process simulation has also been applied to the fabrication of large ceramic components, demonstrating its usefulness for predicting geometry-dependent deformation and supporting process planning [150].

Modeling of debinding and sintering is especially critical in ceramic EAM because final dimensions and properties are strongly influenced by binder removal, densification kinetics, pore evolution, grain growth, and thermal gradients. Variations in green density, heterogeneous binder distribution, and anisotropic filament architectures can lead to differential shrinkage, warpage, residual stresses, and crack formation during thermal treatment. Predictive frameworks that link printing parameters to green-body characteristics and subsequent sintering behavior can help compensate for dimensional changes before fabrication and reduce postprocessing defects. Looking ahead, intelligent ceramic EAM systems are expected to integrate feedstock databases, in situ monitoring, process simulation, and machine learning-based optimization within closed-loop manufacturing platforms. Such systems will enable improved dimensional accuracy, enhanced reproducibility, reduced defect formation, and more efficient process development.

Although process parameter optimization has enhanced extrusion stability, several open questions remain regarding in situ control and modeling. Which real-time monitoring techniques can be adapted or developed to assess layer deposition accuracy, nozzle clogging, or paste consistency during printing? How do variations in nozzle geometry, pressure, and shear rate collectively influence filament shape retention and dimensional accuracy, and can these effects be captured in predictive models?

15272648, 2026, 16, Downloaded from https://advanced.onlinelibrary.wiley.com/doi/10.1002/adem.71089 by Abdollah Saboori - Politecnico Di Torino Sist. Bibl Del Polit Di Torino , Wiley Online Library on [27/09/2026]. See the Terms and Conditions (https://onlinelibrary.wiley.com/terms-and-conditions) on Wiley Online Library for rules of use; OA articles are governed by the applicable Creative Commons License

Additionally, what physical mechanisms dominate filament swelling, and how can extrusion systems dynamically compensate for these phenomena?

5 | Strengthening Processing

Controlling defects in ceramic parts is challenging because such defects often occur randomly and are difficult to predict. However, optimizing process parameters and applying densification and strengthening treatments can significantly reduce or even eliminate these defects [184]. The property enhancement process, including preprocessing and postprocessing steps to achieve fully dense ceramic components, is illustrated in Figure 11.

5.1 | Preprocessing

In ceramics EAM, preprocessing methods play a crucial role in preparing the ceramic material for printing and optimizing the overall process. However, these techniques also have limitations, and parts produced through them can still prone to defects, including cracks that may form and propagate during use. For instance, AM has recently been employed to fabricate ceramic "muscles," enabling rapid production of high-quality components at reduced cost [185–188]. Most ceramic muscles are oxide-based, with alumina, comprising a significant portion; the properties of alumina ceramic muscles used in turbine blades directly influence blade performance [189].

Conventional methods, such as precision casting, make it difficult to produce complex alumina parts, and fabricating multicomponent assemblies using these techniques is often time-consuming and expensive [190]. Consequently, EAM has attracted considerable interest from researchers and practitioners for the production of ceramic muscles. Nevertheless, given the operational conditions of these parts, often involving high temperatures and mechanical stresses and are in direct contact with molten metals, removing porosity and other defects in their structure is critical [191].

For this reason, a large part of the activities carried out by researchers has been devoted to strengthening and densifying the produced parts and building ceramic muscles through AM. Choi et al. [192] employed a combined approach using 3D printing and the organic–inorganic conversion process. Li et al. [193] developed alumina parts with silica as an additive and found that the formation of mullite (aluminosilicate) phases increased the bending strength of the ceramic muscles. They attempted to build alumina muscles using 3D printing, with samples made at 1500 °C having a bending strength of less than 0.5 MPa. To improve bending strength, the samples were impregnated with ethyl silicate hydrolysate, which increased their bending strength to approximately 10 MPa. Zhao et al. [194] developed calcium oxide-based ceramic muscles and reported that the inclusion of ceramic oxide grains enhanced the hydration resistance of the parts. Park et al. [195] demonstrated that the strength of ceramic muscles increases when the compaction density of the raw material powder is maximized.

UHTCs have high thermal and chemical stability and good mechanical properties at temperatures above 3000 °C [196]. For this reason, these ceramic materials can be widely used for applications such as heat transformer components, heat storage systems of powerhouses, industrial burners, and other applications such as aircraft engine nozzles and other parts used by the aerospace industry. However, due to the wetness and low thermal shock of these materials, their applications are still limited [197–200]. One of the points in the design of these parts is proper heat shock resistance, high oxidation resistance, and high thermal resistance because these parts will undergo various thermal and oxidative stresses during their operation [201, 202]. For instance, SiSiC, which is made as silicon-infiltrated silicon carbide, has various industrial applications and often operates at high temperatures, and today one of the challenges is to manufacture SiSiC parts by AM [203–205]. This has led to using this complex material to create special parts with special engineering

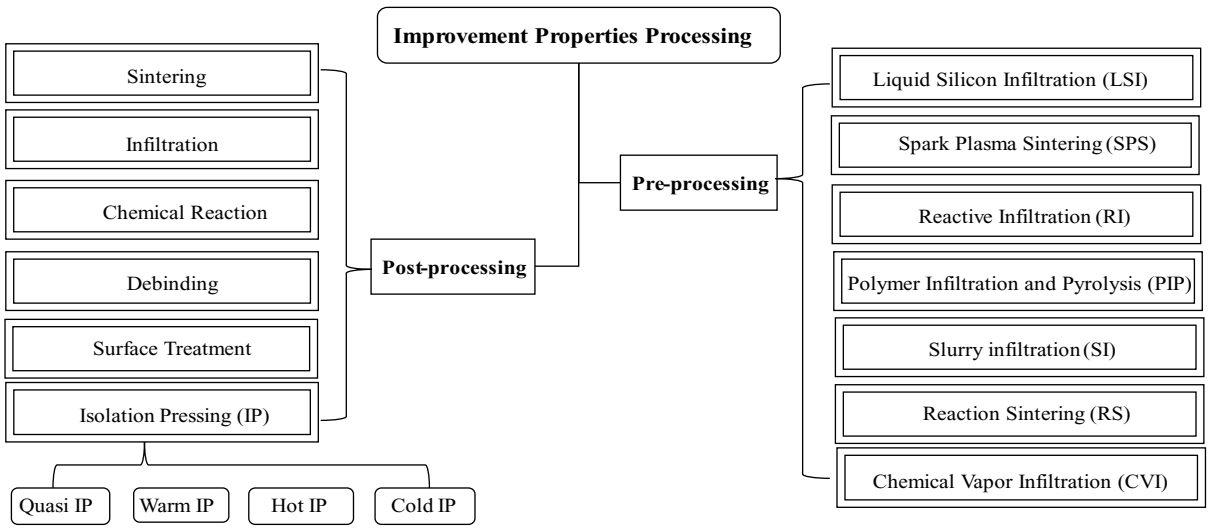


FIGURE 11 | Investigation of methods to improve the properties of ceramics made using AM technology.

15272648, 2026, 16, Downloaded from https://advanced.onlinelibrary.wiley.com/doi/10.1002/adem.71088 by Abdollah Saboori - Politecnico Di Torino Sist. Bibl Del Polit Di Torino , Wiley Online Library on [27/09/2026]. See the Terms and Conditions (https://onlinelibrary.wiley.com/terms-and-conditions) on Wiley Online Library for rules of use; OA articles are governed by the applicable Creative Commons License

shapes, based on which the possibility of using it and its applications has been widely expanded [98, 206, 207]. So far, successful attempts have been made to manufacture these types of parts by a 3D printer using the penetration of molten silicon inside the carbon preform produced by the 3D printer.

The main problem of these parts is the lack of proper density and porosity of the created structure, which leads to decrease in the strength and low resolution of the manufactured parts. For instance, the relative density of SiC ceramic parts made by AM methods is often less than 90%, and their bending strength is low. It usually does not exceed 350 MPa, indicating the high strength of the parts made by conventional methods compared to AM [90]. In this section, to study the nature of the pores created in part, it can be said that the viscous flow does not control the infiltration process, but the reaction at the infiltration front. This reaction occurs between carbon and silicon and leads to the formation of a dense surface. As a result, the penetration of the liquid phase into the pores is restricted, and the pores practically remain in the part [208, 209]. The following section discusses the methods used to densify and strengthen nonoxide ceramics and silicon carbide parts produced by AM.

5.1.1 | *LSI*

LSI involves infiltrating porous C/C materials with molten silicon to form silicon carbide within the structure. This process enhances its properties such as thermal stability, thermal conductivity, and abrasion resistance.

5.1.2 | *SPS*

SPS is a technique that uses pulsed direct current and applied pressure to rapidly sinter powders, enabling precise control over temperature, pressure, and heating rate to produce materials with unique microstructures and properties [210]. A schematic of the SPS process is shown in Figure 12.

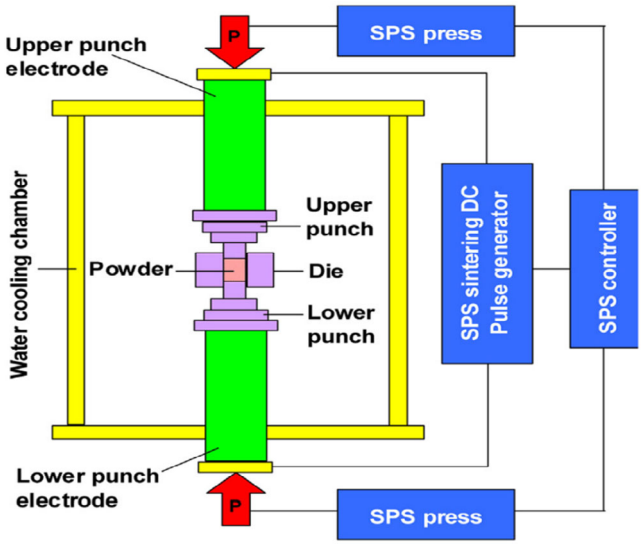


FIGURE 12 | Schematic of the SPS process. Reproduced with permission [210]. Copyright 2014, Elsevier.

5.1.3 | *Reactive Infiltration*

Reactive infiltration (RI) is a process in which a fluid infiltrates a porous medium, inducing chemical reactions to alter the material's properties. It is crucial for fabricating composites with tailored microstructures.

5.1.4 | *PIP*

This technique involves impregnating a porous substrate with a polymeric resin precursor, followed by pyrolysis to convert the polymer into a ceramic material. The pyrolysis process allows for the removal of the organic components, leaving behind a dense ceramic matrix. PIP is particularly effective for fabricating composites with silicon carbide or other silicon-based matrices, offering advantages such as shorter processing times and lower costs than other densification methods like CVI. By controlling the pyrolysis temperature and environment, it is possible to produce ceramics with precise stoichiometric compositions and tailored mechanical properties, making PIP a valuable method for enhancing the strength and density of ceramic components.

5.1.5 | *Slurry Infiltration*

The slurry infiltration (SI) process involves creating a slurry by dissolving TiC particles with graphite powders in deionized water, followed by ball milling. Subsequently, molten silicon infiltrates C/SiC–TiC–C composites at high temperatures under vacuum conditions, filling the internal bundle pores of the composite with TiC–C particles. SI alters material properties and implications, enhancing wear resistance and morphological changes in bulk graphite composites like SiC. The SI process generates denser structures with lower shrinkage than sol–gel infiltration due to increased solid content driven by capillary forces. SI offers advantages such as low porosity rates and good mechanical properties, making it suitable for manufacturing simple and compact parts with improved material characteristics.

5.1.6 | *RS*

The RS process involves the RI of liquid silicon or silicon alloy into a carbon-containing porous ceramic blank. The reaction between the infiltrating agent and the carbon in the blank generates silicon carbide, which combines with the original silicon carbide particles in the blank. The infiltrating agent fills the remaining pores in the blank, completing the densification process. The advantages of RS include a relatively low sintering temperature of around 1600 °C, short sintering times of about 1–2 h, and the ability to effectively prepare large-sized and complex-shaped SiC ceramics. However, there are challenges associated with this method, such as uneven density in sintered products, susceptibility to cracking, insufficient silicon penetration during sintering, high requirements of raw materials, high energy consumption, and elevated production costs. Despite these drawbacks, RS remains a valuable technique for producing silicon carbide ceramics with specific properties and shapes.

5.1.7 | *CVI*

CVI is a technique where a porous substrate is infiltrated by gaseous species that undergo chemical reactions to form a solid

15272648, 2026, 16, Downloaded from https://advanced.onlinelibrary.wiley.com/doi/10.1002/adem.71089 by Abdollah Saboori - Politecnico Di Torino Sist. Bibl Del Polit Di Torino , Wiley Online Library on [27/09/2026]. See the Terms and Conditions (https://onlinelibrary.wiley.com/terms-and-conditions) on Wiley Online Library for rules of use; OA articles are governed by the applicable Creative Commons License

ceramic material within the substrate. CVI is crucial for densifying the porous substrates, offering specific advantages in tailoring material properties. The CVI process is established for various ceramic matrices, including carbon and SiC, allowing for the creation of dense ceramic materials with enhanced strength and unique microstructures. By understanding the specific requirements of CVI processing, it becomes possible to achieve the desired state of densification in ceramics and SiC parts. These methods play a vital role in enhancing the density and strength of nonoxide ceramics and SiC parts manufactured through AM processes, ensuring the production of high-performance materials with specific characteristics tailored to various applications.

The selection of an appropriate densification or strengthening strategy for EAM-fabricated ceramics depends strongly on factors such as ceramic composition, initial porosity, component geometry, target density, and required mechanical performance. Oxide ceramics, including Al_2O_3 and ZrO_2, can often be densified effectively through conventional sintering, with HIP employed when the elimination of residual porosity is required. In contrast, nonoxide ceramics such as SiC, B_4C, Si_3N_4, and UHTCs are inherently more difficult to densify because of their strong covalent bonding, limited self-diffusion, and high sintering temperatures. Consequently, advanced processing techniques, including SPS, LSI, PIP, CVI, RS, and isostatic pressing, are frequently adopted to enhance densification, reduce residual porosity, and improve mechanical reliability. Table 12 compares the principal densification and strengthening routes used for EAM-fabricated ceramics in terms of processing principle, applicable ceramic systems, densification capability, mechanical property enhancement, process cost, advantages, limitations, and typical application areas. As summarized in Table 12, SPS is among the most effective techniques for achieving rapid densification and superior mechanical properties in SiC, B_4C, Al_2O_3, ZrO_2, and UHTC systems. However, its application is generally limited to relatively small components and simple geometries because of die-size constraints and the requirement for uniaxial pressure. HIP is particularly effective for eliminating residual pores in previously sintered oxide and nonoxide ceramics, making it highly attractive for applications requiring exceptional reliability. Nevertheless, the high capital and operating costs of HIP restrict its use primarily to high-value or safety-critical components.

For SiC-based EAM structures, LSI and RS are especially attractive because molten silicon can infiltrate interconnected porosity and react with carbon to generate additional SiC, thereby enabling near-net-shape densification of complex SiC/SiSiC components. In contrast, PIP and CVI are better suited for porous ceramics and fiber-reinforced ceramic matrix composites (CMCs), where matrix continuity, oxidation resistance, and damage tolerance are critical. Their main limitations are the need for multiple processing cycles in PIP and the relatively long processing times associated with CVI. Cold isostatic pressing (CIP) and warm isostatic pressing (WIP) are commonly employed to increase green density prior to sintering; however, their applicability to highly complex additively manufactured geometries may be limited by the potential for dimensional distortion during compaction.

Gomez et al. [86] fabricated a SiC part using 3D printing via the EFF method. The final part was formed after SPS sintering and exhibited a porosity range of 65%–85% porosity. Pelanconi et al. [217] investigated the fabrication of a dense part, by first producing a polymeric preform using the SLS method, followed by LSI applied to the pyrolyzed preform to strengthen the part [212]. In general, by selecting appropriate printing parameters, the density can be controlled, which subsequently affects the infiltration rate and shrinkage after the first pyrolysis cycle. During pyrolysis of preceramic precursor, a SiC preform is created; the amorphous SiC transition to a crystalline structure at high temperatures and shrinks, enabling complete Si penetration. Ultimately, the final density for the 45 vol% SiC + 55 vol% Si part reached 98.3%, and the biaxial strength of the specimens was approximately 127 MPa [212]. In another study, Cai et al. [38] used RC to fabricate SiC ceramic specimens, which were then densified and strengthened using the SPS method, achieving a final density of 97%. Wahl et al. [40] developed SiC/C paste and produced green bodies using RC, followed by reactive sintering and LSI to produce the final part. The density of the final part was 98%, and its four-point bending strength was 224 MPa. Finally, Fielden et al. [39] developed HfB_2 components for high-temperature applications and densified them using pressureless sintering. Table 13 shows the strength and density of 3D-printed SiSiC ceramics postprocessed by various LSI methods.

Recently, some researchers have addressed the challenges of fabricating UHTs ceramic parts by making composites reinforced with chopped carbon fibers [219–221]. Compared to continuous fibers, using chopped fibers facilitates the fabrication of these parts via AM processes [222]. For instance, the DIW method has recently been used to fabricate composites containing directional chopped carbon fibers [223–225]. Franchin et al. prepared a SiC ceramic suspension containing 30% chopped carbon fibers, fabricated the parts using the DIW method, and observed that chopped fibers reduced the cracking within the parts [49]. In another study, Lu et al. [216] fabricated Csf/ZrB_2-SiC composite parts reinforced with directional chopped carbon fibers. First, the Csf precursor was orientated, and DIW was used to form a homogeneous PyC/SiC phase. A slurry of SiC and ZrB_2 was then prepared and applied to the preform via slurry impregnation and reactive melt infiltration. The final specimen, containing ZrB_2 (volume fraction 29.4%) and SiC (volume fraction 30.7%), exhibited a porosity of 18.8% and a density of 2.47 g/cm^3. Due to the relatively poor bonding between the matrix and the fibers, failures in the composite were nonbrittle. This, combined with mechanisms such as crack deflection, bridging, and fiber pullout, enhanced the toughness of the samples. Figure 13 shows the crack behavior and propagation observed after the bending test.

Lu et al. [226] used chopped carbon fibers to make C/SiC composites via PIP and CVI, achieving a fracture toughness of 5.84 MPa·m$^{1/2}$ and a three-point bending strength of 274 MPa. Larson et al. [227] prepared SiC components for optical applications using the DIW method. They applied a low-viscosity SiC suspension to fabricate a green part, followed by liquid-phase sintering at 1800 °C to achieve the final shape. Xiong et al. [213] investigated the fabrication of SiC_w/SiC composites using CVI method, where SiC whiskers were penetrated into the SiC preform using a polycarbosilane suspension, resulting in a part with a bending strength of 47.3 MPa. Gomez et al. [228] fabricated a SiC part by printing filament, followed by SPS sintering to finalize the specimens; the final part exhibited a porosity of 15%–40%. Zhu et al. [214] used high-strength oriented SiC nanowires (SiCNW) as reinforcement in SiC. They first created a SiCNW preform via DIW and then infiltrated SiC into the preform using

15272648, 2026, 16, Downloaded from https://advanced.onlinelibrary.wiley.com/doi/10.1002/adem.71088 by Abdollah Saboori - Politecnico Di Torino Sist. Bibl Del Polit Di Torino , Wiley Online Library on [27/09/2026]. See the Terms and Conditions (https://onlinelibrary.wiley.com/terms-and-conditions) on Wiley Online Library for rules of use; OA articles are governed by the applicable Creative Commons License

TABLE 12 | Comparative analysis of densification and strengthening processes for EAM-fabricated ceramics.

Densification process	Process principle	Applicable ceramic systems	Typical density improvement/final density	Mechanical performance improvement	Process cost	Main advantages	Main limitations	Suitable application scenarios	Ref.
Spark plasma sintering (SPS)	Pulsed electric current and uniaxial pressure promote rapid densification	SiC, B_4C, Al_2O_3, ZrO_2, UHTCs	High; SiC parts can reach ~97% density	Improves strength, hardness, and microstructural compactness by reducing porosity	High	Rapid heating; short sintering time; high density; limited grain growth	Limited part size; expensive equipment; simple geometries preferred	High-performance dense ceramics and research-scale optimization	[210]
Hot isostatic pressing (HIP)	High temperature and isostatic gas pressure close residual pores	Al_2O_3, ZrO_2, Si_3N_4, SiC, AM ceramics after sintering	High; alumina AM parts reached 96% final density after isostatic pressing and HIP	Improves fatigue resistance, fracture strength, and reliability by closing residual pores	Very high	Excellent pore closure; uniform pressure; suitable for high-performance parts	High cost; long cycle; limited accessibility; may require presintered body	Aerospace, biomedical, and high-reliability structural ceramics	[211]
Liquid silicon infiltration (LSI)	Molten Si infiltrates carbon-containing porous preform and reacts to form SiC	SiC, C/SiC, SiSiC	Very high; SiC/SiSiC parts can reach ~98%–100% density depending on preform and infiltration route	Improves flexural strength, thermal conductivity, oxidation resistance, and wear resistance	Medium–High	Effective for complex SiC parts; relatively lower temperature than full sintering; near-net-shape capability	Residual free Si; reaction gradients; limited to carbon/SiC systems	Complex SiC/SiSiC structures, heat exchangers, aerospace and thermal protection components	[8, 19, 40]
Polymer infiltration and pyrolysis (PIP)	Preceramic polymer infiltrates pores and converts to ceramic after pyrolysis	SiC, SiOC, C/SiC composites	Moderate to high after repeated cycles; residual porosity often remains	Improves matrix continuity, oxidation resistance, damage tolerance, and toughness	Medium	Suitable for porous and complex geometries; lower equipment cost than CVI/HIP	Multiple cycles required; shrinkage during pyrolysis; residual porosity remains	Ceramic matrix composites, porous SiC structures, fiber-reinforced ceramics	[212]

(Continues)

15272648, 2026, 16, Downloaded from https://advanced.onlinelibrary.wiley.com/doi/10.1002/adem.71088 by Abdollah Sabouri - Politecnico Di Torino Sist. Bibl Del Polit Di Torino , Wiley Online Library on [27/09/2026]. See the Terms and Conditions (https://onlinelibrary.wiley.com/terms-and-conditions) on Wiley Online Library for rules of use; OA articles are governed by the applicable Creative Commons License

TABLE 12 | (Continued)

Densification process	Process principle	Applicable ceramic systems	Typical density improvement/final density	Mechanical performance improvement	Process cost	Main advantages	Main limitations	Suitable application scenarios	Ref.
Chemical vapor infiltration (CVI)	Gaseous precursors infiltrate porous preform and deposit ceramic matrix by chemical reaction	SiC, C/SiC, SiC/SiC composites	Moderate to high depending on infiltration time and pore connectivity	Enhances high-temperature stability, matrix bonding, and toughness in composites	Very high	Excellent control of matrix composition; suitable for fiber composites	Very slow process; high cost; density gradients possible	High-temperature ceramic matrix composites and aerospace components	[213, 214]
Cold/warm isostatic pressing (CIP/WIP)	Uniform hydrostatic pressure compacts green bodies before sintering	Al_2O_3, ZrO_2, B_4C, SiC, powder-based ceramics	Improves green density; final density depends on subsequent debinding and sintering; WIP-assisted 3DP alumina reached 97.8% final density	Improves dimensional stability and reduces large pores before sintering	Medium	Simple; effective for increasing green density; reduces initial porosity	Risk of deformation in complex AM geometries; requires careful support	Simple or moderately complex green parts before sintering	[211, 215]
Slurry infiltration (SI)	Ceramic or reactive particles are introduced into open porosity through a slurry, followed by drying and thermal treatment	SiC, C/SiC, TiC-modified SiC composites, UHTC composites	Moderate to high depending on pore accessibility and slurry solid loading	Improves matrix filling, wear resistance, and microstructural uniformity	Medium	Relatively simple, useful for introducing secondary phases, suitable for porous preforms	Limited penetration into fine or closed pores, possible particle agglomeration, drying shrinkage	Porous SiC/UHTC preforms and particle-reinforced ceramic composites	[216]
Reaction sintering (RS)	Liquid Si or a reactive phase infiltrates a carbon/ceramic porous blank and reacts to form SiC or secondary ceramic phases	SiC, SiSiC, C/SiC	High; often >95% when pore network and carbon content are well controlled	Improves density, flexural strength, thermal stability, and damage tolerance	Medium	Lower sintering temperature; short processing time; suitable for large SiC parts	Residual silicon; uneven infiltration; crack risk	Large SiC parts, wear-resistant and thermal components	[40, 216]

15272648, 2026, 16, Downloaded from https://advanced.onlinelibrary.wiley.com/doi/10.1002/adem.71088 by Abdollah Saboori - Politecnico Di Torino Sist. Bibl Del Polit Di Torino , Wiley Online Library on [27/09/2026]. See the Terms and Conditions (https://onlinelibrary.wiley.com/terms-and-conditions) on Wiley Online Library for rules of use; OA articles are governed by the applicable Creative Commons License

TABLE 13 | Comparison between strength and density of different SiSiC AM ceramics combined with LSI.

Processing method	LSI			LSI + PIP	LSI + CIP	Ref.
AM method	RC	Binder jetting	SLS	SLS	SLS	[40, 211, 212, 218]
Density, g/cm^3	2.94 (∼98%)	3.05 (∼100%)	2.69	2.718 (∼98%)	2.96	
Flexural strength, MPa	224	358–380	200	127	292–348	

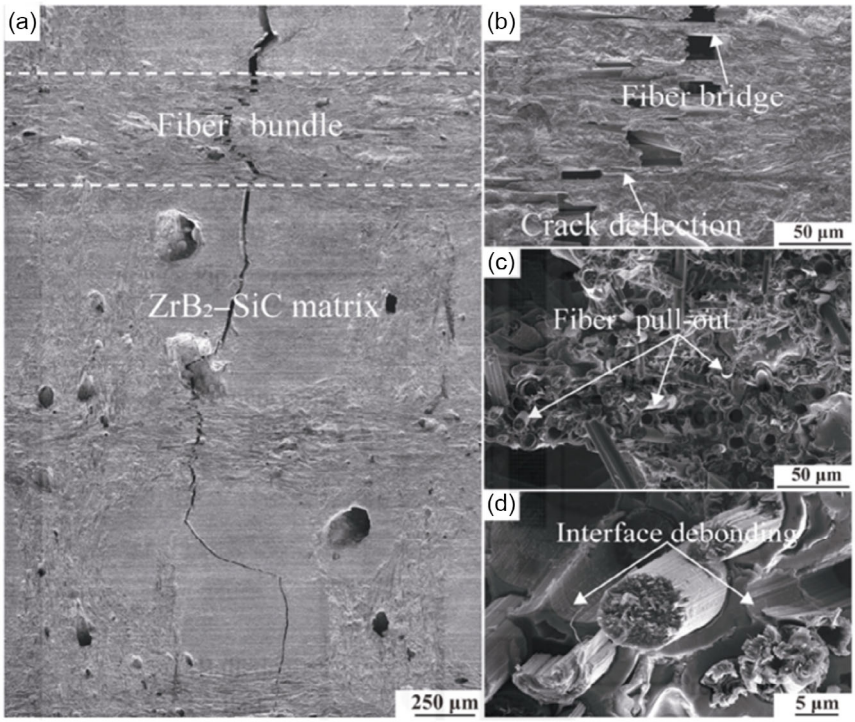


FIGURE 13 | SEM image of crack propagation mechanism and fracture surfaces of ZrB2/SiC composites after bending testing: (a) pattern of crack propagation path within the fiber, (b) crack deflection fiber bridge, (c) fiber pullout, and (d) interface bonding. Reproduced with permission [216]. Copyright 2021, Tsinghua University Press.

the CVI method. The resulting SiCNW/SiC part achieved a final density of 58.7%, along with enhanced compressive strength.

5.2 | Postprocessing

Postprocessing is a crucial stage in AM, necessary for improving part quality by enhancing surface characteristics and mechanical properties. It typically involves clean-up, debinding of any support material, and densification of the ceramic product.

5.2.1 | *Isolation Pressing*

Pressure can be applied to a part in its green (raw) state, sintered state, or during sintering to increase its density. For instance, HIP, CIP, or WIP can be used, where the applied temperature significantly affects the densification [229]. Liu et al. [211] prepared PVA-epoxy-coated alumina particles and fabricated parts using SLS. After cold static pressing at 200 MPa, the parts underwent debinding at 1000 °C and sintering at 1600 °C. Subsequently, the parts were subjected to HIP, resulting in a 32% increase in density, with the final density reaching 96%. Table 14 presents two examples of density increases achieved through sintering and isostatic pressing of green parts. While densification of green and sintered bodies is possible under isostatic pressing, this method is not suitable for complex geometries, as shape distortion may occur.

5.2.1.1 | *CIP.* The CIP is a preprocessing method used in the AM of ceramics. This technique involves subjecting components

TABLE 14 | Investigating the effect of increasing sintering temperature and applying WIP on the final density of ceramic parts produced by the AM method.

Ceramic powder	AM method	Densification method	Density improvement rate	Ref.
B_4C	RC	Sintering	Increased 20%	[229]
Al_2O_3	Powder-based binder jet	WIP (warm isostatic press)	Green density: 36% Final density: 97.8%	[215]

15272648, 2026, 16, Downloaded from https://advanced.onlinelibrary.wiley.com/doi/10.1002/adem.71088 by Abdollah Saboori - Politecnico Di Torino Sist. Bibl Del Polit Di Torino , Wiley Online Library on [27/09/2026]. See the Terms and Conditions (https://onlinelibrary.wiley.com/terms-and-conditions) on Wiley Online Library for rules of use; OA articles are governed by the applicable Creative Commons License

or powder in molds to extreme isostatic pressure, up to 600 MPa, at ambient temperature. CIP consolidates metal and ceramic powders to create a "green" part that can undergo further treatment, such as rolling, machining, or sintering. As a powder-forming technology, it compresses powder materials into various shapes by applying uniform pressure and is widely recognized as an effective forming method in ceramics and powder metallurgy.

5.2.1.2 | *HIP.* The HIP is a manufacturing process used to reduce the porosity of metals and increase the density of many ceramic materials. This technique involves subjecting components to elevated temperature and isostatic gas pressure within a high-pressure containment vessel. The pressurizing gas, commonly argon, prevents chemical reactions in the material. HIP can be applied to produce waste form classes, consolidate metal powders, fabricate ceramic composites and metal cladding, reduce microshrinkage, and improve fatigue resistance. It is also used as a post-processing step in AM and in the processing of radioactive waste to minimize volume during disposal and transport.

5.2.1.3 | *Quasi-Isostatic Pressing.* Quasi-isostatic pressing (QIP) is a preprocessing method used in the AM of ceramic materials. This technique involves subjecting components or powder in molds to extreme isostatic pressure at ambient temperature, up to 600 MPa (87,022 psi). QIP consolidates polymer, metallic, and ceramic materials, ensuring density and removing porosity. By applying QIP, manufacturers can improve the mechanical properties and overall quality of ceramic components produced through AM processes.

5.2.1.4 | *WIP.* WIP is a technique used in AM to enhance the properties of ceramic materials. This method involves subjecting components or powders in molds to extreme isostatic pressures at ambient temperature, up to 600 MPa. WIP can use water, emulsion, or oil as pressure medium and is effective in consolidating polymer, metallic, and ceramic materials, improving density and reducing porosity. By applying WIP, manufacturers can enhance the mechanical properties and overall quality of ceramic components produced through AM.

5.2.2 | *Sintering*

Sintering is the process by which components are compacted to form a dense body through the application of heat. This technique is widely used to achieve densification and is considered a crucial step in AM of ceramics. The primary driving factor behind densification during sintering is the reduction in surface energy achieved by minimizing the solid/liquid interface. Porous structures with significant free space exhibit high surface energy. Applying heat to the initial green part forms solid bonds between particles, thereby reducing the surface energy. Subsequent heat treatment causes progressive growth of the neck between particles, filling the pores, decreasing porosity, and producing a fully densified final product. As mentioned above, sintering is one of the key methods to enhance microstructure quality and part density. Its parameters, such as duration, atmosphere, and temperature, significantly influence densification and microstructure improvement [230, 231]. For instance, in some multistage AM of alumina parts, or in EAM technique used to produce Si_3N_4 [232], alumina [55], and zirconia [233, 234] components, sintering is often applied in a complementary stage. In this stage, conventional sintering processes can be employed to achieve maximum density, improved surface quality, and optimal mechanical properties without the need for applied pressure or atmospheric control. Figures 14 and 15 show the heat treatment and debinding cycle of a barium titanate part fabricated using AM.

Another point effect of sintering is the removal of voids within parts produced by the AM. Since most AM methods build components layer-by-layer, performing heat treatment at an appropriate temperature and duration reduces the interlayer spacing in the structure, in addition to decreasing the overall porosity of the part [237]. For instance, Figure 16 shows a scanning electron microscopic image of a part fabricated by stereolithography.

The following images show the surface of the part after binder removal and densification through heat treatment of varying durations, clearly illustrating the effect of debinding and heat treatment on the structural densification and the elimination of porosity and interlayer gaps. In Figure 17, it can be seen that longer heat treatment reduces the distance between the layers in the structure. The optimal heat treatment duration for minimizing interlayer spacing is approximately 60–90 min. However, extending the treatment beyond 90 min has little additional effect on reducing this distance.

A recent ultrafast high-temperature sintering (UHS) technique was documented [238]. UHS is characterized by its rapid heating and cooling speed, reaching up to 104 °C/min, and a high sintering temperature of up to 3000 °C. Compared to the traditional furnace sintering method, which is slow and time-consuming,

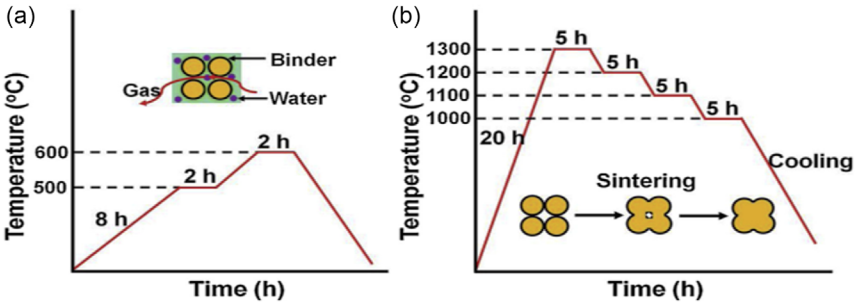


FIGURE 14 | Heat treatment cycle applied to (a) debinding and (b) sintering barium titanate component. Reproduced with permission [235]. Copyright 2020, Elsevier.

15272648, 2026, 16, Downloaded from https://advanced.onlinelibrary.wiley.com/doi/10.1002/adem.71088 by Abdollah Saboori - Politecnico Di Torino Sist. Bibl Del Polit Di Torino , Wiley Online Library on [27/09/2026]. See the Terms and Conditions (https://onlinelibrary.wiley.com/terms-and-conditions) on Wiley Online Library for rules of use; OA articles are governed by the applicable Creative Commons License

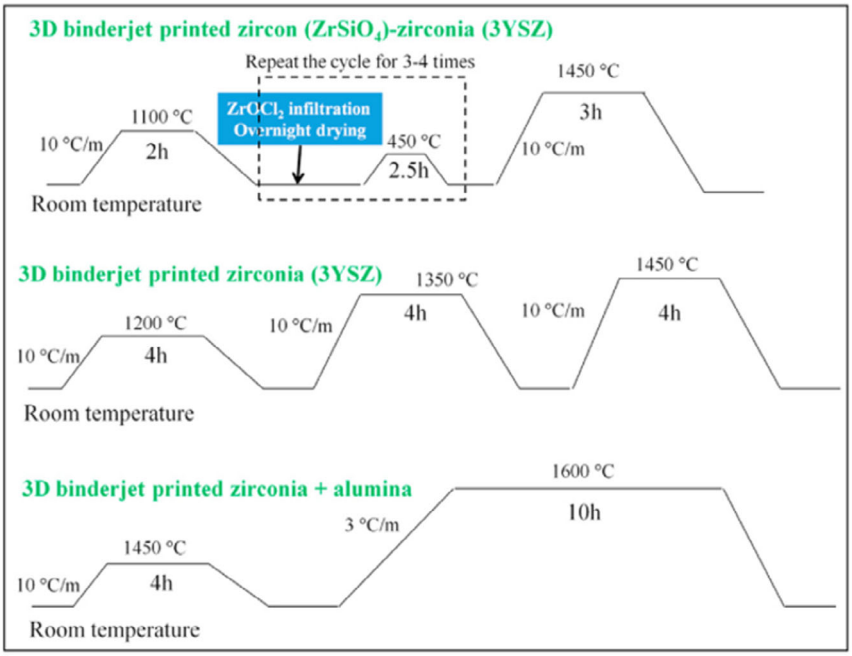


FIGURE 15 | Sintering and postprocessing diagram of zirconia (3YSZ), zircon–zirconia, and zirconia–alumina-based bioceramics. Reproduced with permission [236]. Copyright 2020, Elsevier.

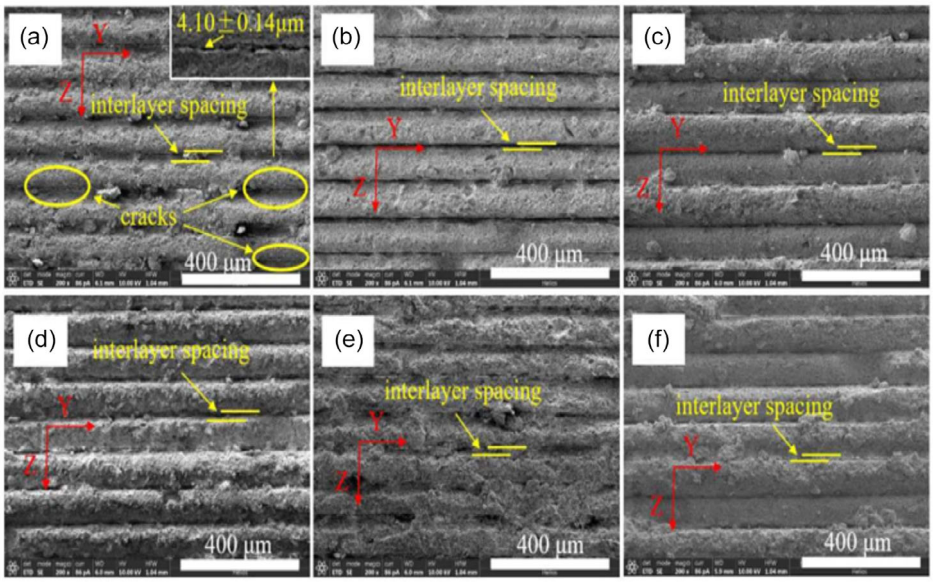


FIGURE 16 | Scanning electron microscope (SEM) images of an alumina part made by stereolithography placed at different times of heat treatment (a: 30 min, b: 60 min, c: 90 min, d: 120 min, e: 150 min, f: 180 min). Reproduced with permission [237]. Copyright 2020, Frontiers.

UHS surpasses it significantly by operating at extremely high temperatures. The procedure entails placing the green components between two Joule heating carbon strips. As the sintering process takes place, the carbon strips quickly heat up, establishing an environment of ultrahigh temperature for solid-state reactions and reactive sintering in an inert atmosphere. The brief sintering duration helps to prevent undesired interdiffusions and volatile evaporation. Wang et al. [239] concluded from their study that the UHS technique is suitable for precursors fabricated through AM. A 3D-printed SiOC polymer precursor underwent successful sintering using the UHS method, resulting in uniform shrinkage and a well-preserved structure.

5.2.3 | *Infiltration*

Another method of increasing the density is the injection of melt or suspension containing ceramic particles and ceramic precursors inside the porous ceramic structure [240], which later penetrates the pores with the assistance of heat treatment and applying pressure. These treatments assist to fill the cavities and solidify as represented in Figure 18. Table 15 presents review of the research conducted on ceramics produced via AM using melt injection as a prefabrication process. The predominant technique for infiltration is known as melt infiltration. In a study conducted by Nan et al. [99], TiC ceramic material underwent infiltration in molten

15272648, 2026, 16, Downloaded from https://advanced.onlinelibrary.wiley.com/doi/10.1002/adem.71088 by Abdollah Saboori - Politecnico Di Torino Sist. Bibl Del Polit Di Torino , Wiley Online Library on [27/09/2026]. See the Terms and Conditions (https://onlinelibrary.wiley.com/terms-and-conditions) on Wiley Online Library for rules of use; OA articles are governed by the applicable Creative Commons License

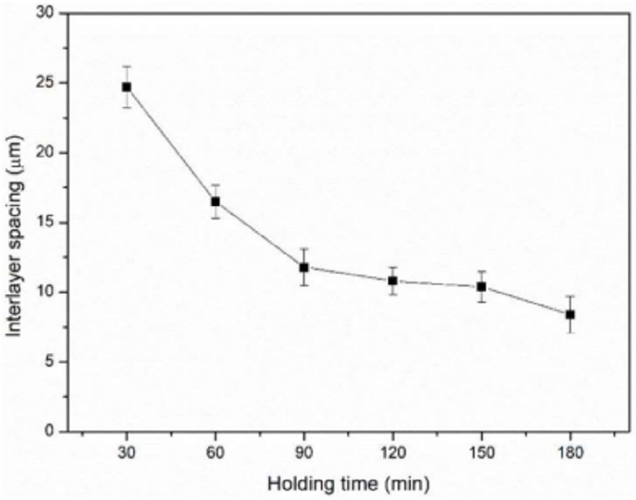


FIGURE 17 | Variation in interlayer spacing of stereolithography-fabricated alumina parts as a function of heat-treatment duration. Reproduced with permission [237]. Copyright 2020, Frontiers.

silicon at temperatures ranging from 1600 to 1700 °C over 1 h, followed by annealing at 1400 °C for 2 h, resulting in the formation of Ti_3SiC_2 and SiC. An alternative approach is solution infiltration, wherein a fine powder is combined with a solvent and submerged in the solution. The key factor influencing the infiltration process is solid loading. The higher levels of solid loading was resulted into reduced infiltration depth.

5.2.4 | *Chemical Reaction*

The phenomenon of chemical reaction represents an additional viable approach for enhancing the sintered density within ceramic materials. Several chemical reactions can be utilized for this purpose, such as the pyrolysis of preceramic polymers, metal oxidation, and the immersion of calcium phosphate material into phosphoric acid. The pyrolysis of preceramic polymers involves use of a precursor as the primary material and then subjecting it to high temperatures for part formation. This methodology, however, is restricted to specific materials suitable for use such as preceramic polymers. Alternatively, the metal oxidation technique employs metal powder as the feedstock material, which is then converted into ceramic through oxidation during fabrication. Lastly, the phosphoric acid immersion method employs phosphoric acid as a binding agent for calcium phosphate components, achieved by immersing the calcium phosphate material in the acid solution.

5.2.5 | *Debinding*

Debinding refers to the removal of polymeric binders without altering the shape of the additively manufactured ceramic

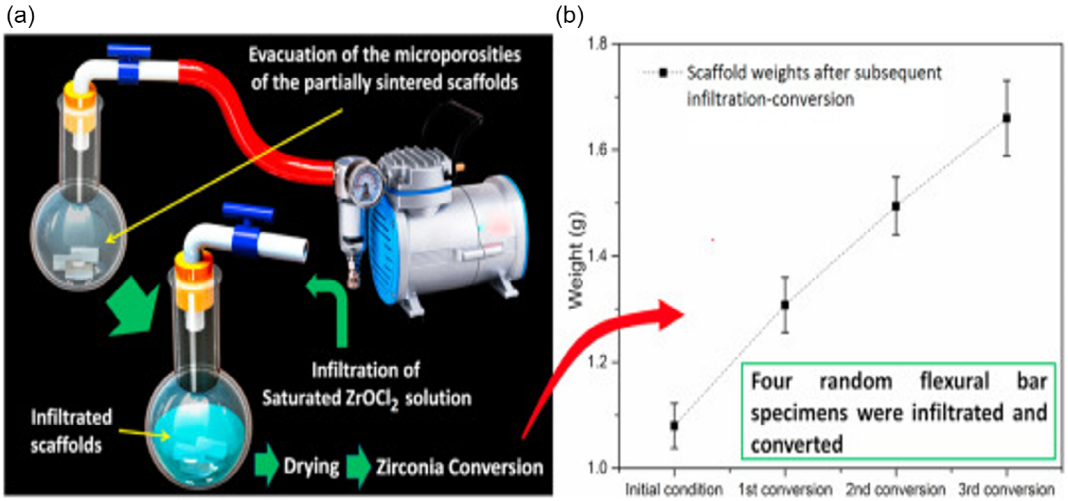


FIGURE 18 | (a) Schematic of infiltration of saturated $ZrOCl_2$ solution in zirconia–alumina-based ceramics and (b) diagram of weight-infiltration cycle that as a result by increasing the infiltration cycle, the weight of ceramic increased. Reproduced with permission [236]. Copyright 2020, Elsevier.

TABLE 15 | Infiltration process for densification of ceramic preform by AM.

Ceramic type	Infiltration method	Melt, suspension, or preceramic polymer	Ceramic preform	Ref.
Al_2O_3/glass composite	pressureless	LAS glass	Al_2O_3 preform	[100]
RBSiC	Liquid silicon infiltration	Molten silicon	SiC or C perform	[218]
SiC	Pressure infiltration and pyrolysis (PIP)	Preceramic polymer liquid	C or SiC preform	[240]
RBSiC	Impregnation and infiltration	Impregnation with graphite suspension Infiltration with Si molten	SiSiC preform	[98]

15272648, 2026, 16, Downloaded from https://advanced.onlinelibrary.wiley.com/doi/10.1002/adem.71089 by Abdollah Saboori - Politecnico Di Torino Sist. Bibl Del Polit Di Torino , Wiley Online Library on [27/09/2026]. See the Terms and Conditions (https://onlinelibrary.wiley.com/terms-and-conditions) on Wiley Online Library for rules of use; OA articles are governed by the applicable Creative Commons License

component. This step is essential because any residual binder can significantly impact the quality and properties of the end product, especially in ceramics fabricated using MEX technologies. These technologies typically involve filaments with a substantial proportion of polymers serving as binders. Gonzalez-Gutierrez and colleagues [118, 146] have identified thermal, solvent, and catalyst methods as the primary debinding techniques.

5.2.6 | *Surface Treatment*

Some AM processes produce ceramic components with subpar surface quality and notable defects. In contrast to AM metals, which can be readily machined and ground, enhancing the surface of AM ceramics is often more complex and may involve thermomechanical treatments. Burkhardt et al. [241] conducted grinding, sandblasting, and laser structuring experiments on shaped parts fabricated from extruded material. Grinding and sandblasting were applied for 25 s to reduce the depth of the spaces between strands. Subsequently, a low-power laser was applied to the part surface for an additional 25 s. The laser energy induced particle mass transport and redistributed the part surface, resulting in no visible strand marks following the surface treatment procedure [242].

Postprocessing, especially debinding and sintering, remains a major source of dimensional distortion and part failure in EAM. Key open questions include how microstructural gradients evolve during the thermal cycle of complex geometries, and to what extent shrinkage and internal stresses can be predicted prior to actual sintering. Are there reliable, noncontact methods such as thermal imaging, acoustic sensing, or dilatometry that can monitor sintering progression in real time? Moreover, what is the critical range of shrinkage mismatch or porosity distribution that leads to cracking, especially in unsupported or overhanging features?

6 | Applications of EAM

Rapidly becoming a key technology for producing advanced ceramic components, EAM enables the construction of complex, near-net-shape structures with tailored microstructures and functional properties that surpass the limits of conventional ceramic manufacturing techniques. Extrusion-based techniques including DIW, RC, and FFF are used to precisely deposit a ceramic-containing paste, slurry, or filament layer by layer. These approaches provide significant design flexibility, facilitating the production of intricate geometries for high-performance applications across various domains, including biology, aerospace, electronics, energy, and more. This section comprehensively examines the cutting-edge applications of EAM in advanced ceramics, including technological concepts, material versatility, application areas, recent advancements, and major challenges.

6.1 | Biomedical Applications: Scaffolds, Implants, and Regenerative Medicine

Thanks to EAM's ability to generate bioceramic structures that precisely replicate the complex morphology and hierarchical porosity of natural bone and tooth tissues, the biomedical sector has experienced transformative breakthroughs. Scaffolds for bone tissue engineering made from hydroxyapatite, tricalcium phosphate, and zirconia provide the exact macro/microarchitecture needed for cell attachment, proliferation, and vascularization. Gradients and customized pore geometries achievable through DIW allow the fabrication of patient-specific implants and scaffolds with precisely controlled mechanical and biological characteristics. Extrusion-based printing guarantees accurate fit and reduces the need for post-fabrication machining; consequently, dental prostheses including crowns and bridges made of dense zirconia represent another important application. Additionally, this approach benefits preoperative planning models and custom maxillofacial implants. Recent studies indicate that bioactive molecules or multimaterial techniques can be incorporated to provide additional therapeutic benefits including controlled drug release and antibacterial activity [243].

Rossi et al. [244] reviewed current advancements in biomedical applications of extrusion-based bioprinting, highlighting the significance of biomaterials and bioinks in the development of this transformative technology. Their review identifies key issues that arise from extrusion-based bioprinting, particularly the resolution, accuracy, and cell viability, and emphasizing the importance of these factors for creating functional tissues and organs, especially in applications such as vascularization. The review underscores the potential of bioprinting to fabricate complex structures that replicate natural tissues, which is critical for regenerative medicine. The authors highlight the dual necessity in bioink design: achieving rheological properties suitable for smooth extrusion while maintaining geometric fidelity, accuracy, and stability post-printing, all while preserving cell viability. They distinguish bioinks into "structural" and "functional" types. Structural bioinks prioritize mechanical stability and shape integrity as a top priority using materials including alginate, gelatin, and decellularized extracellular matrix. Conversely, functional bioinks are designed to actively support cellular functions including growth, differentiation, and proliferation by incorporating biological cues or geometric signals within the printed structure.

The multidisciplinary framework of 3D bioprinting, which combines advanced imaging, computer-aided design (CAD), and conventional 3D printing technologies with bioinks made of cells, growth factors, and hydrogels, is shown in Figure 19. This integrated approach enables the fabrication of biologically and functionally relevant tissue constructs. Apart from the manufacturing of animal-free meat for the food sector, 3D bioprinting finds uses in regenerative medicine for organ transplantation and tissue repair, in vitro tissue models for drug discovery, disease modeling, and consumer care testing. Moreover, its capacity to support sustainable biotechnology solutions, including the production of animal-free meat, positions bioprinting as a transformative technology in both healthcare and industry [245].

Bioprinting commences with the acquisition of the anatomical structure of the target tissue by appropriate imaging modalities, such as computed tomography (CT) and magnetic resonance imaging (MRI). Specialist software is employed to convert the image into a CAD drawing of cross-sectional layers, enabling the printing device to add them in a layer-by-layer manner. By combining a range of printing materials including scaffolds, bioinks, and additional additive components (refer Figure 20), the bioprinting device then fabricates the tissue using a designated printing technique including inkjet 3D bioprinting, microextrusion 3D bioprinting, laser-assisted 3D bioprinting, and stereolithography [245]. Skin, cardiac tissue, cartilage, and blood

15272648, 2026, 16, Downloaded from https://advanced.onlinelibrary.wiley.com/doi/10.1002/adem.71088 by Abdollah Saboori - Politecnico Di Torino Sist. Bibl Del Polit Di Torino , Wiley Online Library on [27/09/2026]. See the Terms and Conditions (https://onlinelibrary.wiley.com/terms-and-conditions) on Wiley Online Library for rules of use; OA articles are governed by the applicable Creative Commons License

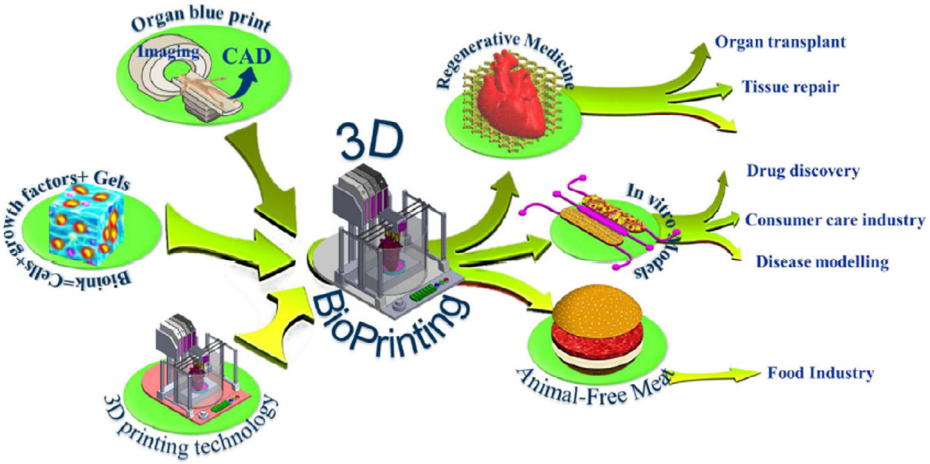


FIGURE 19 | Conventional 3D printing technology, cutting-edge imaging, and cell-laden hydrogels are combined in 3D bioprinting to produce functionally active tissues. Applications in regenerative medicine, pharmaceutical preclinical drug testing, and the manufacturing of meat free of animals are being made possible by this adaptable technology. Reproduced with permission [245]. Copyright 2021, Frontiers.

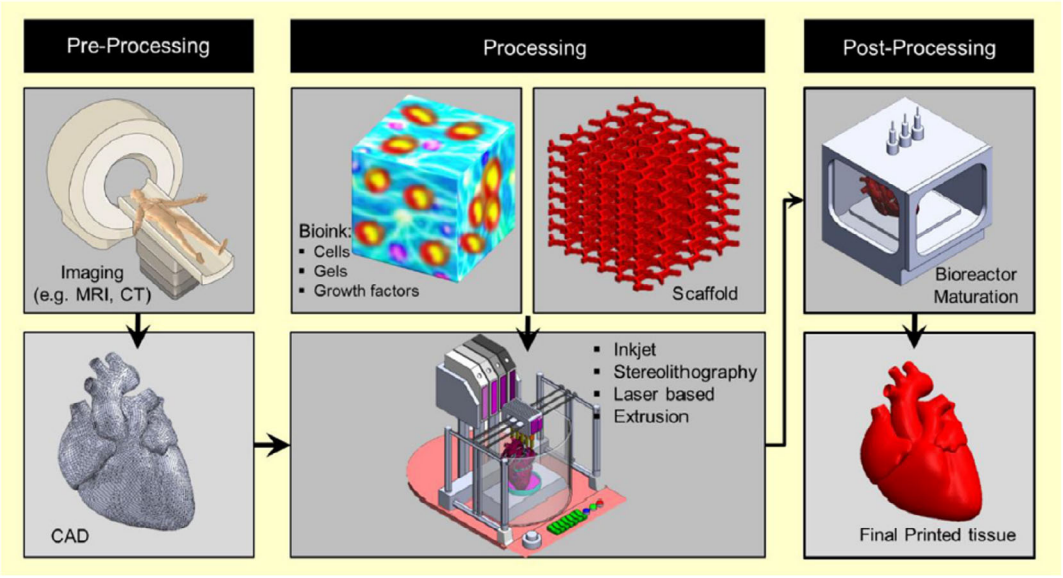


FIGURE 20 | An overview schematic illustrating the sequential stages of the bioprinting process. Reproduced with permission [245]. Copyright 2021, Frontiers.

vessels exemplify bioprinted tissues that illustrate the technology's growing potential for biomedical applications. Researchers have effectively employed a dual-material printing process in 3D bioprinting to fabricate a left ventricular model, utilizing a blend of cardiomyocytes and collagen to reproduce complex, functional biological structures (refer Figure 21) [246].

Among these developments, AI has become increasingly important since it improves bioprinting processes' reliability, efficiency, and accuracy. Figure 22 underscores the evolution of 3D bioprinting from a laboratory technique to a clinically applicable technology, propelled by the incorporation of AI [247]. It delineates a systematic, quality-by-design (QbD) approach that integrally links every phase of the bioprinting process encompassing bioink formulation, anatomical modeling, printing, maturation, and functional evaluation. This methodology guarantees precision, reliability, and biological functionality at each stage through the integration of AI-driven data analysis, sophisticated sensing technologies, and real-time process management. The framework is intended to enable the production of patient-specific, bioengineered tissues that may safely move from laboratory settings to clinical use [247].

Several enterprises have commenced employing EAM techniques for biological applications. Lithoz GmbH utilizes feedstocks that can be extruded to create bioresorbable ceramic scaffolds tailored to the specific requirements of each patient. Similarly, 3DCeram has developed RC methods capable of producing bespoke cranial implants and dental restorations. The commercial applications demonstrate the versatility of EAM in producing biocompatible components with regulated porosity and intricate geometries. Despite increased adoption across several industries, obtaining regulatory permission remains a significant challenge.

15272648, 2026, 16, Downloaded from https://advanced.onlinelibrary.wiley.com/doi/10.1002/adem.71089 by Abdollah Saboori - Politecnico Di Torino Sist. Bibl Del Polit Di Torino , Wiley Online Library on [27/09/2026]. See the Terms and Conditions (https://onlinelibrary.wiley.com/terms-and-conditions) on Wiley Online Library for rules of use; OA articles are governed by the applicable Creative Commons License

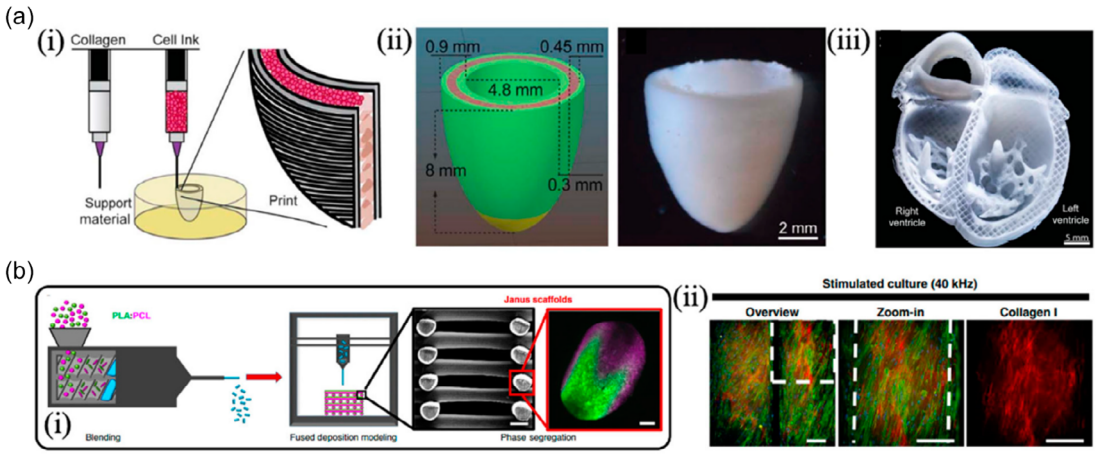


FIGURE 21 | (a) (i) Dual-material printing based on collagen ink and cell ink schematically shown here. (ii) Model and micrograph of a printed ventricle including cardiac cells, collagen shells, and a section dedicated only to collagen. (iii) High-fidelity image of the trabeculae in the left ventricle and the septal wall separating ventricles, together with a cross-sectional view of the collagen heart. (b) (i) Schematic map of the method to produce phase-segregated scaffolds under dynamic conditions. (ii) Bone mesenchymal stem cells grown for 21 days on Janus scaffolds show collagen deposition. Reproduced with permission [246]. Copyright 2019, American Association for the Advancement of Science (AAAS).

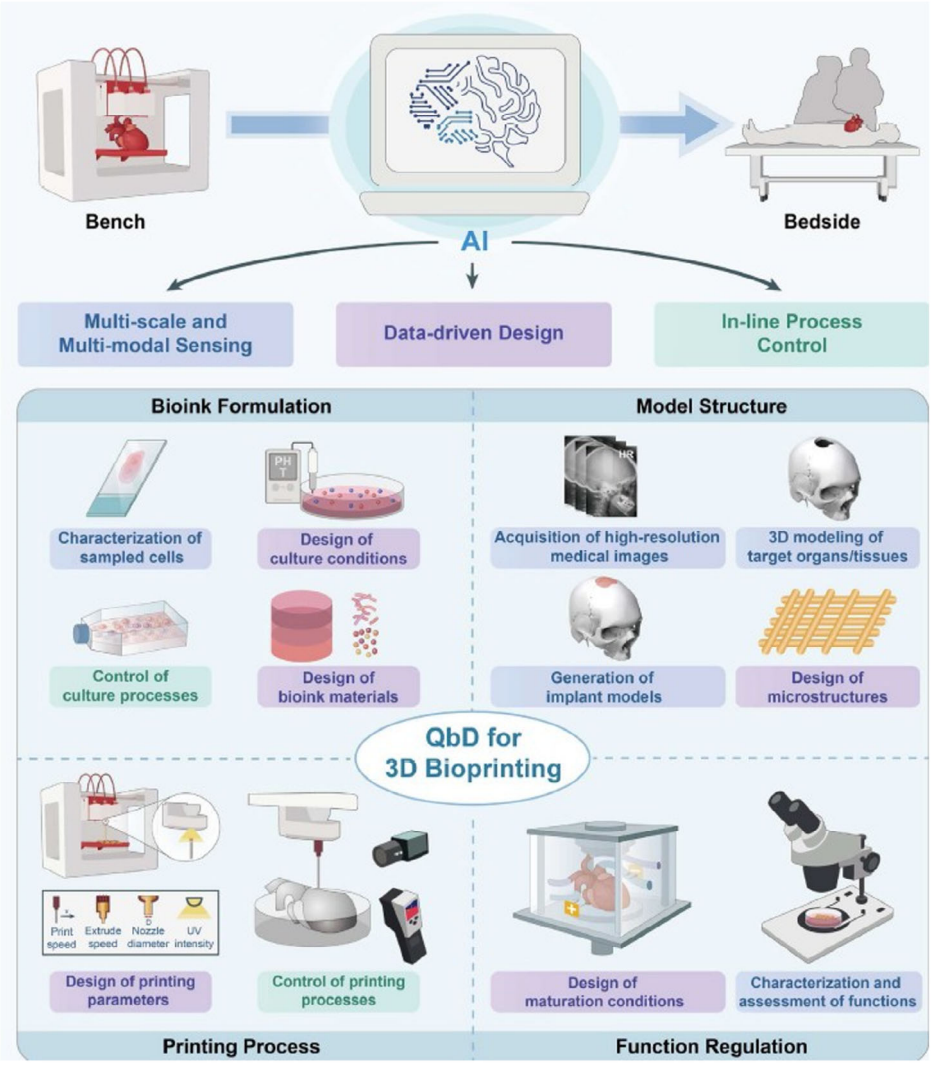


FIGURE 22 | Roadmap of AI-driven QbD for 3D bioprinting. Reproduced with permission [247]. Copyright 2025, Elsevier.

15272648, 2026, 16, Downloaded from https://advanced.onlinelibrary.wiley.com/doi/10.1002/adem.71089 by Abdollah Saboori - Politecnico Di Torino Sist. Bibl Del Polit Di Torino , Wiley Online Library on [27/09/2026]. See the Terms and Conditions (https://onlinelibrary.wiley.com/terms-and-conditions) on Wiley Online Library for rules of use; OA articles are governed by the applicable Creative Commons License

Ceramic implants must comply with the biocompatibility criteria established by ISO 10993 and the regulatory norms of FDA Class III or CE marking, contingent upon their market location. Standard testing methods for additively made ceramics are lacking, complicating their rapid application in clinical environments, particularly for load-bearing implants.

6.2 | Aerospace and High-Temperature Applications

Advanced ceramics EAM shows remarkable properties suitable for demanding conditions including high temperatures, corrosive surroundings, and heavy mechanical loads. Notable materials include reinforced zirconia composites, which have been directly produced into complex forms for aerospace propulsion, thermal protection systems, and insulating components [248]. UHTCs, such as ZrB_2, HfC, are also widely used. These materials are essential for lightweight structural elements and hypersonic vehicle nose cones. The layer-by-layer management of the technology helps to build complex structures improving thermal shock resistance and lowering thermal conductivity. The aerospace and defense sectors benefit from the ability to quickly prototype and improve new designs for engine components, nozzles, and other necessary elements in cases when conventional ceramic production becomes economically unfeasible due to tooling costs and geometric restrictions [249, 250]. As an example, ceramic heaters exhibiting a positive temperature coefficient of resistance (PTCR) can be fabricated by AM, providing improved performance for automotive and aerospace applications. This work emphasizes the successful production of PTCR heating elements in various forms and sizes, including complex honeycomb lattice structures, with a single MEX technique. These findings highlight the versatility and efficacy of AM in producing intricate heater designs (refer Figure 23) [251].

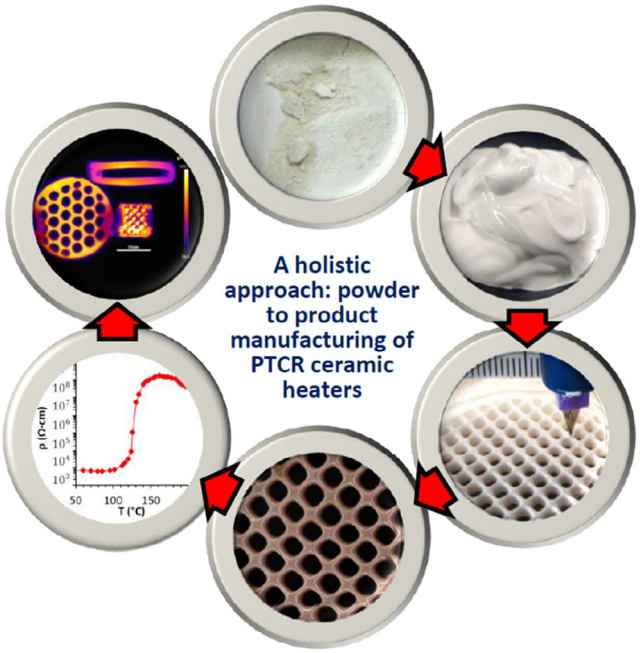


FIGURE 23 | Process of making PTCR ceramic heaters. Reproduced with permission [251]. Copyright 2019, Loughborough University.

The RC process successfully produced a series of ceramic heating elements with well-defined geometries and tailored porosity, as illustrated in Figure 24 [251, 252].

The sequential printing of a hollow circular heating element is shown in Figure 24a, followed by the deposition of a honeycomb-structured specimen using a 50 mm nozzle (Figure 24b). Whereas the top view (Figure 24d) guarantees the homogeneity of the honeycomb pore structure before sintering, the side view of the as-printed green body (Figure 24c) reveals exact layer stacking with consistent interlayer adhesion. The optical micrograph in Figure 24e shows a full-size, sintered specimen measuring roughly 40 mm in diameter, thus postsintering the honeycomb elements maintained their structural integrity with minimum dimensional shrinkage. With an average pore size of 5 mm, a higher magnification image (Figure 24f) shows the sintered

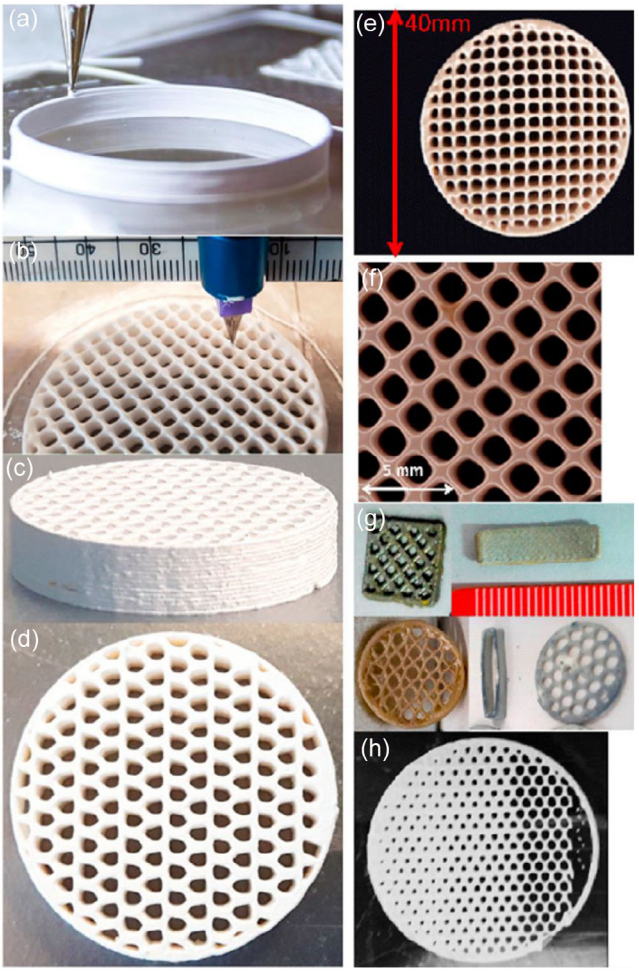


FIGURE 24 | (a) Image of a hollow circular heating element in the printing process, (b) image of the RC nozzle 3D printing the foundational layers of a honeycomb heating element (50 mm diameter), (c) lateral perspective of green printed BT honeycomb specimen, (d) superior perspective of green printed BT honeycomb specimen, (e) top view optical micrograph of a sintered full-size honeycomb heating element, (f) optical micrograph of a sintered heating element featuring a square grid structure, (g) images of typical circular, elliptical, square, and rectangular strip-printed heating elements exhibit customizable porosity, and (h) a 3D-printed green sample featuring a graded porous structure. Reproduced with permission [252]. Copyright 2019, Elsevier.

15272648, 2026, 16, Downloaded from https://advanced.onlinelibrary.wiley.com/doi/10.1002/adem.71088 by Abdollah Saboori - Politecnico Di Torino Sist. Bibl Del Polit Di Torino , Wiley Online Library on [27/09/2026]. See the Terms and Conditions (https://onlinelibrary.wiley.com/terms-and-conditions) on Wiley Online Library for rules of use; OA articles are governed by the applicable Creative Commons License

open-cell grid with outstanding homogeneity of density during sintering, so reflecting the printed geometry. Figure 24g shows a range of sintered heating elements made in different geometries, including square, rectangular, and circular forms, so stressing the adaptability of the RC method for creating bespoke parts. By simply changing the nozzle path and print parameters, the porosity and internal architecture of these elements could be readily tuned, so allowing the production of components with mechanical and thermal characteristics relevant to their application. Especially, Figure 24h shows a 3D-printed green sample with a graded porous architecture, demonstrating the capacity of the technique to generate functionally graded materials (FGMs) with either continuous or discrete porosity variations, providing improved performance in applications needing either controlled fluid flow or tailored heat distribution [252].

In another study, Schwarzer-Fischer et al. [253] developed alumina-based photocurable ceramic resins specifically for the additive fabrication of cold-gas satellite thrusters capable of producing 2.5 and 10 N of thrust (refer Figure 25). The authors emphasized the significant role of monomer selection in determining the rheological properties of the resin during printing. They emphasized the necessity of precise resin formulation to achieve a regulated and effective debinding degree. This modification ultimately enabled the production of components with a final sintered density exceeding 99% of the theoretical value.

Companies such as HRL Laboratories and 3DCeram are employing EAM to produce UHTC components, including heat shields and thruster nozzles, for the aerospace sector. These components must withstand severe temperatures and oxidative environments [254]. NASA has funded programs exploring DIW and RC for the development of CMCs intended for reusable hypersonic vehicles. Aerospace applications have stringent qualifying criteria, including reliable performance under extreme conditions and compliance with ASTM C1161 (flexural strength), ASTM C1421 (fracture toughness), and AS9100D production standards. The absence of long-term performance data on AM ceramics complicates the acquisition of aeronautical certification for additional applications.

Although EAM has demonstrated potential in biomedical and structural ceramic applications, there are still significant gaps in regulatory frameworks and certification readiness. Which specific ASTM or ISO standards need to be developed or adapted to validate mechanical performance and durability of EAM-printed parts? How can repeatability and reproducibility be established under variable environmental and printer-specific conditions? In high-stakes sectors such as aerospace or clinical implants, what technical evidence or long-term reliability data are needed to gain regulatory approval for EAM components, and how can the qualification process be streamlined for customized or patient-specific geometries?

6.3 | Electronics and Energy: Sensors, Actuators, and Functional Devices

The rising demand for high-performance, compact, and multifunctional electronic devices has prompted significant research into improved ceramic materials due to their superior mechanical strength, thermal stability, electrical insulation, and piezoelectric characteristics. EAM is gaining favor in the energy and electrical industries for producing ceramic components with complex geometries and multimaterial interfaces. It involves the fabrication of sensors, capacitors, piezoelectric actuators, and dielectric substrates using advanced electrotechnical ceramics including barium titanate ($BaTiO_3$), alumina, and silicon carbide. Accurate positioning of functional elements, small channels, and gradients improving device performance and integration is made possible by extrusion-based printing. Micropatterned solid oxide fuel cell components, high-surface-area electrodes, ionic conductors, and flexible sensor systems are fabricated with EAM. The process's flexibility helps to create custom ceramic enclosures for small electronics and enables the direct deposition of lead zirconate titanate (PZT) for piezoelectric devices. Extrusion-printed ceramics find use in battery electrodes, fuel cell microtubular supports, and thermoelectric modules in the rapidly expanding fields of energy storage and harvesting. The emergence of functional inks using 2D materials like graphene or MXenes has initiated a novel phase of flexible, high-conductivity device layers. Additionally, the alteration of microstructure by the incorporation of whiskers, fibers, or nanoparticles aims to enhance both electrical and mechanical performance [255–257].

The direct synthesis of geometrically intricate piezoelectric devices, crucial for sophisticated intelligent sensors, transducers, and energy harvesters, has been facilitated by EAM. In contrast to conventional mold-based methods, EAM enables the alteration

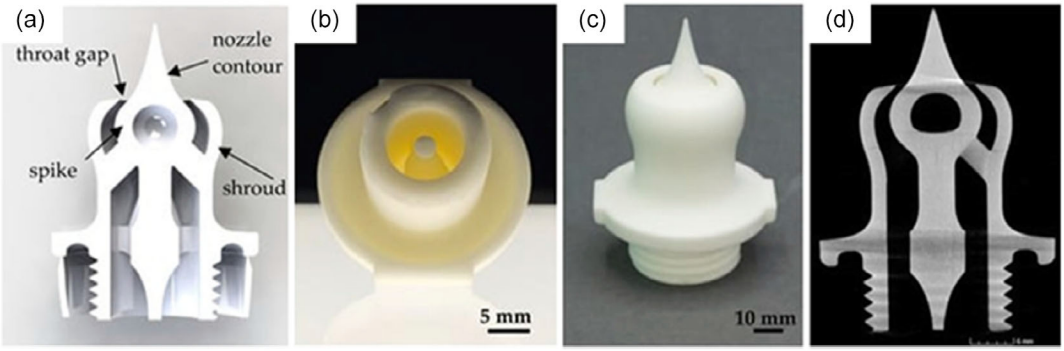


FIGURE 25 | Al_2O_3 nozzles produced via additive manufacturing utilizing the CeraFab 7500 printing apparatus. Sectional representation of an aerospike nozzle (a), 2.5 N nozzle (b), 10 N nozzle (c), and computed tomography image of the 10 N nozzle (d). Reproduced with permission [253]. Copyright 2022, MDPI.

15272648, 2026, 16, Downloaded from https://advanced.onlinelibrary.wiley.com/doi/10.1002/adem.71088 by Abdollah Saboori - Politecnico Di Torino Sist. Bibl Del Polit Di Torino , Wiley Online Library on [27/09/2026]. See the Terms and Conditions (https://onlinelibrary.wiley.com/terms-and-conditions) on Wiley Online Library for rules of use; OA articles are governed by the applicable Creative Commons License

of functional connectivity while promoting rapid prototyping and small-scale manufacturing of innovative device designs, such as multilayer stacks, honeycomb configurations, and curved geometries (Figure 26) [258].

Extrusion-based 3D printing has also opened new possibilities for creating high surface-area electrodes used in batteries and supercapacitors. By using direct ink writing to print graphene–ceramic composites, researchers can fine-tune both the porosity and the pathways for charge transport, leading to better energy storage performance and longer device lifespans [259, 260]. Tethon3D and other firms produce printable ceramic pastes utilized for the fabrication of dielectric layers, sensors, and insulating substrates in electronics. CeramTec and Kyocera are exploring EAM for the production of multimaterial ceramic packages for compact energy systems and embedded electronic modules. The design flexibility of EAM is particularly advantageous for applications involving components that are non-planar or multilayered.

7 | Classification of Defect and Porosities

Based on the provided sources, pores can be classified into different categories based on their characteristics. They are generally smaller than the dimensions of the grains in the structure and can be open, blind, through, or closed. Some of these pores are known as engineering porosities and can be controlled by adjusting temperature and sintering time. In addition, porosities related to sintering and hollow defects may also occur in the structure due to extrusion processes or as by-products of manufacturing and processing [261–263]. Figure 27 illustrates the type of porosities in AM of advanced ceramics.

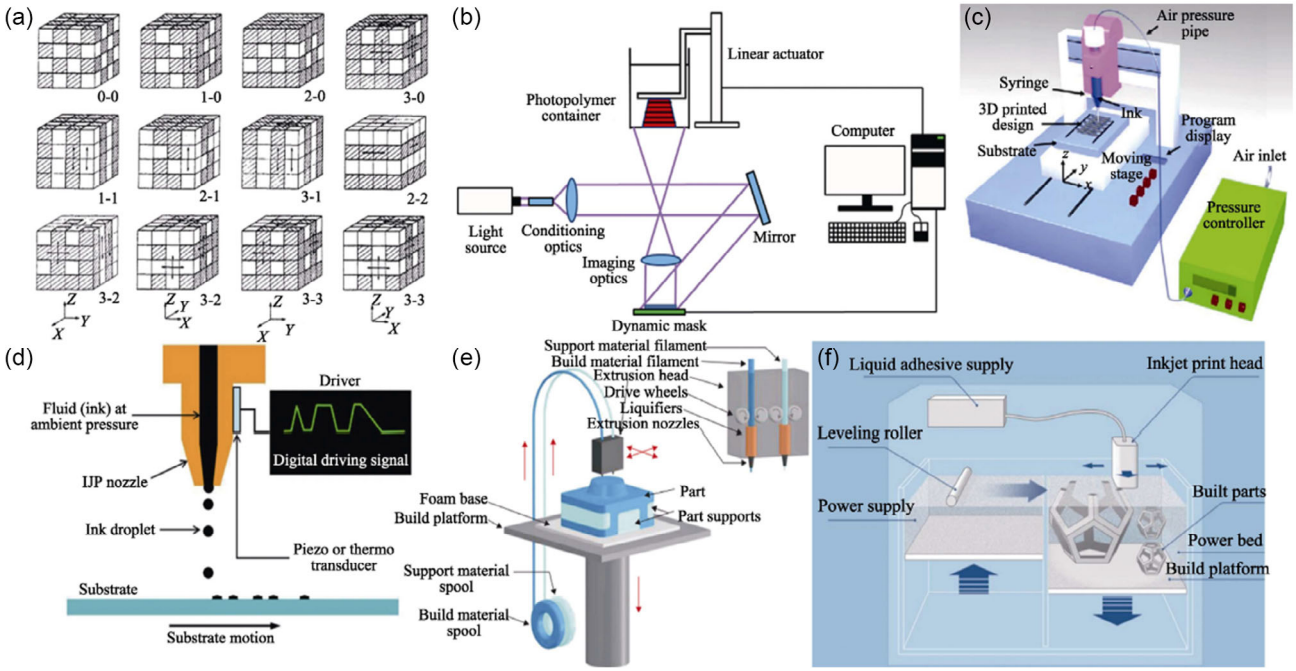


FIGURE 26 | Connections of piezoelectric ceramics and graphic representations of commonly utilized additive manufacturing techniques for the preparation of piezoelectric ceramics. Reproduced with permission [258]. Copyright 2022, Science Press.

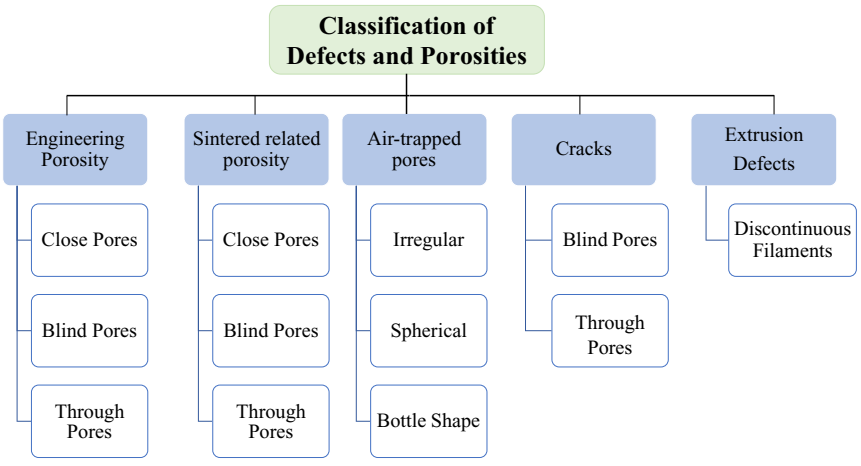


FIGURE 27 | Type of porosities in AM of advanced ceramic.

15272648, 2026, 16, Downloaded from https://advanced.onlinelibrary.wiley.com/doi/10.1002/adem.71089 by Abdollah Saboori - Politecnico Di Torino Sist. Bibl Del Polit Di Torino , Wiley Online Library on [27/09/2026]. See the Terms and Conditions (https://onlinelibrary.wiley.com/terms-and-conditions) on Wiley Online Library for rules of use; OA articles are governed by the applicable Creative Commons License

In EAM methods, technical extrusion problems such as improper velocity and nozzle clogging temporarily interrupt melt flow from the nozzle and create pores in the fabricated layers. The suspension in the nozzle itself can have bubbles [170]. These bubbles can cause closed pores inside the grains to join and cause cracking during debinding and sintering [262]. As a result, ceramic parts made by AM technologies can have several types of hollow defects, including intergranular porosities, air cavities, cracks, and gaps [37]. Intergranular porosity results from poor compression during sintering when pressure is not used. The wide distribution of intergranular pores results from the gradient of suspension density inside the printer. This is where the air bubbles enter the created suspension, which is considered a negative factor. Cracks also form due to capillary suction forces between the particles during drying [37]. Pores and defects size scale in extrusion 3D ceramic printing are shown in Figure 28.

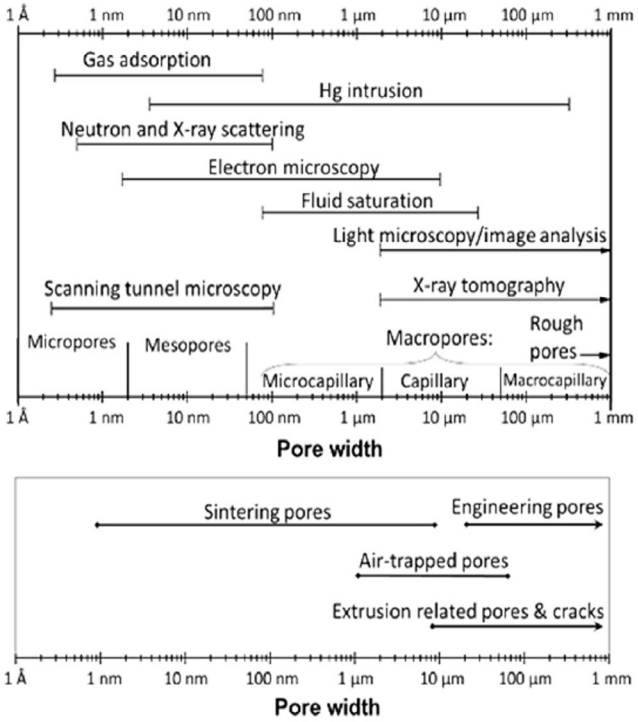


FIGURE 28 | Investigation of porosities and defects length in EAM ceramics. Reproduced with permission [37]. Copyright 2021, Elsevier.

7.1 | Detection Method of Porosities

Examining porosities and their essential parameters, such as volume fraction, porosity size distribution, defect length, topology distribution, and geometry, enables researchers to investigate what has happened in the structure [264, 265]. In this regard, there are many methods to determine the porosities and their effective parameters [266, 267]. Detection methods to assess the porosities and defects are presented in Figure 29.

In general, MIP, N_2 adsorption, and water saturation methods are desirable for detecting open pores at different longitudinal scales, and N_2 adsorption and MIP are used to detect the size distribution of porosities using theoretical models [265]. 2D image analysis reaches the nature of three-dimensional porosities and their parameters by analyzing the porous regions observed on the two-dimensional cross section, which are specifically dependent on the morphology of the pores. If the pore size exceeds the 3D rendering resolution, the 3D analysis by µCT method can be used. Figure 30 displays a micro-CT (µ-CT) schematic as a defect detection method.

SEM can be used for small pores to examine the surface morphology and porosity distribution. The set of open and closed porosities depends on the total volume of pores and the apparent volume of the material. It can be proportional to them, thus obtaining the difference between total and open porosity, indicating closed porosity [269]. MIP, N_2 adsorption, and µ-CT can be used to study quantitatively the distribution of porosity sizes at the nano- and microscale. Other inexpensive methods provide good information, such as water saturation and the apparent and structural density ratio study. Of course, while using several

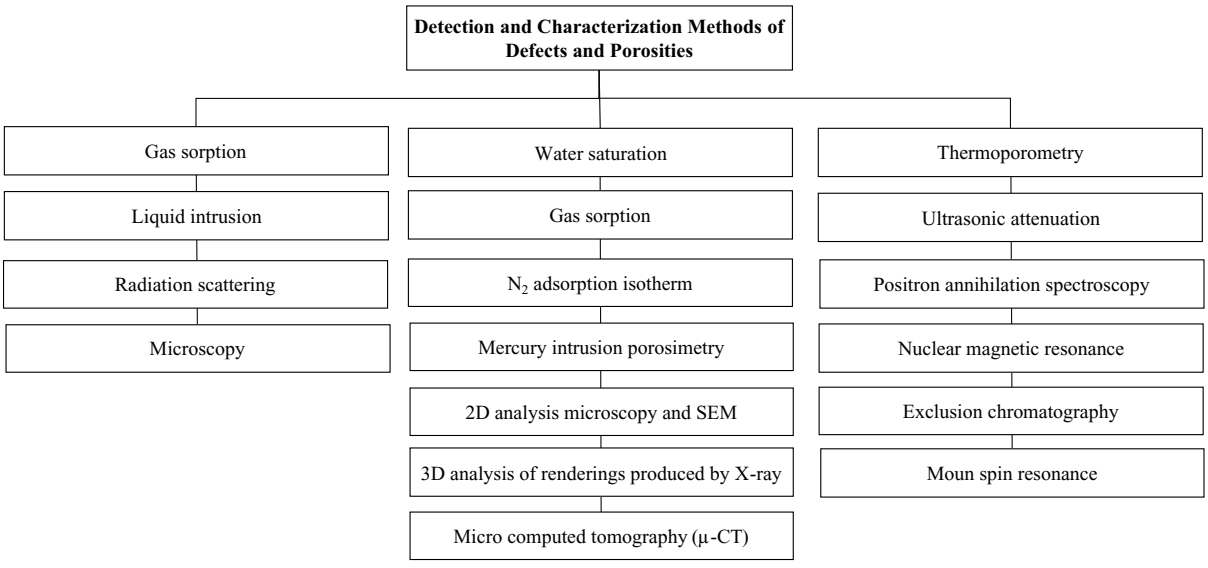


FIGURE 29 | Detection and characterization methods of defects and porosities.

15272648, 2026, 16, Downloaded from https://advanced.onlinelibrary.wiley.com/doi/10.1002/adem.71088 by Abdollah Saboori - Politecnico Di Torino Sist. Bibl Del Polit Di Torino , Wiley Online Library on [27/09/2026]. See the Terms and Conditions (https://onlinelibrary.wiley.com/terms-and-conditions) on Wiley Online Library for rules of use; OA articles are governed by the applicable Creative Commons License

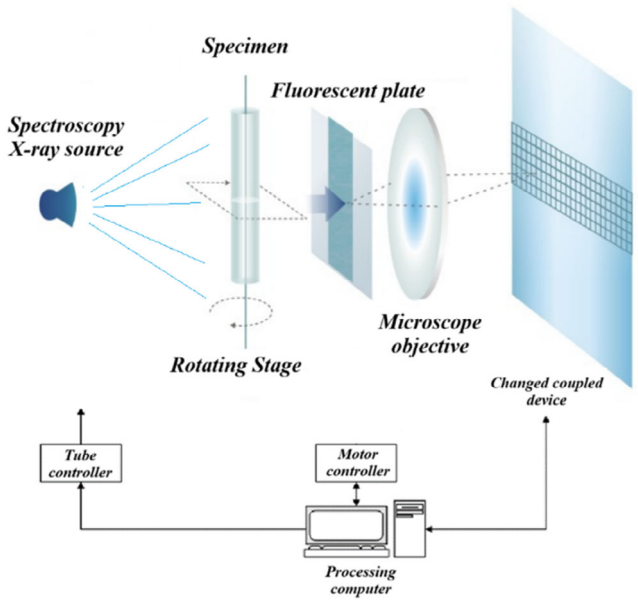


FIGURE 30 | Schematic of micro-computed tomography (μ-CT). Reproduced with permission [268]. Copyright 2012, IntechOpen.

methods, differences in the numbers obtained to understand the size and number may occur, which is due to differences in the basics defined for each method to identify, measure, and escape, and ultimately, choosing the correct method required for accurate analysis of the size of specific pores of the material in question, the shape and geometric dimensions of the part investigated, and the tools needed to work [270, 271]. The advantages, disadvantages, and limitations of the detection and characterization methods of defects are presented in Figure 31.

Recent developments in in situ structural health monitoring and machine learning applications have significantly enhanced flaw detection in EAM. Continuous monitoring of internal state changes made possible by the integration of self-sensing fibers in the printed structure facilitates the early identification of defect formation. Machine learning algorithms trained on large datasets derived from imaging or sensor inputs have demonstrated a 25%–30% improvement in detection sensitivity and reliability compared to conventional nondestructive testing methods. This enables real-time defect classification and supports adaptive process control. Furthermore, the creation of digital twins and self-reporting composites helps to create dynamic feedback loops bridging the gap between intelligent defect mitigation and process monitoring [272].

8 | Conclusion

This review has examined the current landscape of AM technologies for advanced ceramics, with particular emphasis on extrusion-based methods. AM offers transformative potential for the ceramics industry by enabling greater design flexibility, reduced material waste, and cost-effective production of geometrically complex, low-volume components. Despite its advantages over traditional techniques such as injection molding, the AM of ceramics remains significantly more challenging than that of polymers or metals because of the intrinsic properties of ceramics, including high melting points, brittleness, and low defect tolerance. Although notable progress has been made over the past two decades, the widespread industrial adoption of ceramic AM is still constrained by unresolved technical limitations and insufficient process standardization. The selection of a suitable AM process depends on multiple criteria, including material type, target part density, surface finish, dimensional requirements, and application-specific performance. While some AM technologies and ceramic formulations have demonstrated mechanical performance comparable to conventionally manufactured parts, consistent quality remains difficult to achieve. Defects such as intergranular porosity, trapped-air voids, and microcracks, often introduced during extrusion, drying, debinding, or sintering, continue to undermine structural integrity. These defects may also overlap with intentionally designed porosity, making performance prediction more complex. Therefore, pre- and postprocessing techniques remain indispensable for improving surface quality, densification, microstructural integrity, and mechanical

Method	Advantages	Disadvantages	Limitations
N_2 adsorption	Accurate Provides pore size distribution Non-destructive	Sample degassing Requires the skeletal density of the material	Open pores
Water saturation	Easy and cheap Non-destructive	No pore size distribution. No pore shape determined No useful for sensible to corrosion or water-reactive materials Generally underestimated values	Open pores
2D image analysis	Direct visualization of pores Possible estimation of pore size and other geometrical parameters	Destructive Large number of images at different magnifications Extrapolation of 2D results. Not always provide reliable estimations	Open and closed pores
μ-CT	Accurate Direct visualization of pores in 3D Reliable estimation of pore size and other geometrical parameters Non-destructive	Smallest detectable feature depends on the linear voxel size. Time-consuming processing of the results	Open and closed pores
MIP	Accurate Provides pore size distribution	Destructive. Sample must be inert with mercury Restricted to small samples Mercury is highly toxic	Open pores

FIGURE 31 | Advantages and disadvantages of porosity detection methods.

15272648, 2026, 16, Downloaded from https://advanced.onlinelibrary.wiley.com/doi/10.1002/adem.71089 by Abdollah Saboori - Politecnico Di Torino Sist. Bibl Del Polit Di Torino , Wiley Online Library on [27/09/2026]. See the Terms and Conditions (https://onlinelibrary.wiley.com/terms-and-conditions) on Wiley Online Library for rules of use; OA articles are governed by the applicable Creative Commons License

robustness. Future research in ceramic EAM should focus on four closely connected areas: materials, processes, applications, and detection. A major materials challenge is the development of ceramic feedstocks with high solid loading while maintaining sufficient flexibility, stable rheological behavior, clean debinding, and low sintering shrinkage. This issue is especially critical for ceramic filaments and thermoplastic feedstocks, where increasing ceramic content can improve final densification but may also increase brittleness, feeding instability, and extrusion difficulty. Further progress will require improved binder systems, optimized particle size distributions, powder surface modification, printable multimaterial formulations, and feedstocks suitable for UHTC systems. More reliable process control is also required to improve deposition stability, interlayer bonding, dimensional accuracy, and defect suppression. Key challenges include nozzle clogging, filament swelling, layer misalignment, anisotropic shrinkage, drying-induced deformation, and sintering distortion. These limitations can be addressed through adaptive toolpath planning, optimized nozzle design, real-time parameter adjustment, and predictive process modeling. Application-oriented research should move beyond demonstrating printable geometries toward qualification of ceramic EAM components for biomedical, aerospace, thermal protection, electronic, sensor, and energy-related systems. In parallel, in situ monitoring and intelligent defect recognition should become integral parts of future ceramic EAM platforms. Early detection of filament discontinuity, pore formation, interlayer gaps, crack initiation, surface irregularities, and sintering-induced deformation, supported by machine vision, thermal monitoring, pressure feedback, extrusion-force measurement, acoustic sensing, and AI-assisted analysis, will be essential for improving repeatability, reliability, and industrial scalability.

Acknowledgments

The authors have nothing to report.

Open access publishing facilitated by Politecnico di Torino, as part of the Wiley - CRUI-CARE agreement.

Funding

The authors have nothing to report.

Conflicts of Interest

The authors declare no conflicts of interest.

Data Availability Statement

The data that support the findings of this study are available from the corresponding author upon reasonable request.

References

1. I. Gibson, D. W. Rosen, B. Stucker, et al., *Additive Manufacturing Technologies* (Springer, 2021).

2. R. Ghanavati, E. Lannunziata, E. Norouzi, S. Bagherifard, L. Iuliano, and A. Saboori, "Design and Development of SS316L-IN718 Functionally Graded Materials via Laser Powder Bed Fusion," *Materials Letters* 349 (2023): 134793.

3. A. Saboori, M. Toushekhah, A. Aversa, et al., "Critical Features in the Microstructural Analysis of AISI. 316L Produced by Metal Additive Manufacturing," *Metallography, Microstructure, and Analysis* 9, no. 1 (2020): 92–96.

4. P. Fino, L. Montanaro, M. Lombardi, S. Biamino, and A. Saboori, "In Situ Synthesis, Densification and Shaping of Non-Oxide Ceramics by Vacuum Additive Manufacturing Technologies," ed: Google Patents, 2024.

5. J. Farajian, O. Hatami, M. Bakhtiari, B. Darabinajand, and M. Mahboubkhah, "Investigation of Mechanical Properties of 3D-Printed PLA Coated with PU/MWCNTs in a Corrosive Environment," *Arabian Journal for Science and Engineering* 49, no. 8 (2024): 11181–11193, https://doi.org/10.1007/s13369-023-08632-9.

6. K. Shahzad, J. Deckers, J.-P. Kruth, and J. Vleugels, "Additive Manufacturing of Alumina Parts by Indirect Selective Laser Sintering and Post Processing," *Journal of Materials Processing Technology* 213, no. 9 (2013): 1484–1494, https://doi.org/10.1016/j.jmatprotec.2013.03.014.

7. M. Dadkhah, J.-M. Tulliani, A. Saboori, and L. Iuliano, "Additive Manufacturing of Ceramics: Advances, Challenges, and Outlook," *Journal of the European Ceramic Society* 43, no. 15 (2023): 6635–6664, https://doi.org/10.1016/j.jeurceramsoc.2023.07.033.

8. D. Jang, D. Kim, and J. Moon, "Influence of Fluid Physical Properties on Ink-Jet Printability," *Langmuir* 25, no. 5 (2009): 2629–2635, https://doi.org/10.1021/la900059m.

9. E. Lannunziata, M. H. Mosallanejad, M. Galati, G. Piscopo, and A. Saboori, "Analyzing the Interplay of Sintering Conditions on Microstructure and Hardness in Indirect Additive Manufacturing of 17-4PH Stainless Steel," *Acta Metallurgica Sinica (English Letters)* 37, no. 9 (2024): 1611–1620.

10. Z. Chen, Z. Li, J. Li, et al., "3D Printing of Ceramics: A Review," *Journal of the European Ceramic Society* 39, no. 4 (2019): 661–687, https://doi.org/10.1016/j.jeurceramsoc.2018.11.013.

11. G. Zhang, J. Gu, H. Shi, et al., "Microstructures and Mechanical Properties Analysis of TiAl Joints Using Novel Brazing Filler Metal," *Welding in the World* 70, no. 6 (2026): 2237–2251, https://doi.org/10.1007/s40194-025-02210-3.

12. Z. Yang, J. Yi, F. Li, et al., "Static Mechanical Cloaking and Camouflage From Disorder," *Nature Communications* 16, no. 1 (2025): 8858, https://doi.org/10.1038/s41467-025-63939-5.

13. C. Y. Yap, C. K. Chua, Z. L. Dong, et al., "Review of Selective Laser Melting: Materials and Applications," *Applied Physics Reviews* 2, no. 4 (2015): 041101, https://doi.org/10.1063/1.4935926.

14. R. Lian, X. Xu, K. Zhao, X. Fei, W. Cao, and J. Zhu, "Advancements in Laser Processes for Additive Manufacturing: Techniques and Future Directions," *Journal of Materials Research and Technology* 41 (2026): 2428–2451, https://doi.org/10.1016/j.jmrt.2026.01.173.

15. E. Juste, F. Petit, V. Lardot, and F. Cambier, "Shaping of Ceramic Parts by Selective Laser Melting of Powder Bed," *Journal of Materials Research* 29, no. 17 (2014): 2086–2094, https://doi.org/10.1557/jmr.2014.127.

16. P. Klobes and R. Munro, *Porosity and Specific Surface Area Measurements for Solid Materials* (Special Publication (NIST SP), National Institute of Standards and Technology, 2006).

17. T. Chartier, M. Ferrato, and J. J. C. Baumard, "Debinding of Ceramics: A Review," *Ceramicaacta* 6 (1994): 17–27.

18. Q. Wang, X. Chen, Q. An, M. Chen, H. Guo, and Y. He, "Optimization Strategy for Tool Life Based on Dynamic Modal Parameter Identification," *International Journal of Advanced Manufacturing Technology* 139, no. 1 (2025): 343–353, https://doi.org/10.1007/s00170-025-15902-3.

19. M. Schwentenwein and J. Homa, "Additive Manufacturing of Dense Alumina Ceramics," *International Journal of Applied Ceramic Technology* 12, no. 1 (2015): 1–7, https://doi.org/10.1111/ijac.12319.

15272648, 2026, 16, Downloaded from https://advanced.onlinelibrary.wiley.com/doi/10.1002/adem.71089 by Abdollah Saboori - Politecnico Di Torino Sist. Bibl Del Polit Di Torino , Wiley Online Library on [27/09/2026]. See the Terms and Conditions (https://onlinelibrary.wiley.com/terms-and-conditions) on Wiley Online Library for rules of use; OA articles are governed by the applicable Creative Commons License

20. T. J. Hensen, T. G. Aguirre, C. L. Cramer, et al., "Additive Manufacturing of Ceramic Nanopowder by Direct Coagulation Printing," *Additive Manufacturing* 23 (2018): 140–150, https://doi.org/10.1016/j.addma.2018.07.010.

21. B. Ren, J. Liu, Y. Wang, et al., "Hierarchical Cellular Scaffolds Fabricated via Direct Foam Writing Using Gelled Colloidal Particle-Stabilized Foams as the Ink," *Journal of the American Ceramic Society* 102, no. 11 (2019): 6498–6506, https://doi.org/10.1111/jace.16543.

22. W. M. Sigmund, N. S. Bell, and L. Bergström, "Novel Powder-Processing Methods for Advanced Ceramics," *Journal of the American Ceramic Society* 83, no. 7 (2000): 1557–1574, https://doi.org/10.1111/j.1151-2916.2000.tb01432.x.

23. A. Badev, Y. Abouliatim, T. Chartier, et al., "Photopolymerization Kinetics of a Polyether Acrylate in the Presence of Ceramic Fillers Used in Stereolithography," *Journal of Photochemistry and Photobiology A: Chemistry* 222, no. 1 (2011): 117–122, https://doi.org/10.1016/j.jphotochem.2011.05.010.

24. M. Fanous, S. Gold, S. Muller, S. Hirsch, J. Ogorka, and G. Imanidis, "Simplification of Fused Deposition Modeling 3D-Printing Paradigm: Feasibility of 1-Step Direct Powder Printing for Immediate Release Dosage Form Production," *International Journal of Pharmaceutics* 578 (2020): 119124, https://doi.org/10.1016/j.ijpharm.2020.119124.

25. A. Goyanes, N. Allahham, S. J. Trenfield, E. Stoyanov, S. Gaisford, and A. W. Basit, "Direct Powder Extrusion 3D Printing: Fabrication of Drug Products Using a Novel Single-Step Process," *International Journal of Pharmaceutics* 567 (2019): 118471, https://doi.org/10.1016/j.ijpharm.2019.118471.

26. T. A. Baer, J. Cesarano III, and P. Calvert, "Recent Developments in Freeform Fabrication of Dense Ceramics From Slurry Deposition," in *Proceedings of the 8th Annual International Solid Freeform Fabrication* (University of Texas at Austin, 1997), 25–32.

27. M.-C. Leu, L. Tang, B. K. Deuser, et al., "Freeze-Form Extrusion Fabrication of Composite Structures," in *Proceedings of the 22nd Annual International Solid Freeform Fabrication Symposium* (University of Texas at Austin, 2011), 111–124.

28. L. Rueschhoff, W. Costakis, M. Michie, J. Youngblood, and R. Trice, "Additive Manufacturing of Dense Ceramic Parts via Direct Ink Writing of Aqueous Alumina Suspensions," *International Journal of Applied Ceramic Technology* 13, no. 5 (2016): 821–830, https://doi.org/10.1111/ijac.12557.

29. T. Schlordt, S. Schwanke, F. Keppner, T. Fey, N. Travitzky, and P. Greil, "Robocasting of Alumina Hollow Filament Lattice Structures," *Journal of the European Ceramic Society* 33, no. 15 (2013): 3243–3248, https://doi.org/10.1016/j.jeurceramsoc.2013.06.001.

30. W. J. Costakis, L. M. Rueschhoff, A. I. Diaz-Cano, J. P. Youngblood, and R. W. Trice, "Additive Manufacturing of Boron Carbide via Continuous Filament Direct Ink Writing of Aqueous Ceramic Suspensions," *Journal of the European Ceramic Society* 36, no. 14 (2016): 3249–3256, https://doi.org/10.1016/j.jeurceramsoc.2016.06.002.

31. F. J. Martínez-Vázquez, A. Pajares, and P. Miranda, "A Simple Graphite-Based Support Material for Robocasting of Ceramic Parts," *Journal of the European Ceramic Society* 38, no. 4 (2018): 2247–2250, https://doi.org/10.1016/j.jeurceramsoc.2017.10.016.

32. M. Acosta, V. L. Wiesner, C. J. Martinez, R. W. Trice, and J. P. Youngblood, "Effect of Polyvinylpyrrolidone Additions on the Rheology of Aqueous, Highly Loaded Alumina Suspensions," *Journal of the American Ceramic Society* 96, no. 5 (2013): 1372–1382, https://doi.org/10.1111/jace.12277.

33. S. S. Nadkarni and J. E. Smay, "Concentrated Barium Titanate Colloidal Gels Prepared by Bridging Flocculation for Use in Solid Freeform Fabrication," *Journal of the American Ceramic Society* 89, no. 1 (2006): 96–103, https://doi.org/10.1111/j.1551-2916.2005.00646.x.

34. L. C. Hwa, S. Rajoo, A. M. Noor, N. Ahmad, and M. B. Uday, "Recent Advances in 3D Printing of Porous Ceramics: A Review," *Current Opinion in Solid State and Materials Science* 21, no. 6 (2017): 323–347, https://doi.org/10.1016/j.cossms.2017.08.002.

35. J. A. Lewis, J. E. Smay, J. Stuecker, and J. Cesarano, "Direct Ink Writing of Three-Dimensional Ceramic Structures," *Journal of the American Ceramic Society* 89, no. 12 (2006): 3599–3609, https://doi.org/10.1111/j.1551-2916.2006.01382.x.

36. M. Mohammadi, P. Pascaud-Mathieu, V. Allizond, et al., "Robocasting of Single and Multi-Functional Calcium Phosphate Scaffolds and Its Hybridization with Conventional Techniques: Design, Fabrication and Characterization," *Applied Sciences* 10, no. 23 (2020): 8677.

37. L. Čelko, V. Gutiérrez-Cano, M. Casas-Luna, et al., "Characterization of Porosity and Hollow Defects in Ceramic Objects Built by Extrusion Additive Manufacturing," *Additive Manufacturing* 47 (2021): 102272, https://doi.org/10.1016/j.addma.2021.102272.

38. K. Cai, B. Román-Manso, J. E. Smay, et al., "Geometrically Complex Silicon Carbide Structures Fabricated by Robocasting," *Journal of the American Ceramic Society* 95, no. 8 (2012): 2660–2666, https://doi.org/10.1111/j.1551-2916.2012.05276.x.

39. E. Feilden, D. Glymond, E. Saiz, and L. Vandeperre, "High Temperature Strength of an Ultra High Temperature Ceramic Produced by Additive Manufacturing," *Ceramics International* 45, no. 15 (2019): 18210–18214, https://doi.org/10.1016/j.ceramint.2019.05.032.

40. L. Wahl, M. Lorenz, J. Biggemann, and N. Travitzky, "Robocasting of Reaction Bonded Silicon Carbide Structures," *Journal of the European Ceramic Society* 39, no. 15 (2019): 4520–4526, https://doi.org/10.1016/j.jeurceramsoc.2019.06.049.

41. J. E. Smay, J. Cesarano, and J. A. Lewis, "Colloidal Inks for Directed Assembly of 3-D Periodic Structures," *Langmuir* 18, no. 14 (2002): 5429–5437, https://doi.org/10.1021/la0257135.

42. B. A. Tuttle, J. E. Smay, J. Cesarano, et al., "Robocast Pb(Zr0.95Ti0.05) O3 Ceramic Monoliths and Composites," *Journal of the American Ceramic Society* 84, no. 4 (2001): 872–874, https://doi.org/10.1111/j.1151-2916.2001.tb00756.x.

43. E. Feilden, E. G.-T. Blanca, F. Giuliani, E. Saiz, and L. Vandeperre, "Robocasting of Structural Ceramic Parts with Hydrogel Inks," *Journal of the European Ceramic Society* 36, no. 10 (2016): 2525–2533, https://doi.org/10.1016/j.jeurceramsoc.2016.03.001.

44. Y. Xia, Z. Lu, J. Cao, K. Miao, J. Li, and D. Li, "Microstructure and Mechanical Property of Cf/SiC Core/Shell Composite Fabricated by Direct Ink Writing," *Scripta Materialia* 165 (2019): 84–88, https://doi.org/10.1016/j.scriptamat.2019.02.016.

45. J. W. Kemp, N. S. Hmeidat, and B. G. Compton, "Boron Nitride-Reinforced Polysilazane-Derived Ceramic Composites via Direct-Ink Writing," *Journal of the American Ceramic Society* 103, no. 8 (2020): 4043–4050, https://doi.org/10.1111/jace.17084.

46. P. Miranda, E. Saiz, K. Gryn, and A. P. Tomsia, "Sintering and Robocasting of β-Tricalcium Phosphate Scaffolds for Orthopaedic Applications," *Acta Biomaterialia* 2, no. 4 (2006): 457–466, https://doi.org/10.1016/j.actbio.2006.02.004.

47. H. Elsayed, F. Carraro, S. Agnoli, et al., "Direct Ink Writing of Silica-Carbon-Calcite Composite Scaffolds From a Silicone Resin and Fillers," *Journal of the European Ceramic Society* 38, no. 15 (2018): 5200–5207, https://doi.org/10.1016/j.jeurceramsoc.2018.07.049.

48. H. Shao, X. Yang, Y. He, et al., "Bioactive Glass-Reinforced Bioceramic Ink Writing Scaffolds: Sintering, Microstructure and Mechanical Behavior," *Biofabrication* 7, no. 3 (2015): 035010, https://doi.org/10.1088/1758-5090/7/3/035010.

49. G. Franchin, L. Wahl, and P. Colombo, "Direct Ink Writing of Ceramic Matrix Composite Structures," *Journal of the American*

15272648, 2026, 16, Downloaded from https://advanced.onlinelibrary.wiley.com/doi/10.1002/adem.71088 by Abdollah Saboori - Politecnico Di Torino Sist. Bibl Del Polit Di Torino , Wiley Online Library on [27/09/2026]. See the Terms and Conditions (https://onlinelibrary.wiley.com/terms-and-conditions) on Wiley Online Library for rules of use; OA articles are governed by the applicable Creative Commons License

Ceramic Society 100, no. 10 (2017): 4397–4401, https://doi.org/10.1111/jace.15045.

50. T. Huang, M. S. Mason, G. E. Hilmas, and M. C. Leu, "Freeze-Form Extrusion Fabrication of Ceramic Parts," *Virtual and Physical Prototyping* 1, no. 2 (2006): 93–100, https://doi.org/10.1080/17452750600649609.

51. M. P. Serdeczny, R. Comminal, D. B. Pedersen, and J. Spangenberg, "Experimental and Analytical Study of the Polymer Melt Flow through the Hot-End in Material Extrusion Additive Manufacturing," *Additive Manufacturing* 32 (2020): 100997, https://doi.org/10.1016/j.addma.2019.100997.

52. X. Ren, H. Shao, T. Lin, and H. Zheng, "3D Gel-Printing—An Additive Manufacturing Method for Producing Complex Shape Parts," *Materials & Design* 101 (2016): 80–87, https://doi.org/10.1016/j.matdes.2016.03.152.

53. W. Li, A. Armani, D. McMillen, M. Leu, G. Hilmas, and J. Watts, "Additive Manufacturing of Zirconia Parts with Organic Sacrificial Supports," *International Journal of Applied Ceramic Technology* 17, no. 4 (2020): 1544–1553, https://doi.org/10.1111/ijac.13520.

54. W. Li, A. Ghazanfari, D. McMillen, M. C. Leu, G. E. Hilmas, and J. Watts, "Fabricating Ceramic Components with Water Dissolvable Support Structures by the Ceramic On-Demand Extrusion Process," *CIRP Annals* 66, no. 1 (2017): 225–228, https://doi.org/10.1016/j.cirp.2017.04.129.

55. A. Ghazanfari, W. Li, M. Leu, J. Watts, and G. Hilmas, "Mechanical Characterization of Parts Produced by Ceramic on-Demand Extrusion Process," *International Journal of Applied Ceramic Technology* 14, no. 3 (2017): 486–494, https://doi.org/10.1111/ijac.12665.

56. W. Li, A. Ghazanfari, D. McMillen, M. C. Leu, G. E. Hilmas, and J. Watts, "Characterization of Zirconia Specimens Fabricated by Ceramic on-Demand Extrusion," *Ceramics International* 44, no. 11 (2018): 12245–12252, https://doi.org/10.1016/j.ceramint.2018.04.008.

57. J. A. Lewis, "Colloidal Processing of Ceramics," *Journal of the American Ceramic Society* 83, no. 10 (2000): 2341–2359, https://doi.org/10.1111/j.1151-2916.2000.tb01560.x.

58. L. J. P. D. T. Rueschhoff, "Ceramic Near-Net Shaped Processing Using Highly-Loaded Aqueous Suspensions," Ph.D. thesis, (Purdue University, ProQuest Dissertations Publishing, 2017).

59. D. McMillen, W. Li, M. C. Leu, G. E. Hilmas, and J. Watts, "Designed Extrudate for Additive Manufacturing of Zirconium Diboride by Ceramic on-Demand Extrusion," in *Proceedings of the 27th Annual International Solid Freeform Fabrication* (University of Texas at Austin, 2016), 929–938.

60. H. Gong, D. Snelling, K. Kardel, and A. Carrano, "Comparison of Stainless Steel 316L Parts Made by FDM- and SLM-Based Additive Manufacturing Processes," *JOM* 71, no. 3 (2019): 880–885, https://doi.org/10.1007/s11837-018-3207-3.

61. M. Agarwala, R. v Weeren, A. Bandyopadhyay, P. Whalen, A. Safari, and S. Danforth, "Fused Deposition of Ceramics and Metals: An Overview," in *Proceedings of the 7th Annual International Solid Freeform Fabrication* (University of Texas at Austin, 1996), 385–392.

62. K. Rane and M. Strano, "A Comprehensive Review of Extrusion-Based Additive Manufacturing Processes for Rapid Production of Metallic and Ceramic Parts," *Advances in Manufacturing* 7, no. 2 (2019): 155–173.

63. D. Kupp, H. Eifert, M. Greul, and M. Kunstner, "Rapid Prototyping of Functional Metal and Ceramic Components by the Multiphase Jet Solidification (MJS) Process," in *Proceedings of the 8th Annual International Solid Freeform Fabrication* (University of Texas at Austin, 1997), 203–210.

64. M. Greul and R. Lenk, *Near-Net-Shape Ceramic and Composite Parts by Multiphase Jet Solidification (MJS)* (Industrial Ceramics, 2000).

65. R. Vaidyanathan, J. Lombardi, J. Walsh, S. Kasichainula, P. Calvert, and K. Cooper, "Extrusion Freeform Fabrication of Functional Ceramic Prototypes," in *24th Annual Conference on Composites, Advanced Ceramics, Materials, and Structures: B: Ceramic Engineering and Science Proceedings* (John Wiley & Sons, 2000), 121–128, https://doi.org/10.1002/9780470294635.ch16.

66. K. Stuffle, A. Mulligan, J. Lombardi, P. Calvert, and B. Fabes, "Solid Freebody Forming of Ceramics From PolymerizableSlurry," *MRS Proceedings* 346 (1994): 1027, https://doi.org/10.1557/PROC-346-1027.

67. Y. Lakhdar, C. Tuck, J. Binner, A. Terry, and R. Goodridge, "Additive Manufacturing of Advanced Ceramic Materials," *Progress in Materials Science* 116 (2021): 100736, https://doi.org/10.1016/j.pmatsci.2020.100736.

68. M. Agarwala, A. Bandyopadhyay, R. V. Weeren, et al., "Fused Deposition of Ceramics (FDC) for Structural Silicon Nitride Components," in *Proceedings of the 7th Annual International Solid Freeform Fabrication* (University of Texas at Austin, 1996), 335–344.

69. S. Cailleaux, N. M. Sanchez-Ballester, Y. A. Gueche, B. Bataille, and I. Soulairol, "Fused Deposition Modeling (FDM), the New Asset for the Production of Tailored Medicines," *Journal of Controlled Release* 330 (2021): 821–841, https://doi.org/10.1016/j.jconrel.2020.10.056.

70. N. Dumpa, A. Butreddy, H. Wang, N. Komanduri, S. Bandari, and M. A. Repka, "3D Printing in Personalized Drug Delivery: An Overview of Hot-Melt Extrusion-Based Fused Deposition Modeling," *International Journal of Pharmaceutics* 600 (2021): 120501, https://doi.org/10.1016/j.ijpharm.2021.120501.

71. C. Parulski, O. Jennotte, A. Lechanteur, and B. Evrard, "Challenges of Fused Deposition Modeling 3D Printing in Pharmaceutical Applications: Where are We Now?," *Advanced Drug Delivery Reviews* 175 (2021): 113810, https://doi.org/10.1016/j.addr.2021.05.020.

72. A. Melocchi, F. Briatico-Vangosa, M. Uboldi, et al., "Quality Considerations on the Pharmaceutical Applications of Fused Deposition Modeling 3D Printing," *International Journal of Pharmaceutics* 592 (2021): 119901, https://doi.org/10.1016/j.ijpharm.2020.119901.

73. J. Macedo, A. Samaro, V. Vanhoorne, C. Vervaet, and J. F. Pinto, "Processability of Poly(vinyl Alcohol) Based Filaments With Paracetamol Prepared by Hot-Melt Extrusion for Additive Manufacturing," *Journal of Pharmaceutical Sciences* 109, no. 12 (2020): 3636–3644, https://doi.org/10.1016/j.xphs.2020.09.016.

74. S. J. Trenfield, A. Awad, A. Goyanes, S. Gaisford, and A. W. Basit, "3D Printing Pharmaceuticals: Drug Development to Frontline Care," *Trends in Pharmacological Sciences* 39, no. 5 (2018): 440–451, https://doi.org/10.1016/j.tips.2018.02.006.

75. E. Fuenmayor, M. Forde, A. V. Healy, et al., "Material Considerations for Fused-Filament Fabrication of Solid Dosage Forms," *Pharmaceutics* 10, no. 2 (2018): 44.

76. P. Xu, J. Li, A. Meda, et al., "Development of a Quantitative Method to Evaluate the Printability of Filaments for Fused Deposition Modeling 3D Printing," *International Journal of Pharmaceutics* 588 (2020): 119760, https://doi.org/10.1016/j.ijpharm.2020.119760.

77. J. Aho, J. P. Bøtker, N. Genina, M. Edinger, L. Arnfast, and J. Rantanen, "Roadmap to 3D-Printed Oral Pharmaceutical Dosage Forms: Feedstock Filament Properties and Characterization for Fused Deposition Modeling," *Journal of Pharmaceutical Sciences* 108, no. 1 (2019): 26–35, https://doi.org/10.1016/j.xphs.2018.11.012.

78. B. Shaqour, M. Abuabiah, S. Abdel-Fattah, et al., "Gaining a Better Understanding of the Extrusion Process in Fused Filament Fabrication 3D Printing: A Review," *International Journal of Advanced Manufacturing Technology* 114, no. 5 (2021): 1279–1291, https://doi.org/10.1007/s00170-021-06918-6.

79. H. Masuda, Y. Ohta, and M. Kitayama, "Additive Manufacturing of SiC Ceramics with Complicated Shapes Using the FDM Type 3D-Printer," *Journal of Materials Science and Chemical Engineering* 7, no. 1 (2019): 1–12, https://doi.org/10.4236/msce.2019.72001.

80. U. Scheithauer, E. Schwarzer, H.-J. Richter, and T. Moritz, "Thermoplastic 3D Printing—An Additive Manufacturing Method for

15272648, 2026, 16, Downloaded from https://advanced.onlinelibrary.wiley.com/doi/10.1002/adem.71089 by Abdollah Saboori - Politecnico Di Torino Sist. Bibl Del Polit Di Torino , Wiley Online Library on [27/09/2026]. See the Terms and Conditions (https://onlinelibrary.wiley.com/terms-and-conditions) on Wiley Online Library for rules of use; OA articles are governed by the applicable Creative Commons License

Producing Dense Ceramics," *International Journal of Applied Ceramic Technology* 12, no. 1 (2015): 26–31, https://doi.org/10.1111/ijac.12306.

81. S. Iyer, J. McIntosh, A. Bandyopadhyay, et al., "Microstructural Characterization and Mechanical Properties of Si_3N_4 Formed by Fused Deposition of Ceramics," *International Journal of Applied Ceramic Technology* 5, no. 2 (2008): 127–137, https://doi.org/10.1111/j.1744-7402.2008.02193.x.

82. M. Greulich, M. Greul, and T. Pintat, "Fast, Functional Prototypes via Multiphase Jet Solidification," *Rapid Prototyping Journal* 1, no. 1 (1995): 20–25, https://doi.org/10.1108/13552549510146649.

83. I. Grida and J. R. G. Evans, "Extrusion Freeforming of Ceramics through Fine Nozzles," *Journal of the European Ceramic Society* 23, no. 5 (2003): 629–635, https://doi.org/10.1016/S0955-2219(02)00163-2.

84. M. Atif Yardimci and S. Güçeri, "Conceptual Framework for the Thermal Process Modelling of Fused Deposition," *Rapid Prototyping Journal* 2, no. 2 (1996): 26–31, https://doi.org/10.1108/13552549610128206.

85. M. Saha and M. Mallik, "Additive Manufacturing of Ceramics and Cermets: Present Status and Future Perspectives," *Sādhanā* 46, no. 3 (2021): 162, https://doi.org/10.1007/s12046-021-01685-2.

86. A. Gómez-Gómez, J. J. Moyano, M. I. Osendi, M. Belmonte, and P. Miranzo, "The Effect of Rod Orientation on the Strength of Highly Porous Filament Printed 3D SiC Ceramic Architectures," *Boletín de la Sociedad Española de Cerámica y Vidrio* 60, no. 2 (2021): 119–127, https://doi.org/10.1016/j.bsecv.2020.01.013.

87. H. Zhang, Y. Yang, B. Liu, and Z. Huang, "The Preparation of SiC-Based Ceramics by One Novel Strategy Combined 3D Printing Technology and Liquid Silicon Infiltration Process," *Ceramics International* 45, no. 8 (2019): 10800–10804, https://doi.org/10.1016/j.ceramint.2019.02.154.

88. M. S. McClain, I. E. Gunduz, and S. F. Son, "Additive Manufacturing of Ammonium Perchlorate Composite Propellant with High Solids Loadings," *Proceedings of the Combustion Institute* 37, no. 3 (2019): 3135–3142, https://doi.org/10.1016/j.proci.2018.05.052.

89. T. Huang, M. S. Mason, X. Zhao, G. E. Hilmas, and M. C. Leu, "Aqueous-Based Freeze-Form Extrusion Fabrication of Alumina Components," *Rapid Prototyping Journal* 15, no. 2 (2009): 88–95, https://doi.org/10.1108/13552540910943388.

90. R. He, N. Zhou, K. Zhang, et al., "Progress and Challenges towards Additive Manufacturing of SiC Ceramic," *Journal of Advanced Ceramics* 10, no. 4 (2021): 637–674, https://doi.org/10.1007/s40145-021-0484-z.

91. U. Scheithauer, J. Pötschke, S. Weingarten, et al., "Droplet-Based Additive Manufacturing of Hard Metal Components by Thermoplastic 3D Printing (T3DP)," *Journal of Ceramic Science and Technology* 8, no. 1 (2017): 155–160, https://doi.org/10.4416/JCST2016-00104.

92. M. Faes, J. Vleugels, F. Vogeler, and E. Ferraris, "Extrusion-Based Additive Manufacturing of ZrO2 Using Photoinitiated Polymerization," *CIRP Journal of Manufacturing Science and Technology* 14 (2016): 28–34, https://doi.org/10.1016/j.cirpj.2016.05.002.

93. A. Ghazanfari, W. Li, M. C. Leu, J. L. Watts, and G. E. Hilmas, "Additive Manufacturing and Mechanical Characterization of High Density Fully Stabilized Zirconia," *Ceramics International* 43, no. 8 (2017): 6082–6088, https://doi.org/10.1016/j.ceramint.2017.01.154.

94. R. Spina and L. Morfini, "Material Extrusion Additive Manufacturing of Ceramics: A Review on Filament-Based Process," *Materials* 17, no. 11 (2024): 2779.

95. A. Zocca, P. Colombo, C. M. Gomes, and J. Günster, "Additive Manufacturing of Ceramics: Issues, Potentialities, and Opportunities," *Journal of the American Ceramic Society* 98, no. 7 (2015): 1983–2001, https://doi.org/10.1111/jace.13700.

96. S. A. Rasaki, D. Xiong, S. Xiong, F. Su, M. Idrees, and Z. Chen, "Photopolymerization-Based Additive Manufacturing of Ceramics: A Systematic Review," *Journal of Advanced Ceramics* 10, no. 3 (2021): 442–471, https://doi.org/10.1007/s40145-021-0468-z.

97. Z. Wang, C. Huang, J. Wang, and B. Zou, "Development of a Novel Aqueous Hydroxyapatite Suspension for Stereolithography Applied to Bone Tissue Engineering," *Ceramics International* 45, no. 3 (2019): 3902–3909, https://doi.org/10.1016/j.ceramint.2018.11.063.

98. S. Meyers, L. De Leersnijder, J. Vleugels, and J.-P. Kruth, "Direct Laser Sintering of Reaction Bonded Silicon Carbide with Low Residual Silicon Content," *Journal of the European Ceramic Society* 38, no. 11 (2018): 3709–3717, https://doi.org/10.1016/j.jeurceramsoc.2018.04.055.

99. B. Nan, X. Yin, L. Zhang, and L. Cheng, "Three-Dimensional Printing of Ti_3SiC_2-Based Ceramics," *Journal of the American Ceramic Society* 94, no. 4 (2011): 969–972, https://doi.org/10.1111/j.1551-2916.2010.04257.x.

100. W. Zhang, R. Melcher, N. Travitzky, R. K. Bordia, and P. Greil, "Three-Dimensional Printing of Complex-Shaped Alumina/Glass Composites," *Advanced Engineering Materials* 11, no. 12 (2009): 1039–1043, https://doi.org/10.1002/adem.200900213.

101. D. A. Klosterman, R. P. Chartoff, N. R. Osborne, et al., "Development of a Curved Layer LOM Process for Monolithic Ceramics and Ceramic Matrix Composites," *Rapid Prototyping Journal* 5, no. 2 (1999): 61–71, https://doi.org/10.1108/13552549910267362.

102. W. Wang, J. Sun, B. Guo, X. Chen, K. P. Ananth, and J. Bai, "Fabrication of Piezoelectric Nano-Ceramics via Stereolithography of Low Viscous and Non-Aqueous Suspensions," *Journal of the European Ceramic Society* 40, no. 3 (2020): 682–688, https://doi.org/10.1016/j.jeurceramsoc.2019.10.033.

103. G. Franchin, H. Elsayed, R. Botti, et al., "Additive Manufacturing of Ceramics From Liquid Feedstocks," *Chinese Journal of Mechanical Engineering: Additive Manufacturing Frontiers* 1, no. 1 (2022): 100012, https://doi.org/10.1016/j.cjmeam.2022.100012.

104. K. Rane, L. Di Landro, and M. Strano, "Processability of SS316L Powder - Binder Mixtures for Vertical Extrusion and Deposition on Table Tests," *Powder Technology* 345 (2019): 553–562, https://doi.org/10.1016/j.powtec.2019.01.010.

105. R. M. German, "Injection Molding of Metals and Ceramics," *Powder Metallurgy* 42 (1997): 157–160.

106. M. Trunec, "Fabrication of Zirconia- and Ceria-Based Thin-Wall Tubes by Thermoplastic Extrusion," *Journal of the European Ceramic Society* 24, no. 4 (2004): 645–651, https://doi.org/10.1016/S0955-2219(03)00258-9.

107. J. B. Li, Z. G. Xie, X. H. Zhang, Q. G. Zeng, and H. J. Liu, "Study of Metal Powder Extrusion and Accumulating Rapid Prototyping," *Key Engineering Materials* 443 (2010): 81–86, https://doi.org/10.4028/www.scientific.net/KEM.443.81.

108. D. Pettas, G. Karapetsas, Y. Dimakopoulos, and J. Tsamopoulos, "On the Origin of Extrusion Instabilities: Linear Stability Analysis of the Viscoelastic Die Swell," *Journal of Non-Newtonian Fluid Mechanics* 224 (2015): 61–77, https://doi.org/10.1016/j.jnnfm.2015.07.011.

109. L. Ren, X. Zhou, Z. Song, et al., "Process Parameter Optimization of Extrusion-Based 3D Metal Printing Utilizing PW-LDPE–SA Binder System," *Materials* 10, no. 3 (2017): 305.

110. K. K. Rane and P. P. Date, "Rheological Investigation of MIM Feedstocks for Reducing Frictional Effects during Injection Moulding," *Advanced Materials Research* 966–967 (2014): 196–205, https://doi.org/10.4028/www.scientific.net/AMR.966-967.196.

111. M. Khakbiz, A. Simchi, and R. Bagheri, "Analysis of the Rheological Behavior and Stability of 316L Stainless Steel-TiC Powder Injection Molding Feedstock," *Materials Science and Engineering: A* 407, no. 1 (2005): 105–113, https://doi.org/10.1016/j.msea.2005.06.057.

112. D. Nötzel and T. Hanemann, "New Feedstock System for Fused Filament Fabrication of Sintered Alumina Parts," *Materials* 13, no. 19 (2020): 4461.

113. M. Orlovská, Z. Chlup, Ľ. Bača, M. Janek, and M. Kitzmantel, "Fracture and Mechanical Properties of Lightweight Alumina

15272648, 2026, 16, Downloaded from https://advanced.onlinelibrary.wiley.com/doi/10.1002/adem.71089 by Abdollah Saboori - Politecnico Di Torino Sist. Bibl Del Polit Di Torino , Wiley Online Library on [27/09/2026]. See the Terms and Conditions (https://onlinelibrary.wiley.com/terms-and-conditions) on Wiley Online Library for rules of use; OA articles are governed by the applicable Creative Commons License

Ceramics Prepared by Fused Filament Fabrication," *Journal of the European Ceramic Society* 40, no. 14 (2020): 4837–4843, https://doi.org/10.1016/j.jeurceramsoc.2020.02.026.

114. M. Orlovská, M. Hain, M. Kitzmantel, et al., "Monitoring of Critical Processing Steps during the Production of High Dense 3D Alumina Parts Using Fused Filament Fabrication Technology," *Additive Manufacturing* 48 (2021): 102395, https://doi.org/10.1016/j.addma.2021.102395.

115. L. Gorjan, C. Galusca, M. Sami, T. Sebastian, and F. Clemens, "Effect of Stearic Acid on Rheological Properties and Printability of Ethylene Vinyl Acetate Based Feedstocks for Fused Filament Fabrication of Alumina," *Additive Manufacturing* 36 (2020): 101391, https://doi.org/10.1016/j.addma.2020.101391.

116. V. Truxová, J. Šafka, J. Sobotka, J. Macháček, and M. Ackermann, "Alumina Manufactured by Fused Filament Fabrication: A Comprehensive Study of Mechanical Properties and Porosity," *Polymers* 14, no. 5 (2022): 991.

117. A. Smirnov, A. Seleznev, P. Peretyagin, et al., "Rheological Characterization and Printability of Polylactide (PLA)-Alumina (Al_2O_3) Filaments for Fused Deposition Modeling (FDM)," *Materials* 15, no. 23 (2022): 8399.

118. C. Tosto, M. Bragaglia, F. Nanni, G. Recca, and G. Cicala, "Fused Filament Fabrication of Alumina/Polymer Filaments for Obtaining Ceramic Parts after Debinding and Sintering Processes," *Materials* 15, no. 20 (2022): 7399, https://doi.org/10.3390/ma15207399.

119. A. Hadian, B. Morath, M. Biedermann, M. Meboldt, and F. Clemens, "Selected Design Rules for Material Extrusion-Based Additive Manufacturing of Alumina Based Nozzles and Heat Exchangers considering Limitations in Printing, Debinding, and Sintering," *Additive Manufacturing* 75 (2023): 103719, https://doi.org/10.1016/j.addma.2023.103719.

120. I. Özden, A. Iveković, and A. Kocjan, "Additive Manufacturing of Ceramics From Thermoplastic Feedstocks," *Open Ceramics* 6 (2021): 100129, https://doi.org/10.1016/j.oceram.2021.100129.

121. D. Nötzel, R. Eickhoff, and T. Hanemann, "Fused Filament Fabrication of Small Ceramic Components," *Materials* 11, no. 8 (2018): 1463.

122. S. Cano, H. Cajner, J. Gonzalez-Gutierrez, et al., "Optimization of Material Properties for Highly-Filled Thermoplastic Polymers Used in Fused Filament Fabrication of Ceramics," *AIP Conference Proceedings* 2065, no. 1 (2019): 030058, https://doi.org/10.1063/1.5088316.

123. S. Weingarten, U. Scheithauer, R. Johne, et al., "Multi-Material Ceramic-Based Components - Additive Manufacturing of Black-and-White Zirconia Components by Thermoplastic 3D-Printing (CerAM - T3DP)," *Journal of Visualized Experiments* 143 (2019): e57538, https://doi.org/10.3791/57538.

124. R. Eickhoff, S. Antusch, S. Baumgärtner, D. Nötzel, and T. Hanemann, "Feedstock Development for Material Extrusion-Based Printing of Ti6Al4V Parts," *Materials* 15, no. 18 (2022): 6442.

125. H. Oh, T. Im, J. Pyo, J.-s. Lee, and C. S. Lee, "Study of Solid Loading of Feedstock Using Trimodal Iron Powders for Extrusion Based Additive Manufacturing," *Scientific Reports* 13, no. 1 (2023): 4819, https://doi.org/10.1038/s41598-023-32095-5.

126. H. W. Li, Y. P. Zhao, G. Q. Chen, M. H. Li, X. S. Fu, and W. L. Zhou, "Synergy of Low-and High-Density Polyethylene in a Binder System for Powder Injection Molding of SiC Ceramics," *Ceramics International* 48, no. 17 (2022): 25513–25520, https://doi.org/10.1016/j.ceramint.2022.05.230.

127. C. Aumnate, N. Nawaukkaratharnant, and N. Chuankrerkkul, "Preparation of Feedstock Containing Water-Soluble Binder for Powder Injection Moulding of Silver," *Journal of Metals, Materials and Minerals* 32, no. 3 (2022): 75–79, https://doi.org/10.55713/jmmm.v32i3.1271.

128. B. Hausnerova, D. Bleyan, V. Kasparkova, and V. Pata, "Surface Adhesion between Ceramic Injection Molding Feedstocks and Processing Tools," *Ceramics International* 42, no. 1, Part A (2016): 460–465, https://doi.org/10.1016/j.ceramint.2015.08.132.

129. T. Heim, F. Kern, and C. Siligardi, "Influence of the Binder Composition on the Water Debinding Properties of a PVB-PEG-Alumina Feedstock for the Fused Deposition of Ceramic Process," *Open Ceramics* 21 (2025): 100728, https://doi.org/10.1016/j.oceram.2024.100728.

130. A. J. Medesi, D. Nötzel, and T. Hanemann, "PVB/PEG-Based Feedstocks for Injection Molding of Alumina Microreactor Components," *Materials* 12, no. 8 (2019): 1219.

131. R. M. German and A. Bose, *Binder and Polymer Assisted Powder Processing* (ASM International, 2020).

132. H. Ji, J. Zhao, J. Chen, et al., "A Novel Experimental Approach to Quantitatively Evaluate the Printability of Inks in 3D Printing Using Two Criteria," *Additive Manufacturing* 55 (2022): 102846, https://doi.org/10.1016/j.addma.2022.102846.

133. I. Özden Moser, M. Vukšić, M. Dular, A. Iveković, and A. Kocjan, "Tuning the Rheological Properties of Paraffin-Wax Ceramic Feedstocks for Deposition with Thermoplastic 3D Printing," *Journal of the European Ceramic Society* 44, no. 13 (2024): 7791–7800, https://doi.org/10.1016/j.jeurceramsoc.2024.05.057.

134. J.-H. Sim, B.-K. Koo, M. Jung, and D.-S. Kim, "Study on Debinding and Sintering Processes for Ceramics Fabricated Using Digital Light Processing (DLP) 3D Printing," *Processes* 10, no. 11 (2022): 2467.

135. K. Lim, M. D. Hayat, K. D. Jena, et al., "Environmentally Friendly Solvent Debinding Technique of POM Binder System for Titanium Injection Molding," *Journal of Materials Research and Technology* 30 (2024): 1037–1043, https://doi.org/10.1016/j.jmrt.2024.03.064.

136. S. Bose, E. K. Akdogan, V. K. Balla, et al., "3D Printing of Ceramics: Advantages, Challenges, Applications, and Perspectives," *Journal of the American Ceramic Society* 107, no. 12 (2024): 7879–7920, https://doi.org/10.1111/jace.20043.

137. L. Santana, E. Y. Nagata, G. M. O. Barra, et al., "Characterization and Analysis of Printing Challenges with High Filled Alumina Filament in Low-Cost Extrusion-Based Additive Manufacturing," *Polymer Composites* 46, no. 10 (2025): 9586–9612, https://doi.org/10.1002/pc.29581.

138. A. Villa, P. K. Gianchandani, and F. Baino, "Sustainable Approaches for the Additive Manufacturing of Ceramic Materials," *Ceramics* 7, no. 1 (2024): 291–309.

139. L. del-Mazo-Barbara and M.-P. Ginebra, "Rheological Characterisation of Ceramic Inks for 3D Direct Ink Writing: A Review," *Journal of the European Ceramic Society* 41, no. 16 (2021): 18–33, https://doi.org/10.1016/j.jeurceramsoc.2021.08.031.

140. A. M'Barki, L. Bocquet, and A. Stevenson, "Linking Rheology and Printability for Dense and Strong Ceramics by Direct Ink Writing," *Scientific Reports* 7, no. 1 (2017): 6017, https://doi.org/10.1038/s41598-017-06115-0.

141. S. Bhandari, C. Manière, F. Sedona, et al., "Ultra-Rapid Debinding and Sintering of Additively Manufactured Ceramics by Ultrafast High-Temperature Sintering," *Journal of the European Ceramic Society* 44, no. 1 (2024): 328–340, https://doi.org/10.1016/j.jeurceramsoc.2023.08.040.

142. T. Li, G. He, Z. Jiang, Y. Duan, and M. Liu, "Research Advances and New Insights into Multi-Source Solid Waste-Derived Ceramic Foams," *Sustainable Materials and Technologies* 45 (2025): e01535, https://doi.org/10.1016/j.susmat.2025.e01535.

143. C. Duan, L. Guan, Y. Zhu, et al., "Rapid Microwave Heating Synthesis and Microwave Coupling Mechanism of Transition Metal High-Entropy Carbides," *Ceramics International* 51, no. 25, Part C (2025): 47506–47515, https://doi.org/10.1016/j.ceramint.2025.08.308.

144. Y. Huang, J. Wang, F. Wang, et al., "Formation Mechanisms on Amorphous-Enhanced Interfaces of Al/Steel Bimetallic Freeform Components via Wire-Based Friction Stir Additive Manufacturing," *Additive Manufacturing* 119 (2026): 105113, https://doi.org/10.1016/j.addma.2026.105113.

15272648, 2026, 16, Downloaded from https://advanced.onlinelibrary.wiley.com/doi/10.1002/adem.71089 by Abdollah Saboori - Politecnico Di Torino Sist. Bibl Del Polit Di Torino , Wiley Online Library on [27/09/2026]. See the Terms and Conditions (https://onlinelibrary.wiley.com/terms-and-conditions) on Wiley Online Library for rules of use; OA articles are governed by the applicable Creative Commons License

145. N. Travitzky, A. Bonet, B. Dermeik, et al., "Additive Manufacturing of Ceramic-Based Materials," *Advanced Engineering Materials* 16, no. 6 (2014): 729–754, https://doi.org/10.1002/adem.201400097.

146. P. Wang, B. Zou, S. Ding, L. Li, and C. Huang, "Effects of FDM-3D Printing Parameters on Mechanical Properties and Microstructure of CF/PEEK and GF/PEEK," *Chinese Journal of Aeronautics* 34, no. 9 (2021): 236–246, https://doi.org/10.1016/j.cja.2020.05.040.

147. J. Li, Q. Duan, J. Hou, H. Xie, and S. Liu, "In-Situ Monitoring of Substrate Deformation in Directed Energy Deposition Process Using the Coherent Gradient Sensing Method," *Additive Manufacturing* 36 (2020): 101547, https://doi.org/10.1016/j.addma.2020.101547.

148. X. Q. Wang, Z. Jin, B. Zheng, and G. X. Gu, "Transformer-Based Approach for Printing Quality Recognition in Fused Filament Fabrication," *npj Advanced Manufacturing* 2, no. 1 (2025): 15, https://doi.org/10.1038/s44334-025-00025-0.

149. P. B. Chandan and M. R. Sankar, "Extrusion-Based Additive Manufacturing of Alumina Ceramics through Controlled Extrusion Pressure," *International Journal of Applied Ceramic Technology* 22, no. 2 (2025): e14935, https://doi.org/10.1111/ijac.14935.

150. T. Lin, Z. Zhao, T. Wang, and Y.-T. Pan, "Three-Dimensional Printing of Large Ceramic Products and Process Simulation," *Materials* 16, no. 10 (2023): 3815.

151. E. Romanczuk-Ruszuk, B. Sztorch, D. Pakuła, E. Gabriel, K. Nowak, and R. E. Przekop, "3D Printing Ceramics—Materials for Direct Extrusion Process," *Ceramics* 6, no. 1 (2023): 364–385.

152. M. A. N. B. Mohd Khairul Nizam, K. I. B. Ismail, and T. C. Yap, "The Effect of Printing Orientation on the Mechanical Properties of FDM 3D Printed Parts," in *Enabling Industry 4.0 Through Advances in Manufacturing and Materials: Selected Articles From iM3F 2021* (Springer, 2022), 75–85.

153. M. Eryıldız, "Effect of Build Orientation on Mechanical Behaviour and Build Time of FDM. 3D-Printed PLA Parts: An Experimental Investigation," *European Mechanical Science* 5, no. 3 (2021): 116–120, https://doi.org/10.26701/ems.881254.

154. M. Bakhtiari, M. H. Sheikh-Ansari, and B. Darabinajand, "Effect of Raster Angle and Nanocomposite PU-CNTs Coating on 3D Printing PLA: Investigation of Mechanical and Shape Recovery Behaviour Under Marine Environment," *Journal of Polymers and the Environment* 34, no. 1 (2026): 20, https://doi.org/10.1007/s10924-025-03751-w.

155. D. Godec, S. Cano, C. Holzer, and J. Gonzalez-Gutierrez, "Optimization of the 3D Printing Parameters for Tensile Properties of Specimens Produced by Fused Filament Fabrication of 17-4PH Stainless Steel," *Materials* 13, no. 3 (2020): 774.

156. T. Schuller, M. Jalaal, P. Fanzio, and F. J. Galindo-Rosales, "Optimal Shape Design of Printing Nozzles for Extrusion-Based Additive Manufacturing," *Additive Manufacturing* 84 (2024): 104130, https://doi.org/10.1016/j.addma.2024.104130.

157. V. Ermolai and A. I. Irimia, "Influence of Nozzle Parameters in 3D Printing under the Manufacturing Time," *Bulletin of the Polytechnic Institute of Iaşi. Machine Constructions Section* 67, no. 3 (2021): 63–72, https://doi.org/10.2478/bipcm-2021-0017.

158. A. B. Irez and A. Dogru, "The Microstructural Evolution of Material Extrusion Based Additive Manufacturing of Polyetheretherketone under Different Printing Conditions and Application in a Spinal Implant," *Polymer Engineering & Science* 64, no. 11 (2024): 5486–5502, https://doi.org/10.1002/pen.26929.

159. S. Lamnini, H. Elsayed, Y. Lakhdar, F. Baino, F. Smeacetto, and E. Bernardo, "Robocasting of Advanced Ceramics: Ink Optimization and Protocol to Predict the Printing Parameters - A Review," *Heliyon* 8, no. 9 (2022): e10651, https://doi.org/10.1016/j.heliyon.2022.e10651.

160. J. Hergel, K. Hinz, S. Lefebvre, and B. Thomaszewski, "Extrusion-Based Ceramics Printing with Strictly-Continuous Deposition," *ACM Transactions on Graphics* 38, no. 6 (2019): 1–11, https://doi.org/10.1145/3355089.3356509.

161. M. Edward, T. Ellis, and J. Noone, "Real-Time Adaptive Control of Additive Manufacturing Processes Using Machine Learning," ed: Google Patents, 2019.

162. A. Marnot, L. Konzelman, J. M. Jones, C. Hill, and B. Brettmann, "Applicability of UV-Curable Binders in High Solid Suspensions for Direct-Ink-Write 3D Printing in Extremely Cold Temperatures," *ACS Applied Materials & Interfaces* 15, no. 43 (2023): 50378–50390, https://doi.org/10.1021/acsami.3c11742.

163. K. Jakupi, V. Dukovski, and G. Hodolli, "Surface Roughness Modeling of Material Extrusion PLA Flat Surfaces," *International Journal of Polymer Science* 2023, no. 1 (2023): 8844626, https://doi.org/10.1155/2023/8844626.

164. I. Buj-Corral, A. Domínguez-Fernández, and A. Gómez-Gejo, "Effect of Printing Parameters on Dimensional Error and Surface Roughness Obtained in Direct Ink Writing (DIW) Processes," *Materials* 13, no. 9 (2020): 2157.

165. S. C. Altıparmak, V. A. Yardley, Z. Shi, and J. Lin, "Extrusion-Based Additive Manufacturing Technologies: State of the Art and Future Perspectives," *Journal of Manufacturing Processes* 83 (2022): 607–636, https://doi.org/10.1016/j.jmapro.2022.09.032.

166. J. Liu, C. Ma, M. Li, et al., "A Real-Time Spatiotemporal Error Compensation Framework for Face Gear Grinding," *Engineering Applications of Artificial Intelligence* 162 (2025): 112429, https://doi.org/10.1016/j.engappai.2025.112429.

167. J. Zhou, L. Li, L. Lu, and Y. Cheng, "Machine Learning-Based Quality Optimisation of Ceramic Extrusion 3D Printing Deposition Lines," *Materials Today Communications* 41 (2024): 110841, https://doi.org/10.1016/j.mtcomm.2024.110841.

168. K. Rane, M. A. Farid, W. Hassan, and M. Strano, "Effect of Printing Parameters on Mechanical Properties of Extrusion-Based Additively Manufactured Ceramic Parts," *Ceramics International* 47, no. 9 (2021): 12189–12198, https://doi.org/10.1016/j.ceramint.2021.01.066.

169. M. Xiangguang, C. Bin, M. Xiaobo, and W. Liming, "Breakdown Mechanism of Internal Cracks in Porcelain Materials," *Journal of Physics D: Applied Physics* 59, no. 1 (2026): 015504, https://doi.org/10.1088/1361-6463/ae2ae9.

170. K. Rane, S. Petrò, and M. Strano, "Evolution of Porosity and Geometrical Quality through the Ceramic Extrusion Additive Manufacturing Process Stages," *Additive Manufacturing* 32 (2020): 101038, https://doi.org/10.1016/j.addma.2020.101038.

171. O. Bouzaglou, O. Golan, and N. Lachman, "Process Design and Parameters Interaction in Material Extrusion 3D Printing: A Review," *Polymers* 15, no. 10 (2023): 2280.

172. J. D. Kechagias and N. Vidakis, "Parametric Optimization of Material Extrusion 3D Printing Process: An Assessment of Box-Behnken vs. Full-Factorial Experimental Approach," *International Journal of Advanced Manufacturing Technology* 121, no. 5 (2022): 3163–3172, https://doi.org/10.1007/s00170-022-09532-2.

173. A. Gaspar-Cunha, J. A. Covas, and J. Sikora, "Optimization of Polymer Processing: A Review (Part I—Extrusion)," *Materials* 15, no. 1 (2022): 384.

174. Z. Abdelhamid, H. Mohamed, and S. Kelouwani, "The use of Machine Learning in Process-Structure–property Modeling for Material Extrusion Additive Manufacturing: A State-of-the-Art Review," *Journal of the Brazilian Society of Mechanical Sciences and Engineering* 46, no. 2 (2024): 70, https://doi.org/10.1007/s40430-023-04637-5.

175. W.-T. Xie, D.-N. Song, W.-C. Tang, J.-W. Ma, and J.-H. Li, "Auxiliary Support Path Planning for Robot-Assisted Machining of Thin-Walled Parts with Non-Uniform Thickness and Closed Cross-Section Based on

15272648, 2026, 16, Downloaded from https://advanced.onlinelibrary.wiley.com/doi/10.1002/adem.71089 by Abdollah Saboori - Politecnico Di Torino Sist. Bibl Del Polit Di Torino , Wiley Online Library on [27/09/2026]. See the Terms and Conditions (https://onlinelibrary.wiley.com/terms-and-conditions) on Wiley Online Library for rules of use; OA articles are governed by the applicable Creative Commons License

a Neutral Surface," *Journal of Manufacturing Processes* 147 (2025): 16–28, https://doi.org/10.1016/j.jmapro.2025.05.002.

176. Y.-a. Jin, Y. He, J.-z. Fu, W.-f. Gan, and Z.-w. Lin, "Optimization of Tool-Path Generation for Material Extrusion-Based Additive Manufacturing Technology," *Additive Manufacturing* 1–4 (2014): 32–47, https://doi.org/10.1016/j.addma.2014.08.004.

177. Y. Jin, Y. He, G. Fu, A. Zhang, and J. Du, "A Non-Retraction Path Planning Approach for Extrusion-Based Additive Manufacturing," *Robotics and Computer-Integrated Manufacturing* 48 (2017): 132–144, https://doi.org/10.1016/j.rcim.2017.03.008.

178. J. Jiang, X. Xu, and J. Stringer, "Optimization of Process Planning for Reducing Material Waste in Extrusion Based Additive Manufacturing," *Robotics and Computer-Integrated Manufacturing* 59 (2019): 317–325, https://doi.org/10.1016/j.rcim.2019.05.007.

179. J. Ahn, J. Doh, S. Kim, and S.-I. Park, "Knowledge-Based Design Algorithm for Support Reduction in Material Extrusion Additive Manufacturing," *Micromachines* 13, no. 10 (2022): 1672.

180. Z. Wang, Y. Tao, S. Zhang, et al., "Spatial Spiral Tube Multi-Roller Bending: Accurate Axial Prediction Utilizing AWPSO-FECAM-LSTM Framework," *Expert Systems with Applications* 296 (2026): 128960, https://doi.org/10.1016/j.eswa.2025.128960.

181. S. Rahmani Dabbagh, O. Ozcan, and S. Tasoglu, "Machine Learning-Enabled Optimization of Extrusion-Based 3D Printing," *Methods* 206 (2022): 27–40, https://doi.org/10.1016/j.ymeth.2022.08.002.

182. X. Zhou, S.-J. Hsieh, and J.-C. Wang, "Accelerating Extrusion-Based Additive Manufacturing Optimization Processes with Surrogate-Based Multi-Fidelity Models," *International Journal of Advanced Manufacturing Technology* 103, no. 9 (2019): 4071–4083, https://doi.org/10.1007/s00170-019-03813-z.

183. A. Oleff, B. Küster, and L. Overmeyer, "Determination of Quality Classes for Material Extrusion Additive Manufacturing Using Image Processing," *International Journal of Advanced Manufacturing Technology* 132, no. 3 (2024): 1585–1598, https://doi.org/10.1007/s00170-024-13269-5.

184. R. Dasgupta, S. Roy, and S. Tarafdar, "Correlation between Porosity, Conductivity and Permeability of Sedimentary Rocks—A Ballistic Deposition Model," *Physica A: Statistical Mechanics and Its Applications* 275, no. 1 (2000): 22–32, https://doi.org/10.1016/S0378-4371(99)00388-X.

185. H. Li, K. Hu, Y. Liu, Z. Lu, and J. Liang, "Improved Mechanical Properties of Silica Ceramic Cores Prepared by 3D Printing and Sintering Processes," *Scripta Materialia* 194 (2021): 113665, https://doi.org/10.1016/j.scriptamat.2020.113665.

186. H. Li, Y. Liu, W. Li, Y. Liu, and Q. Zeng, "The Effect of Sintering on the Properties of Calcium Oxide Promoted Alumina-Based Ceramic Cores via 3D Printing," *Materials Chemistry and Physics* 263 (2021): 124443, https://doi.org/10.1016/j.matchemphys.2021.124443.

187. H. Li, Y. Liu, Y. Liu, et al., "Influence of Sintering Temperature and CVI Time on Mechanical Properties of 3D-Printed Alumina Ceramics," *Materials Letters* 285 (2021): 129096, https://doi.org/10.1016/j.matlet.2020.129096.

188. H. Li, Y. Liu, Y. Liu, et al., "Influence of Debinding Holding Time on Mechanical Properties of 3D-Printed Alumina Ceramic Cores," *Ceramics International* 47, no. 4 (2021): 4884–4894, https://doi.org/10.1016/j.ceramint.2020.10.061.

189. H. Li, Y. Liu, Y. Liu, et al., "Influence of Vacuum Debinding Temperature on Microstructure and Mechanical Properties of Three-Dimensional-Printed Alumina via Stereolithography," *3D Printing and Additive Manufacturing* 7, no. 1 (2020): 8–18, https://doi.org/10.1089/3dp.2019.0060.

190. S. Ghanizadeh, S. Grasso, P. Ramanujam, et al., "Improved Transparency and Hardness in α-Alumina Ceramics Fabricated by High-Pressure SPS of Nanopowders," *Ceramics International* 43, no. 1, Part A (2017): 275–281, https://doi.org/10.1016/j.ceramint.2016.09.150.

191. E.-H. Kim, H.-H. Choi, and Y.-G. Jung, "Fabrication of a Ceramic Core for an Impeller Blade Using a 3D Printing Technique and Inorganic Binder," *Journal of Manufacturing Processes* 53 (2020): 43–47, https://doi.org/10.1016/j.jmapro.2020.01.055.

192. H.-H. Choi, E.-H. Kim, B.-G. Kim, S. Yang, and Y.-G. Jung, "Improvement of Ceramic Core Strength by Combining 3D Printing Technology and an Organic-Inorganic Conversion Process Using Dual Polymers," *Ceramics International* 47, no. 12 (2021): 17644–17651, https://doi.org/10.1016/j.ceramint.2021.03.083.

193. H. Li, Y. Liu, Y. Liu, Q. Zeng, and J. Liang, "Silica Strengthened Alumina Ceramic Cores Prepared by 3D Printing," *Journal of the European Ceramic Society* 41, no. 4 (2021): 2938–2947, https://doi.org/10.1016/j.jeurceramsoc.2020.11.050.

194. H. Zhao, C. Ye, Z. Fan, and C. Wang, "3D Printing of CaO-Based Ceramic Core Using Nanozirconia Suspension as a Binder," *Journal of the European Ceramic Society* 37, no. 15 (2017): 5119–5125, https://doi.org/10.1016/j.jeurceramsoc.2017.06.050.

195. H.-Y. Park, E.-H. Kim, H.-H. Choi, G.-H. Cho, Y.-G. Jung, and J. Zhang, "New Conversion Process for Fabricating a Ceramic Core by a 3D Printing Technique," *Surface and Coatings Technology* 332 (2017): 527–532, https://doi.org/10.1016/j.surfcoat.2017.07.034.

196. G.-J. Zhang, D.-W. Ni, J. Zou, et al., "Inherent Anisotropy in Transition Metal Diborides and Microstructure/Property Tailoring in Ultra-High Temperature Ceramics—A Review," *Journal of the European Ceramic Society* 38, no. 2 (2018): 371–389, https://doi.org/10.1016/j.jeurceramsoc.2017.09.012.

197. A. Sommers, Q. Wang, X. Han, C. T'Joen, Y. Park, and A. Jacobi, "Ceramics and Ceramic Matrix Composites for Heat Exchangers in Advanced Thermal Systems—A Review," *Applied Thermal Engineering* 30, no. 11 (2010): 1277–1291, https://doi.org/10.1016/j.applthermaleng.2010.02.018.

198. H. J. Strumpf, T. L. Stillwagon, D. M. Kotchick, and M. G. Coombs, "Advanced Industrial Ceramic Heat Pipe Recuperators," *Heat Recovery Systems and CHP* 8, no. 3 (1988): 235–246, https://doi.org/10.1016/0890-4332(88)90059-2.

199. O. Al-Ketan, M. Pelanconi, A. Ortona, and R. K. Abu Al-Rub, "Additive Manufacturing of Architected Catalytic Ceramic Substrates Based on Triply Periodic Minimal Surfaces," *Journal of the American Ceramic Society* 102, no. 10 (2019): 6176–6193, https://doi.org/10.1111/jace.16474.

200. J. Binner, M. Porter, B. Baker, et al., "Selection, Processing, Properties and Applications of Ultra-High Temperature Ceramic Matrix Composites, UHTCMCs – A Review," *International Materials Reviews* 65, no. 7 (2020): 389–444, https://doi.org/10.1080/09506608.2019.1652006.

201. E. Rezaei, S. Haussener, S. Gianella, and A. Ortona, "Early-Stage Oxidation Behavior at High Temperatures of SiSiC Cellular Architectures in a Porous Burner," *Ceramics International* 42, no. 14 (2016): 16255–16261, https://doi.org/10.1016/j.ceramint.2016.07.159.

202. M. Pelanconi, M. Barbato, S. Zavattoni, G. L. Vignoles, and A. Ortona, "Thermal Design, Optimization and Additive Manufacturing of Ceramic Regular Structures to Maximize the Radiative Heat Transfer," *Materials & Design* 163 (2019): 107539, https://doi.org/10.1016/j.matdes.2018.107539.

203. S. Gianella, D. Gaia, and A. Ortona, "High Temperature Applications of Si–SiC Cellular Ceramics," *Advanced Engineering Materials* 14, no. 12 (2012): 1074–1081, https://doi.org/10.1002/adem.201200012.

204. L. Schlier, W. Zhang, N. Travitzky, P. Greil, J. Cypris, and M. Weclas, "Macro-Cellular Silicon Carbide Reactors for Nonstationary Combustion Under Piston Engine-Like Conditions," *International Journal of Applied Ceramic Technology* 8, no. 5 (2011): 1237–1245, https://doi.org/10.1111/j.1744-7402.2010.02591.x.

15272648, 2026, 16, Downloaded from https://advanced.onlinelibrary.wiley.com/doi/10.1002/adem.71089 by Abdollah Saboori - Politecnico Di Torino Sist. Bibl Del Polit Di Torino , Wiley Online Library on [27/09/2026]. See the Terms and Conditions (https://onlinelibrary.wiley.com/terms-and-conditions) on Wiley Online Library for rules of use; OA articles are governed by the applicable Creative Commons License

205. I. Polozov, N. Razumov, D. Masaylo, A. Silin, Y. Lebedeva, and A. Popovich, "Fabrication of Silicon Carbide Fiber-Reinforced Silicon Carbide Matrix Composites Using Binder Jetting Additive Manufacturing From Irregularly-Shaped and Spherical Powders," *Materials* 13, no. 7 (2020): 1766.

206. M. Pelanconi, E. Rezaei, and A. Ortona, "Cellular Ceramic Architectures Produced by Hybrid Additive Manufacturing: A Review on the Evolution of Their Design," *Journal of the Ceramic Society of Japan* 128, no. 9 (2020): 595–604, https://doi.org/10.2109/jcersj2.20071.

207. Q. Wang, X. Chen, Q. An, et al., "Research on the Method for Improving the Cutting Performance of Forming Tools Based on the Non-Uniform Passivation of the Cutting Edge," *International Journal of Advanced Manufacturing Technology* 138, no. 9 (2025): 3975–3987, https://doi.org/10.1007/s00170-025-15719-0.

208. D. Sergi, A. Camarano, J. M. Molina, A. Ortona, and J. Narciso, "Surface Growth for Molten Silicon Infiltration into Carbon Millimeter-Sized Channels: Lattice-Boltzmann Simulations, Experiments and Models," *International Journal of Modern Physics C* 27, no. 06 (2015): 1650062, https://doi.org/10.1142/S0129183116500625.

209. V. Bougiouri, R. Voytovych, N. Rojo-Calderon, J. Narciso, and N. Eustathopoulos, "The Role of the Chemical Reaction in the Infiltration of Porous Carbon by NiSi Alloys," *Scripta Materialia* 54, no. 11 (2006): 1875–1878, https://doi.org/10.1016/j.scriptamat.2006.02.015.

210. Z.-H. Zhang, Z.-F. Liu, J.-F. Lu, X.-B. Shen, F.-C. Wang, and Y.-D. Wang, "The Sintering Mechanism in Spark Plasma Sintering – Proof of the Occurrence of Spark Discharge," *Scripta Materialia* 81 (2014): 56–59, https://doi.org/10.1016/j.scriptamat.2014.03.011.

211. K. Liu, Y. Shi, W. He, C. Li, Q. Wei, and J. Liu, "Densification of Alumina Components via Indirect Selective Laser Sintering Combined with Isostatic Pressing," *International Journal of Advanced Manufacturing Technology* 67, no. 9 (2013): 2511–2519, https://doi.org/10.1007/s00170-012-4668-0.

212. P. Colombo, G. Mera, R. Riedel, and G. D. Sorarù, "Polymer-Derived Ceramics: 40 Years of Research and Innovation in Advanced Ceramics," *Journal of the American Ceramic Society* 93, no. 7 (2010): 1805–1837, https://doi.org/10.1111/j.1551-2916.2010.03876.x.

213. H. Xiong, H. Chen, Z. Chen, X. Xiong, D. Zhang, and K. Zhou, "3D-SiC Decorated with SiC Whiskers: Chemical Vapor Infiltration on the Porous 3D-SiC Lattices Derived From Polycarbosilane-Based Suspensions," *Ceramics International* 46, no. 5 (2020): 6234–6242, https://doi.org/10.1016/j.ceramint.2019.11.092.

214. Q. Zhu, X. Dong, J. Hu, et al., "High Strength Aligned SiC Nanowire Reinforced SiC Porous Ceramics Fabricated by 3D Printing and Chemical Vapor Infiltration," *Ceramics International* 46, no. 5 (2020): 6978–6983, https://doi.org/10.1016/j.ceramint.2019.11.113.

215. J. Yoo, M. Cima, S. Khanuja, and E. Sachs, "Structural Ceramic Components by 3D Printing," *Proceedings of the 4th Annual International Solid Freeform Fabrication* (University of Texas at Austin, 1996), 40–50.

216. J. Lu, D. Ni, C. Liao, et al., "Fabrication and Microstructure Evolution of Csf/ZrB2-SiC Composites via Direct Ink Writing and Reactive Melt Infiltration," *Journal of Advanced Ceramics* 10, no. 6 (2021): 1371–1380, https://doi.org/10.1007/s40145-021-0512-z.

217. M. Pelanconi, G. Bianchi, P. Colombo, and A. Ortona, "Fabrication of Dense SiSiC Ceramics by a Hybrid Additive Manufacturing Process," *Journal of the American Ceramic Society* 105, no. 2 (2022): 786–793, https://doi.org/10.1111/jace.18134.

218. X. Tian, W. Zhang, D. Li, and J. G. Heinrich, "Reaction-Bonded SiC Derived From Resin Precursors by Stereolithography," *Ceramics International* 38, no. 1 (2012): 589–597, https://doi.org/10.1016/j.ceramint.2011.07.047.

219. S. Tang and C. Hu, "Design, Preparation and Properties of Carbon Fiber Reinforced Ultra-High Temperature Ceramic Composites for Aerospace Applications: A Review," *Journal of Materials Science & Technology* 33, no. 2 (2017): 117–130, https://doi.org/10.1016/j.jmst.2016.08.004.

220. B.-W. Chen, D.-W. Ni, C.-J. Liao, Y.-L. Jiang, J. Lu, and S.-M. Dong, "Long-Term Ablation Behavior and Mechanisms of 2D-Cf/ZrB2-SiC Composites at Temperatures up to 2400 °C," *Corrosion Science* 177 (2020): 108967, https://doi.org/10.1016/j.corsci.2020.108967.

221. C. Yan, R. Liu, C. Zhang, Y. Cao, and Y. Wang, "Effects of SiC/HfC Ratios on the Ablation and Mechanical Properties of 3D Cf/HfC-SiC Composites," *Journal of the European Ceramic Society* 37, no. 6 (2017): 2343–2351, https://doi.org/10.1016/j.jeurceramsoc.2017.01.017.

222. M. Shahedi Asl, F. Golmohammadi, M. Ghassemi Kakroudi, and M. Shokouhimehr, "Synergetic Effects of SiC and Csf in ZrB2-Based Ceramic Composites. Part I: Densification Behavior," *Ceramics International* 42, no. 3 (2016): 4498–4506, https://doi.org/10.1016/j.ceramint.2015.11.139.

223. D. E. Yunus, R. He, W. Shi, O. Kaya, and Y. Liu, "Short Fiber Reinforced 3d Printed Ceramic Composite with Shear Induced Alignment," *Ceramics International* 43, no. 15 (2017): 11766–11772, https://doi.org/10.1016/j.ceramint.2017.06.012.

224. H. L. Tekinalp, V. Kunc, G. M. Velez-Garcia, et al., "Highly Oriented Carbon Fiber-Polymer Composites via Additive Manufacturing," *Composites Science and Technology* 105 (2014): 144–150, https://doi.org/10.1016/j.compscitech.2014.10.009.

225. A. A. Stepashkin, D. I. Chukov, F. S. Senatov, A. I. Salimon, A. M. Korsunsky, and S. D. Kaloshkin, "3D-Printed PEEK-Carbon Fiber (CF) Composites: Structure and Thermal Properties," *Composites Science and Technology* 164 (2018): 319–326, https://doi.org/10.1016/j.compscitech.2018.05.032.

226. Z. Lu, Y. Xia, K. Miao, et al., "Microstructure Control of Highly Oriented Short Carbon Fibres in SiC Matrix Composites Fabricated by Direct Ink Writing," *Ceramics International* 45, no. 14 (2019): 17262–17267, https://doi.org/10.1016/j.ceramint.2019.05.283.

227. C. M. Larson, J. J. Choi, P. A. Gallardo, et al., "Direct Ink Writing of Silicon Carbide for Microwave Optics," *Advanced Engineering Materials* 18, no. 1 (2016): 39–45, https://doi.org/10.1002/adem.201500298.

228. A. Gómez-Gómez, J. J. Moyano, B. Román-Manso, M. Belmonte, P. Miranzo, and M. I. Osendi, "Highly-Porous Hierarchical SiC Structures Obtained by Filament Printing and Partial Sintering," *Journal of the European Ceramic Society* 39, no. 4 (2019): 688–695, https://doi.org/10.1016/j.jeurceramsoc.2018.12.034.

229. S. Eqtesadi, A. Motealleh, F. H. Perera, et al., "Fabricating Geometrically-Complex B4C Ceramic Components by Robocasting and Pressureless Spark Plasma Sintering," *Scripta Materialia* 145 (2018): 14–18, https://doi.org/10.1016/j.scriptamat.2017.10.001.

230. S. Kultayeva and Y.-W. Kim, "Mechanical, Thermal, and Electrical Properties of Pressureless Sintered SiC-AlN Ceramics," *Ceramics International* 46, no. 11, Part B (2020): 19264–19273, https://doi.org/10.1016/j.ceramint.2020.04.266.

231. F. Niu, D. Wu, G. Ma, S. Zhou, and B. Zhang, "Effect of Second-Phase Doping on Laser Deposited Al_2O_3 Ceramics," *Rapid Prototyping Journal* 21, no. 2 (2015): 201–206, https://doi.org/10.1108/RPJ-12-2014-0167.

232. G. He, D. Hirschfeld, J. Cesarano III, and J. N. Stuecker, *Robocasting and Mechanical Testing of Aqueous Silicon Nitride Slurries* (Sandia National Lab.(SNL-NM), 2000).

233. H. C. Yen and H. H. Tang, "Study on Direct Fabrication of Ceramic Shell Mold with Slurry-Based Ceramic Laser Fusion and Ceramic Laser Sintering," *International Journal of Advanced Manufacturing Technology* 60, no. 9 (2012): 1009–1015, https://doi.org/10.1007/s00170-011-3664-0.

234. Y. Wang, Y. Peng, W. Qin, et al., "Mechanism of Amorphous SiO_2 Grain Boundary Modulation to Inhibit Abnormal Grain Growth and High-Temperature Strengthening of 3YSZ Ceramic Fibers," *Journal of*

15272648, 2026, 16, Downloaded from https://advanced.onlinelibrary.wiley.com/doi/10.1002/adem.71088 by Abdollah Saboori - Politecnico Di Torino Sist. Bibl Del Polit Di Torino , Wiley Online Library on [27/09/2026]. See the Terms and Conditions (https://onlinelibrary.wiley.com/terms-and-conditions) on Wiley Online Library for rules of use; OA articles are governed by the applicable Creative Commons License

the European Ceramic Society 46, no. 7 (2026): 118128, https://doi.org/10.1016/j.jeurceramsoc.2026.118128.

235. X. Wei, Y. Liu, D. Zhao, and S. S. Ge, "3D Printing of Piezoelectric Barium Titanate with High Density From Milled Powders," *Journal of the European Ceramic Society* 40, no. 15 (2020): 5423–5430, https://doi.org/10.1016/j.jeurceramsoc.2020.06.021.

236. S. Barui, S. Chowdhury, R. Samajdar, S. Chakraborty, M. Gavade, and B. Basu, "Impact of Core-Shell Mode of Printing on Properties of 3D Binderjet Printed Zirconia-Alumina Based Bioceramics," *Open Ceramics* 3 (2020): 100026, https://doi.org/10.1016/j.oceram.2020.100026.

237. Y. Pan, H. Li, Y. Liu, et al., "Effect of Holding Time During Sintering on Microstructure and Properties of 3D Printed Alumina Ceramics," *Frontiers in Materials* 7 (2020): 2020, https://doi.org/10.3389/fmats.2020.00054.

238. M. Kermani, J. Dong, M. Biesuz, et al., "Ultrafast High-Temperature Sintering (UHS) of Fine Grained α-Al_2O_3," *Journal of the European Ceramic Society* 41, no. 13 (2021): 6626–6633, https://doi.org/10.1016/j.jeurceramsoc.2021.05.056.

239. L. Wang and R. Ma, "Effects of Different Polymer Precursors on the Characteristics of SiOC Bulk Ceramics," *Applied Physics A* 125, no. 6 (2019): 395, https://doi.org/10.1007/s00339-019-2680-z.

240. R. He, G. Ding, K. Zhang, Y. Li, and D. Fang, "Fabrication of SiC Ceramic Architectures Using Stereolithography Combined with Precursor Infiltration and Pyrolysis," *Ceramics International* 45, no. 11 (2019): 14006–14014, https://doi.org/10.1016/j.ceramint.2019.04.100.

241. C. Burkhardt, P. Freigassner, O. Weber, P. Imgrund, and S. Hampel, "Fused Filament Fabrication (FFF) of 316L Green Parts for the MIM Process," in *Proceedings of the World PM2016—AM—Deposition Technologies* (European Powder Metallurgy Association (EPMA), 2016).

242. M. Bakhtiari, A. Fayazi Khanigi, and A. Farnia, "Improving the Wear Properties of AISI4130 Steel Using Laser Surface Hardening Treatment," *Arabian Journal for Science and Engineering* 48, no. 9 (2023): 11801–11818, https://doi.org/10.1007/s13369-022-07551-5.

243. S. Sharma, D. Mudgal, and V. Gupta, "Integrating Extrusion Process and Additive Manufacturing for Biomedical Breakthroughs," *International Journal on Interactive Design and Manufacturing* 18, no. 6 (2024): 3547–3570, https://doi.org/10.1007/s12008-023-01632-x.

244. A. Rossi, T. Pescara, A. M. Gambelli, et al., "Biomaterials for Extrusion-Based Bioprinting and Biomedical Applications," *Frontiers in Bioengineering and Biotechnology* 12 (2024): 1393641, https://doi.org/10.3389/fbioe.2024.1393641.

245. Q. Ramadan and M. Zourob, "3D Bioprinting at the Frontier of Regenerative Medicine, Pharmaceutical, and Food Industries," *Frontiers in Medical Technology* 2 (2021): 607648, https://doi.org/10.3389/fmedt.2020.607648.

246. A. Lee, A. R. Hudson, D. J. Shiwarski, et al., "3D Bioprinting of Collagen to Rebuild Components of the Human Heart," *Science* 365, no. 6452 (2019): 482–487, https://doi.org/10.1126/science.aav9051.

247. Z. Zhang, X. Zhou, Y. Fang, Z. Xiong, and T. Zhang, "AI-Driven 3D Bioprinting for Regenerative Medicine: From Bench to Bedside," *Bioactive Materials* 45 (2025): 201–230, https://doi.org/10.1016/j.bioactmat.2024.11.021.

248. Y. Hong, D. D. Dong, G. P. Zou, et al., "The Corrosion Response of the Heterogeneous Nitriding Structure Originated From the Laser Additive Manufactured Steel," *Corrosion Science* 218 (2023): 111188, https://doi.org/10.1016/j.corsci.2023.111188.

249. F. Clemens, F. Sarraf, A. Borzì, A. Neels, and A. Hadian, "Material Extrusion Additive Manufacturing of Advanced Ceramics: Towards the Production of Large Components," *Journal of the European Ceramic Society* 43, no. 7 (2023): 2752–2760, https://doi.org/10.1016/j.jeurceramsoc.2022.10.019.

250. X. Yang, J. Fu, Y. Hu, et al., "Microstructure and Mechanical Properties of Ni Superalloy Fabricated by Laser Directed Energy Deposition (L-DED) versus Laser Powder Bed Fusion (L-PBF)," *Archives of Civil and Mechanical Engineering* 26, no. 3 (2026): 148, https://doi.org/10.1007/s43452-026-01520-7.

251. W. Rowlands, *Additive Manufacturing of Advanced Ceramics for Demanding Applications* (Loughborough University, 2019).

252. W. Rowlands and B. Vaidhyanathan, "Additive Manufacturing of Barium Titanate Based Ceramic Heaters with Positive Temperature Coefficient of Resistance (PTCR)," *Journal of the European Ceramic Society* 39, no. 12 (2019): 3475–3483, https://doi.org/10.1016/j.jeurceramsoc.2019.03.024.

253. E. Schwarzer-Fischer, J. Abel, J. Sieder-Katzmann, et al., "Study on CerAMfacturing of Novel Alumina Aerospike Nozzles by Lithography-Based Ceramic Vat Photopolymerization (CerAM VPP)," *Materials* 15, no. 9 (2022): 3279.

254. H. Yu, Q. Zhao, J. Fu, et al., "The Design of Oxidation Resistant Ni Superalloys for Additive Manufacturing," *Additive Manufacturing* 97 (2025): 104616, https://doi.org/10.1016/j.addma.2024.104616.

255. S. Bhandari, P. Veteška, G. Vajpayee, et al., "Material-Extrusion Based Additive Manufacturing of $BaTiO_3$ Ceramics: From Filament Production to Sintered Properties," *Additive Manufacturing* 88 (2024): 104238, https://doi.org/10.1016/j.addma.2024.104238.

256. M. Christ, C. Zimmermann, S. Neinert, B. Leykauf, K. Döringshoff, and M. Krutzik, "Additively Manufactured Ceramics for Compact Quantum Technologies," *Advanced Quantum Technologies* 7, no. 12 (2024): 2400076, https://doi.org/10.1002/qute.202400076.

257. Y. Ji, W. Bai, A. O. Omoniyi, et al., "One-Stone-Two-Bird Programmable Temperature-Gated 4D Encryption Enabled by Precisely and Synergistically Controlled Shape and Color Transformations of Polyurethane Films," *Chemical Engineering Journal* 526 (2025): 171407, https://doi.org/10.1016/j.cej.2025.171407.

258. B. Nan, J. Zang, W. Lu, T. Yang, S. Zhang, and H. Zhang, "Recent Progress on Additive Manufacturing of Piezoelectric Ceramics," *Journal of Inorganic Materials* 37, no. 6 (2022): 585–595, https://doi.org/10.15541/jim20210358.

259. A. Asghar, K. Khan, M. S. Rashid, et al., "Extrusion-Based Additive Manufacturing of Carbonaceous and Non-Carbonaceous Electrode Materials for Electrochemical Energy Storage Devices," *Advanced Materials Technologies* 10, no. 3 (2025): 2400136, https://doi.org/10.1002/admt.202400136.

260. K. Hassan, M. J. Nine, T. T. Tung, et al., "Functional Inks and Extrusion-Based 3D Printing of 2D Materials: A Review of Current Research and Applications," *Nanoscale* 12, no. 37 (2020): 19007–19042, https://doi.org/10.1039/D0NR04933F.

261. A. Ghazanfari, W. Li, M. C. Leu, and G. E. Hilmas, "A Novel Freeform Extrusion Fabrication Process for Producing Solid Ceramic Components with Uniform Layered Radiation Drying," *Additive Manufacturing* 15 (2017): 102–112, https://doi.org/10.1016/j.addma.2017.04.001.

262. L. Tabard, V. Garnier, E. Prud'Homme, et al., "Robocasting of Highly Porous Ceramics Scaffolds with Hierarchized Porosity," *Additive Manufacturing* 38 (2021): 101776, https://doi.org/10.1016/j.addma.2020.101776.

263. J. Seuba, S. Deville, C. Guizard, and A. J. Stevenson, "Mechanical Properties and Failure Behavior of Unidirectional Porous Ceramics," *Scientific Reports* 6, no. 1 (2016): 24326, https://doi.org/10.1038/srep24326.

264. S.-I. Roohani-Esfahani, P. Newman, and H. Zreiqat, "Design and Fabrication of 3D Printed Scaffolds with a Mechanical Strength Comparable to Cortical Bone to Repair Large Bone Defects," *Scientific Reports* 6, no. 1 (2016): 19468, https://doi.org/10.1038/srep19468.

265. Y. Zou and J. Malzbender, "Development and Optimization of Porosity Measurement Techniques," *Ceramics International* 42, no. 2, Part A (2016): 2861–2870, https://doi.org/10.1016/j.ceramint.2015.11.015.

266. D. Pastorino, C. Canal, and M.-P. Ginebra, "Multiple Characterization Study on Porosity and Pore Structure of Calcium

15272648, 2026, 16, Downloaded from https://advanced.onlinelibrary.wiley.com/doi/10.1002/adem.71089 by Abdollah Saboori - Politecnico Di Torino Sist. Bibl Del Polit Di Torino , Wiley Online Library on [27/09/2026]. See the Terms and Conditions (https://onlinelibrary.wiley.com/terms-and-conditions) on Wiley Online Library for rules of use; OA articles are governed by the applicable Creative Commons License

Phosphate Cements," *Acta Biomaterialia* 28 (2015): 205–214, https://doi.org/10.1016/j.actbio.2015.09.017.

267. L. M. Anovitz and D. R. Cole, "Characterization and Analysis of Porosity and Pore Structures," *Reviews in Mineralogy and Geochemistry* 80, no. 1 (2015): 61–164, https://doi.org/10.2138/rmg.2015.80.04.

268. Z. Tonar, V. Liska, T. Gregor, et al., "Correlating Micro-CT Imaging with Quantitative Histology," in *Injury and Skeletal Biomechanics*, ed. T. Goswami (IntechOpen, 2012).

269. E. N. Kaufmann, "Common Concepts in Materials Characterization," in *Characterization of Materials* (John Wiley & Sons, 2002), https://doi.org/10.1002/0471266965.com001.

270. Y. Zhao, C. Han, Y. Sun, N. N. Danesh, T. Liu, and Y. Gao, "Nano- to Micro-Pore Characterization by Synchrotron Radiation SAXS and Nano-CT for Bituminous Coals," *Frontiers of Earth Science* 15, no. 2 (2021): 189–201, https://doi.org/10.1007/s11707-021-0889-6.

271. S.-Y. Chung, J.-S. Kim, D. Stephan, and T.-S. Han, "Overview of the use of Micro-Computed Tomography (Micro-CT) to Investigate the Relation between the Material Characteristics and Properties of Cement-Based Materials," *Construction and Building Materials* 229 (2019): 116843, https://doi.org/10.1016/j.conbuildmat.2019.116843.

272. D. A. Ashebir, A. Hendlmeier, M. Dunn, et al., "Detecting Multi-Scale Defects in Material Extrusion Additive Manufacturing of Fiber-Reinforced Thermoplastic Composites: A Review of Challenges and Advanced Non-Destructive Testing Techniques," *Polymers* 16, no. 21 (2024): 2986, https://doi.org/10.3390/polym16212986.

Biographies



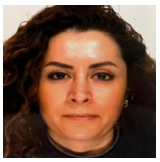
Meisam Bakhtiari received his Ph.D. in materials science and engineering from the Department of Materials Science and Engineering at K.N. Toosi University of Technology. His research focuses on the constitutive modeling of advanced materials, including shape memory polymers (SMPs) and shape memory alloys (SMAs), employing finite element method (FEM) and multiscale modeling approaches. His expertise spans a broad range of topics in advanced materials processing, including micromechanics of solids, additive manufacturing and 3D printing of advanced materials, hot deformation behavior, microstructure simulation using cellular automata (CA), and surface modification treatments such as laser shock peening (LSP).



Mohammad Hadi Sheikh-Ansari received his Ph.D. in materials science and engineering from K.N. Toosi University of Technology, Iran. His primary research focuses on additive manufacturing (3D printing) of polymers and advanced ceramics, encompassing nanocomposite development, print process optimization, and structural performance in aggressive environments. Drawing on his strong background in continuum mechanics and thermomechanical modeling, he also leads R&D initiatives in energy storage materials and battery simulation.



Avinash Borgaonkar, Ph.D., is currently an assistant professor in the Department of Management and Production Engineering at Politecnico di Torino, Italy. Prior to this, he worked as a postdoctoral researcher in the School of Mechanical and Manufacturing Engineering at Dublin City University, Ireland. During his postdoctoral tenure, he focused on enhancing the speed and sustainability of the laser powder bed fusion (LPBF) process and conducted life cycle assessments (LCA) of nano-enabled coatings used in industrial applications. His research interests include metal additive manufacturing, materials structure–property analysis, life cycle assessment, tribology, and sustainable manufacturing.



Mehran Dadkhah, Ph.D., is an R&D Engineer in materials and processes with experience in industrial R&D, advanced materials characterization, and process validation. She received her Ph.D. in materials science and technology from Politecnico di Torino, Italy. From 2021 to 2025, she worked as a postdoctoral research fellow at Politecnico di Torino, contributing to projects on polymer-based formulations, rubber compounds, ceramics, metal oxides, gas sensors, and circular-economy applications. Her research interests include polymer and composite materials, ceramics, metal oxides, process–property relationships, qualification testing, and sustainable materials development.



Abdollah Saboori, Ph.D., is an associate professor in the Department of Management and Production Engineering at Politecnico di Torino, Italy, and a member of the Integrated Additive Manufacturing Center, IAM@PoliTo. He received his Ph.D. in materials science and engineering from Politecnico di Torino, graduating with honors cum laude. His research focuses on metal additive manufacturing, process–structure–property relationships, advanced metallic materials for additive manufacturing, and post-treatment of additively manufactured components. He has contributed to several European and national research projects and serves in editorial roles for journals in materials science and additive manufacturing.

15272648, 2026, 16, Downloaded from https://advanced.onlinelibrary.wiley.com/doi/10.1002/adem.71089 by Abdollah Saboori - Politecnico Di Torino Sist. Bibl Del Polit Di Torino , Wiley Online Library on [27/09/2026]. See the Terms and Conditions (https://onlinelibrary.wiley.com/terms-and-conditions) on Wiley Online Library for rules of use; OA articles are governed by the applicable Creative Commons License